Implementation Of The Arbitrary Lagrangian Eulerian Method In Soft Body Projectile Impacts Against Composite Plates

Lucas Márquez Duque

Master Thesis

presented in partial fulfillment
of the requirements for the double degree:
"Advanced Master in Naval Architecture" conferred by University of Liege
"Master of Sciences in Applied Mechanics, Specialization in Hydrodynamics,
Energetics and Propulsion" conferred by Ecole Centrale de Nantes

developed at Institut Catholique d'arts et métiers, Nantes
in the framework of the

"EMSHIP"
Erasmus Mundus Master Course
in "Integrated Advanced Ship Design"

Ref. 159652-1-2009-1-BE-ERA MUNDUS-EMMC

Supervisor:	Pr. Hervé Le Sourne, Institut Catholique d'arts et métiers, Nantes
Reviewer:	Pr. Gangadhara Prusty, University of New South Wales, Sydney

Nantes, February 2019

Lucas Márquez Duque

This page is intentionally left blank

DECLARATION OF AUTHORSHIP

I, Lucas Márquez Duque declare that this thesis and the work presented in it are my own and has been generated by me as the result of my own original research.

"Implementation of the Arbitrary Lagrangian Eulerian Method in Soft Body Projectile Impacts Against Composite Plates"

I confirm that:

1. This work was done wholly or mainly while in candidature for a research degree at this University;

2. Where any part of this thesis has previously been submitted for a degree or any other qualification at this University or any other institution, this has been clearly stated;

3. Where I have consulted the published work of others, this is always clearly attributed;

4. Where I have quoted from the work of others, the source is always given. With the exception of such quotations, this thesis is entirely my own work;

5. I have acknowledged all main sources of help;

6. Where the thesis is based on work done by myself jointly with others, I have made clear exactly what was done by others and what I have contributed myself;

7. None of this work has been published before submission;

8. I cede copyright of the thesis in favor of Institut Catholique d'Art et Métiers, Nantes Campus.

Signed:

Date:

This page is intentionally left blank

CONTENTS

ABSTRACT

Implementation Of The Arbitrary Lagrangian Eulerian Method In Soft Body Projectile Impacts Against Composite Plates

By Lucas Márquez Duque

Underwater Explosions (UNDEX) have been a subject of high interest not only for military organizations but also for commercial industry. The analytical and numerical tools that have been developed until these days have allowed studying the energy transport mechanisms occurred in UNDEX and its interaction with man-crafted structures, allowing also improving the structural scantlings and defense systems against these kinds of treats. Similar approaches can be used as well to study the instantaneous high-pressure impact loads such as slamming, which is one of the most important design loads in the vast majority of applications in naval engineering. However, performing experimental tests of these mechanisms is not only a costly but also a complicated process, due to the hazards involved in handling explosives and the limited organizations that have licenses to develop such tests.

Under the framework of Project SUCCESS, one of the main objectives is to study the response of Fiber Reinforced Polymers (FRP) structures subjected to slamming and UNDEX, therefore developing accurate calculation tools, which allow the designers to take into account these loads in the design of different naval components. One of the main challenges of the project is to include adequately the intra-laminar and inter-laminar damage mechanisms during these events, which is far more complex to the ones suffered by metallic materials. For these reasons, a series of experimental tests were performed in order to understand the dynamic behavior of FRP square plates subjected to soft body projectile impacts, while validating the numerical models developed.

The research performed in this Master thesis was focused in the use of Arbitrary Lagrangian Eulerian (ALE) methods for solving Fluid Structure Interaction (FSI) problems involving Soft Body Impacts on composite laminates, focusing mainly in the structural behavior of the plates during the impact, especially the intra-laminar damage mechanisms and its evolution. Simplified models of composite damage are used to predict the different phases of the plate response: elastic response, initiation of matrix cracking due to tension loads and finally fiber rupture. The initial results of the numerical models were used as a reference for the gas canon tests performed during the project campaign.

Keywords: Fluid Structure Interaction, Arbitrary-Lagrangian-Eulerian, Intra-laminar damage, Composites Modelling, Soft Body Impact.

LIST OF FIGURES

LIST OF TABLES

NOMENCLATURE

C_0	Isentropic Wave Velocity in Uncompressed Material [m/s]
ρ	Material Density [Kg/m^3]
ρ_1	Material Density before Shockwave [Kg/m^3]
ρ_2	Material Density after Shockwave [Kg/m^3]
D	Cylinder Diameter [m]
F	Force [N]
I	Impulse [N-S]
k	Experimental Constant [DIMENSIONLESS]
L	Cylinder Length [m]
$(L/D)_C$	Cylinder Critical L/D ratio. [DIMENSIONLESS]
P_{sh}	Hugoniot Pressure [Pa]
P_{stag}	Stagnation Pressure [Pa]
P_1	Pressure before Shockwave [Pa]
P_2	Pressure after Shockwave [Pa]
q	Relation between ρ_1 and ρ_2 [DIMENSIONLESS]
V_{sh}	Shockwave Velocity [m/s]
V_{im}	Impact Velocity [m/s]
ν	Poisson ratio [DIMENSIONLESS]
z	Porosity by Volume Fraction [DIMENSIONLESS]
E_{ii}	Young Modulus [Pa]
u_i, v_i, w_i	Particle Velocity components in the eulerian frame [ms]
σ_{ij}	Cauchy tensor [Pa]
μ	Dynamic Viscocity [Kg/m.s]
Y_t	Unidirectional ply tensile strength in the transverse direction [Pa]
Y_c	Unidirectional ply compressive strength in the transverse direction [Pa]
X_t	Unidirectional ply tensile strength in the fiber direction [Pa]
X_c	Unidirectional ply compressive strength in the fiber direction [Pa]
S_c	Unidirectional ply shear strength [Pa]

1. INTRODUCTION

The project SUCCESS was born in France as a partnership between ICAM Engineering School, private companies and the French government, oriented to study the behavior of composite structures submitted to UNDEX and other instantaneous loads. One of its mains objectives is to study the response of Fiber Reinforced Polymers (FRP) structures subjected to slamming and UNDEX, therefore developing accurate calculation tools that allow the designers to take into account these loads in the design of different naval components. One of the main challenges of the project is to include adequately the intra-laminar and inter-laminar damage mechanisms during these events, which is far more complex to the ones suffered by metallic materials. Considering the difficulties involved in performing tests using explosives, another kind of experimental setups were considered for having a preliminary approximation of the damage evolution on composite plates. It was decided that using simple dropping tests and soft body impacts fired with an air gas cannon would allow studying the different composite damage mechanisms in a preliminary phase, where only intra-laminar damage is considered with the objective to implement such solutions at the industrial level (fast calculation tools)

The main objectives of this work are listed as follows:

- To study the interaction of a soft body impactor against a rigid plate whilst identifying the main physical parameters required for modelling such bodies numerically.

- To develop a numerical model based on an Arbitrary Lagrangian Eulerian approach for recreating the kinematics and kinetics behavior involved during Soft Body Impact events at low and high velocities against elastic and elastoplastic target plates.

- To extend the previous numerical model for studying the impact of such bodies against Fiber Reinforced Polymer plates, where an intra-laminar damage model is included.

- To simulate numerically the gel-structure impact tests that were performed at Clement Ader institute, contributing to prepare both pre and post experimental phases.

This work was performed done under the tutelage of Professor Hervé Le Sourne (ICAM) and Jean Christophe Petiteau (MECA CALCUL) in the framework of the project SUCCESS and the academic final dissertation of the ERASMUS MUNDUS program EMSHIP (8TH Cohort). During this project, the academic research was performed at ICAM Nantes campus and the engineering design office of MECA.

2. LITERATURE REVIEW
2.1. Underwater Explosions

Underwater Explosions (UNDEX) has been a topic largely studied after the 20th century due to the proliferation of explosive threats developed for war purposes. Their application goes from the understanding of the charges explosive mechanisms, up to the development of defense systems used in boat structures, aiming to reduce the damage caused by these events. UNDEX are events in which high amounts of energy are transferred at high velocities through a liquid medium. This energy reaches a targeted surface as dynamic loading, affecting directly the integrity of the surface Ex. Ship Structures, Oil platforms, Submarine piping, etc.

A submarine detonation can be divided into two main phases: shockwave generation and gas bubble expansion, both differing in the event lapse time, and the quantity of energy transmitted. When a submarine charge explodes, it generates an instantaneous 3-D spherical shock wave front, which travels faster than the velocity of sound through the fluid. This shock wave generates high-pressure gradients that travel at high velocities, generating an intense impulsive loading to the surrounding fluids and obstacles. When this shockwave reaches the free surface, the impedance difference between air and water reflects the wave, generating a phenomenon called a tensile wave, causing immediately the so-called bulk cavitation. Meanwhile, the shockwave front, which is going towards the bottom, collides and depending on the floor material and characteristics, will be reflected causing tensile waves again. All these events occur in the lapse of milliseconds while carrying the most quantity of energy liberated by the explosion (See Fig. #1). [1]
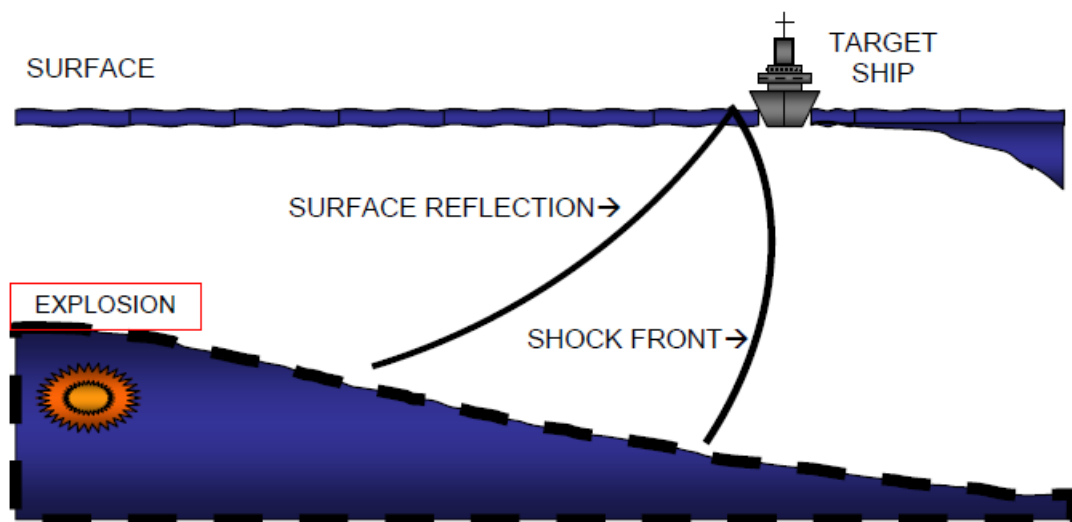
Figure 1. Schematic of the explosion shock wave and free surface reflection. From: [1]
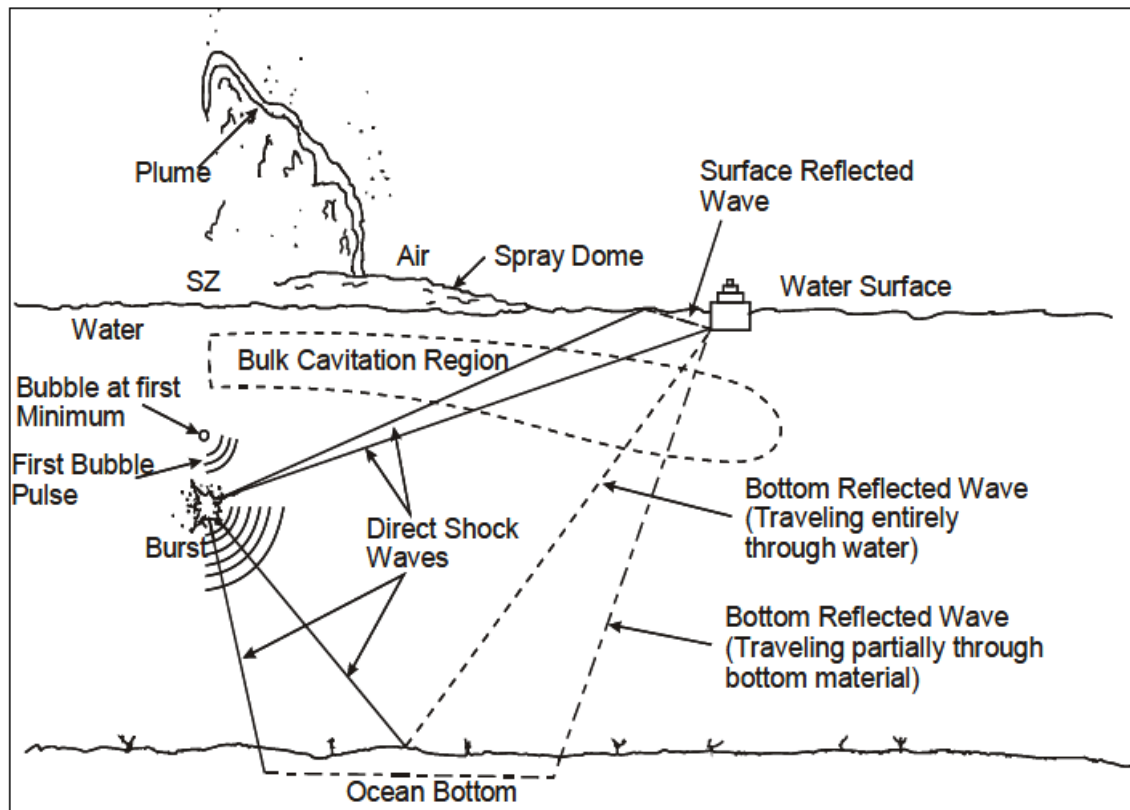
Figure 2. Overall schematic of the principal phenomena after an underwater explosion From:[1]

Parallel to the shock wave generation, a gas bubble, composed mainly by the gaseous products generated by the chemical products of the bomb, begins to expand itself and starts moving up due to buoyancy effects. On its way up, it will be suffering from expansion and contraction due to hydrostatic and hydrodynamic forces. This phase, although does not carry as high as the energy carried by the shock wave propagation, it is important when modelling the structural shock responses. It also participates the so-called "Water Hammer Effect", that occurs when the closing of the bulk cavitated zone and the Gas Bubble encounters, generating this way a compressive pulse. However, the lapse of this phase, that is bubble evolution, is in the order of seconds, being this large time difference compared to the shock wave propagation, which is in the order of milliseconds, one of the main difficulties in the numerical modelling of these events. [1]

In the Fig.2, it is presented a diagram that briefs the events of a UNDEX is presented, starting with the propagation of both shock wave front and gas bubble. Afterwards, the reflection of the shock wave front in both free surface and ocean bottom takes place, generating the bulk cavitation region. Subsequently, the surface interaction takes place, first in form of a spray dome (Due to the shock wave) followed by an explosive expulsion of water called plume (Due to the gas bubble release).

2.2. UNDEX Numerical Approaches

Several numerical approaches have been used to model the Fluid Structure Interaction (FSI) problem caused by UNDEX when interacting with structures. Currently, most part of the research in this topic has been made modelling the problem using Hydrocodes based on formulations such as Lagrangian, Eulerian, Coupled Eulerian-Lagrangian (CEL) and Arbitrary Lagrangian Eulerian (ALE) [2]. In the framework of this research, it has been observed that the formulations preferred not only by being computationally less expensive, but accurate enough, are the Coupled Eulerian-Lagrangian (CEL) [3] and Arbitrary Lagrangian-Eulerian (ALE).

ALE formulations are based on the preservation of a uniform mesh by giving an arbitrary movement to the Eulerian mesh in order to avoid the errors obtained by having big deformations, as it happens in a pure Lagrangian formulation. In ALE formulation, the motion of the solid element is recomputed at each time step in the Eulerian mesh through its boundary, matching the element and the fluid nodes, thus creating this way the Fluid Structure Interaction coupling without the need to define two different coordinate systems as it happens with CEL. However, both CEL and ALE methods should be used having in mind that their results are very sensitive due to dissipative and dispersive problems caused by advection, inherent to the Eulerian Formulations (Fig.#3). [2]
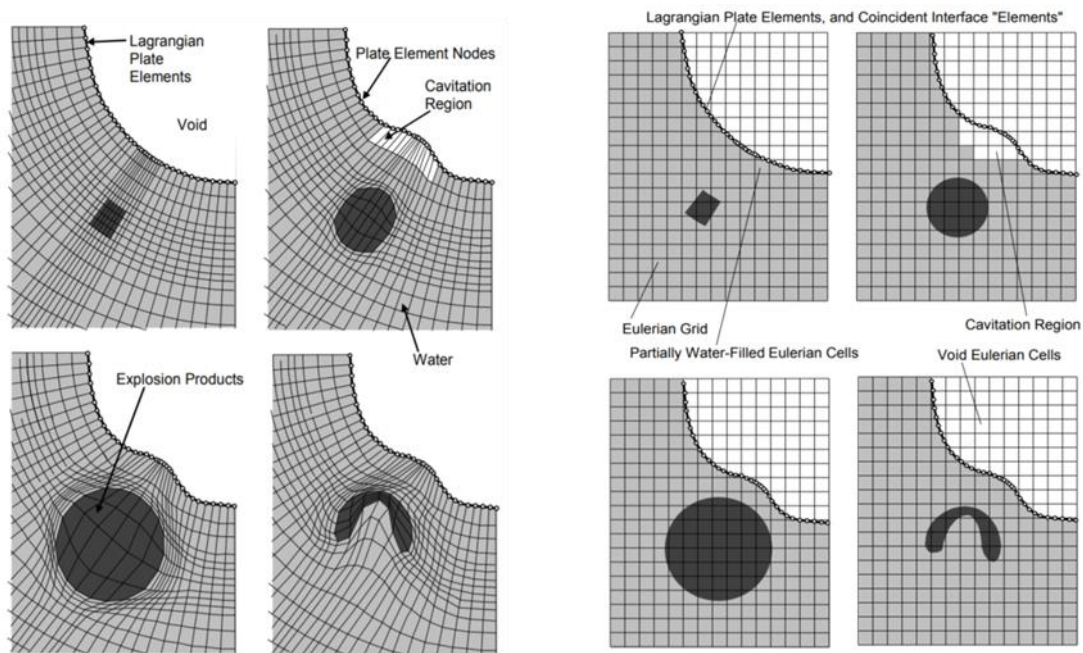
Figure 3. Left: Single material ALE Hydrocode. Right: Coupled Eulerian Lagrangian hydrocode. From: [2]

In the work of Avachat [3], the loading carrying capacity under impulsive loads of different laminates made of Fiber Reinforced Polymers (Fiberglass and Carbon fiber) was studied using FEM. These results were then validated by using a fully 3-D coupled model to account for the effects of fluid structure interactions. In parallel, an experimental setup was developed to study the underwater blast response of the laminates, called Underwater Shock Loading Simulator (USLS, See Fig.5). In this experimental arrangement, a gas shock wave is transmitted from a pressurized reservoir to a shock tube filled with water, the last one being in directly contact with the simply supported air-backed plate as shown in the Fig.5. The experimental data such as deformation and failure was collected using a high-speed camera at the wall-water interface.

Concerning to the numerical simulation, a Coupled Eulerian-Lagrange (CEL) domain was used in order to include the FSI, where Lagrangian elements where assigned to the material whereas the fluid was modeled using a Eulerian formulation. On the other hand, an energy based evolution law was used to include the damage modes in the composite material through all the discretized elements in the domain: Matrix tension, Matrix Compression, Fiber tension, and Fiber compression. For the layers interface, cohesive elements were defined in order to capture with high accuracy the failure due to delamination, which is the dominating failure mode in composite materials exposed to impulsive loads. This way, the discretization of the material domain was divided into two parts: 3-D brick elements were used for the intra-laminar regions whereas cohesive elements of finite thickness were used for inter-laminar regions.

The results obtained by Avachat [3] can be seen in Fig.4, where the experimental evolution of the deflection during the blast is compared to the results obtained by FEM. Some important features can be extrapolated from these results: the experimental results fit really well with the numerical approach for both fiberglass and carbon fiber. In the case of the fiberglass quasi-isotropic laminate, there is an appreciable mismatch of the deflection evolution. Moreover, in overall terms, the maximum deflection of both fiberglass unidirectional laminates is overestimated.
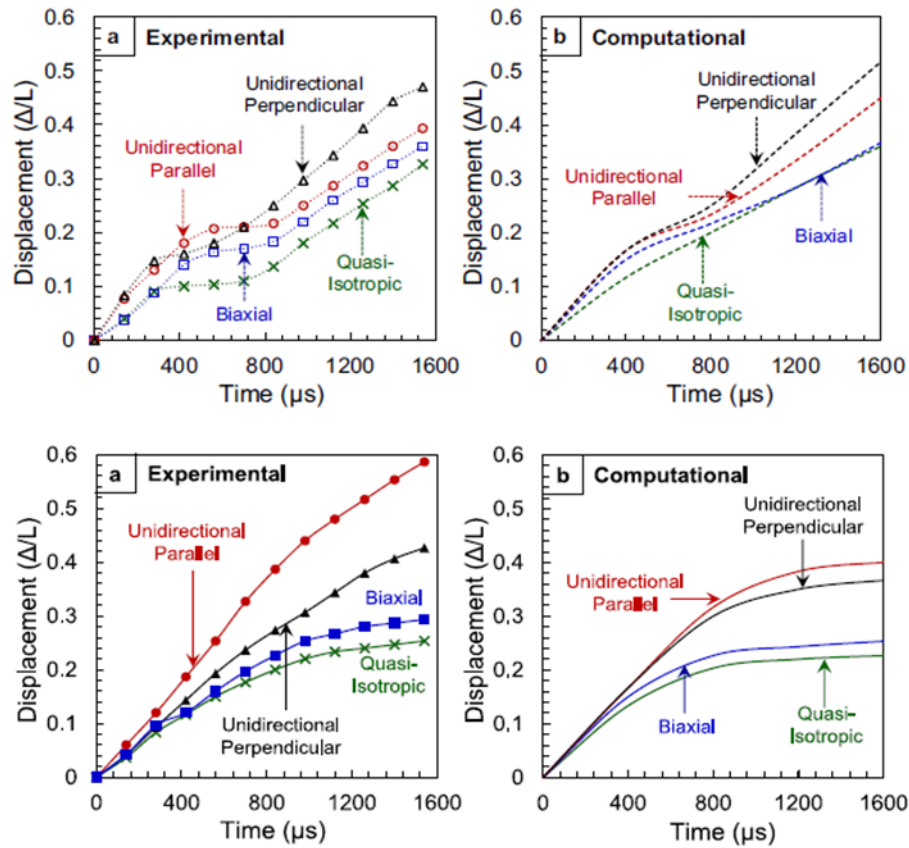
Figure 4.   Non-dimensional displacement obtained by the computational and experimental methodologies used by Avachat. Top: Glass fiber/ epoxy. Bottom: Carbon fiber/ epoxy. From:[3]

For the carbon fiber, despite the similar tendency of both curves that shows an adequate modelling of the failure modes in the numerical formulation, there is an overall underestimation of the deflection in the numerical results. According to Avachat [3], this underestimation is related to the fact that the continuum damage concludes in an artificial softening of the plate, which ends in a lower rate of deformation after failure.

Another important aspect to observe is that in overall terms, the carbon fiber presents an excellent behavior compared to the fiberglass in terms of reduced deflection due to its higher stiffness, overall weight and accumulated damage, which was 25% of the damage experience by glass fiber laminates. Hence, this research shows that its highly important to select correctly the failure model when composite laminates are studied in underwater explosions, as well as the influence that the laminate layup for having the least deflection possible, which is the case for the quasi-isotropic laminates. In overall terms, the numerical results fit really well against the experimental data, indicating the robustness of the Fully Dynamic 3D coupled Eulerian-Lagrangian finite element simulations used in this research.
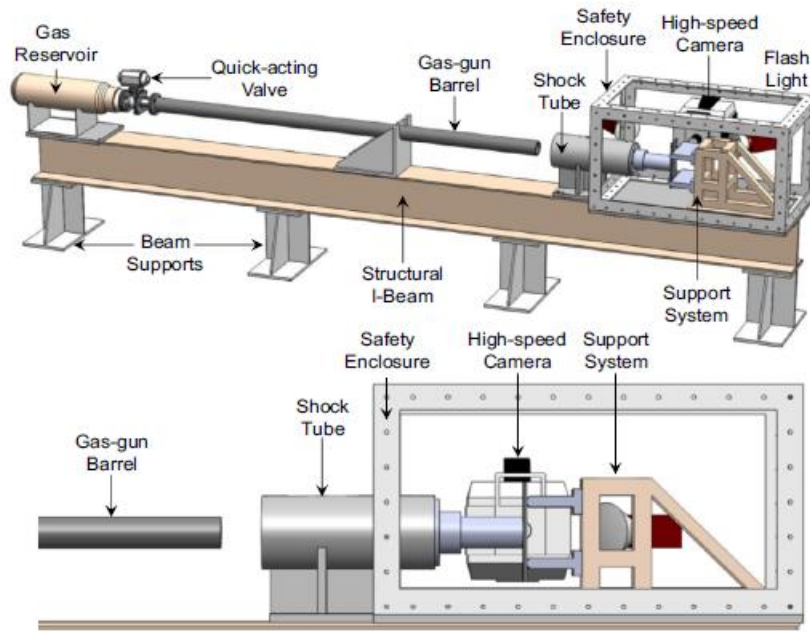
Figure 5. Experimental set up to model the impact of shockwaves using a Gas Shock tube. From:[3]

The analytical and numerical tools that have been developed until these days have allowed studying the energy transport mechanisms occurred in UNDEX and its interaction with man-crafted structures, allowing also improving the structural scantlings and defense systems against these kinds of treats. Similar approaches can be used as well to study the instantaneous high-pressure impact loads such as slamming, which is one of the most important design loads in the vast majority of applications in naval engineering. However, performing experimental tests of these mechanisms is not only a costly but also a complicated process, due to the hazards involved in handling explosives and the limited organisms that have licenses to develop such tests.

The project SUCCESS was born in France, as a partnership between ICAM Engineering School, private companies and the French government, oriented to study the behavior of structures submitted to UNDEX and other instantaneous loads. One of its mains objectives is to study the response of Fiber Reinforced Polymers (FRP) structures subjected to slamming and UNDEX, therefore developing accurate calculation tools that allow the designers to take into account these loads in the design of different naval components. One of the main challenges of the project is to include adequately the intra-laminar and inter-laminar damage mechanisms during these events, which is far more complex to the ones suffered by a metallic material. Considering the difficulties involved in performing tests using explosives, another kind of experimental setups is considered in order to have a preliminary approximation of the damage evolution on these composite plates. It was decided then that using simple dropping tests and

Soft Body Impacts by using an air gas cannon would allow studying the different composite damage mechanisms in a preliminary phase.

2.3. Soft Body Impacts

The events of soft body impacts is a vast field of research in structural engineering due to the difficulties related to the establishment of impact design limits in many collision cases, a consequence of the randomness in projectiles shapes and composition, as well as its "instantaneous" interaction with structural members. This complicates the selection of the initial experimental parameters required for having an ideal response of the plate during a test, which should allow studying properly each damage initiation phase. These events get even more complex when such projectiles impacts structures made of Fiber Reinforced Polymers (FRP) due to the complications related to intra-laminar and inter-laminar damages, a topic that is still under development.

The aerospace industry has been one of the main contributors in developing analytical and numerical methods for calculating such impact events due to the high-load operational conditions of an aircraft, which is always exposed to high velocity collisions with birds, hail, rubber as well as some low velocity impacts such as tool dropping [4]. These methods have helped to predict the damage behavior of these structural members before certification tests, improving this way the design methods and reducing, therefore, the investment in costly experimental tests (See Fig.6).

Figure 6. Platform STIMPACT at Clement Ader institute, Toulouse, France. From: [51]

One of the main references for describing the phenomena behind soft projectile impacts was the analytical model proposed by Wilbeck in 1978 [5]. In this report, the impact theory for soft body impacts is based on the hydrodynamic response of the projectile material when it is considered as a fluid. The general energy transfer mechanisms that occur during these events such as the Hugoniot pressure (Shock Pressure), Stagnation pressure and shock waves evolution is described in an analytical way, subsequently comparing it against different experimental tests with different materials: Birds, Beef, Rubber, porous and non-porous gelatin (See Fig.7). In this work, several experimental tests were performed, in which gelatin projectiles were fired against plates and Hopkinson bars in order to measure the pressure evolution along time.
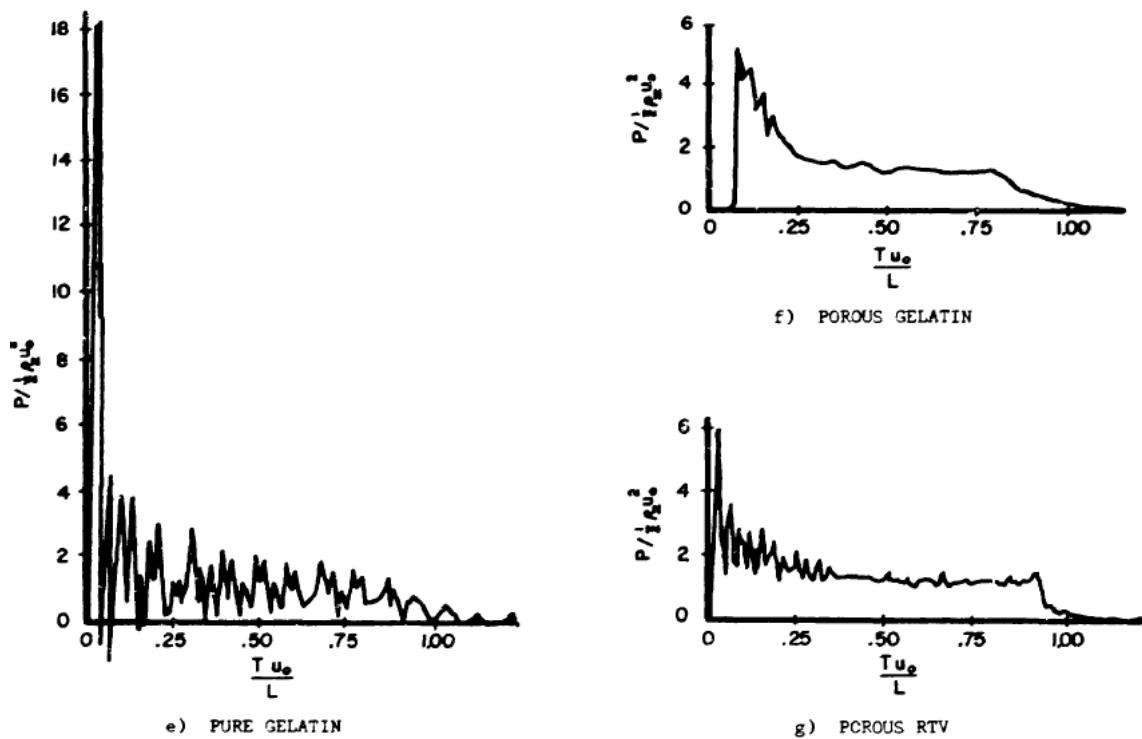
Figure 7. Impact pressure profiles for different materials against a rigid plate. From: [5]

Different kind of approximations has been used for modelling such phenomena, being especially preferred ALE and SPH methods due to their flexibility for modelling Fluid Structure Interaction (FSI) where large deformation exists [6] (See Fig.8). The numerical modelling of these events is usually carried out on FEM software with explicit formulations such as ABAQUS EXPLICIT, RADIOSS, PAM-CRASH, and LS-DYNA.
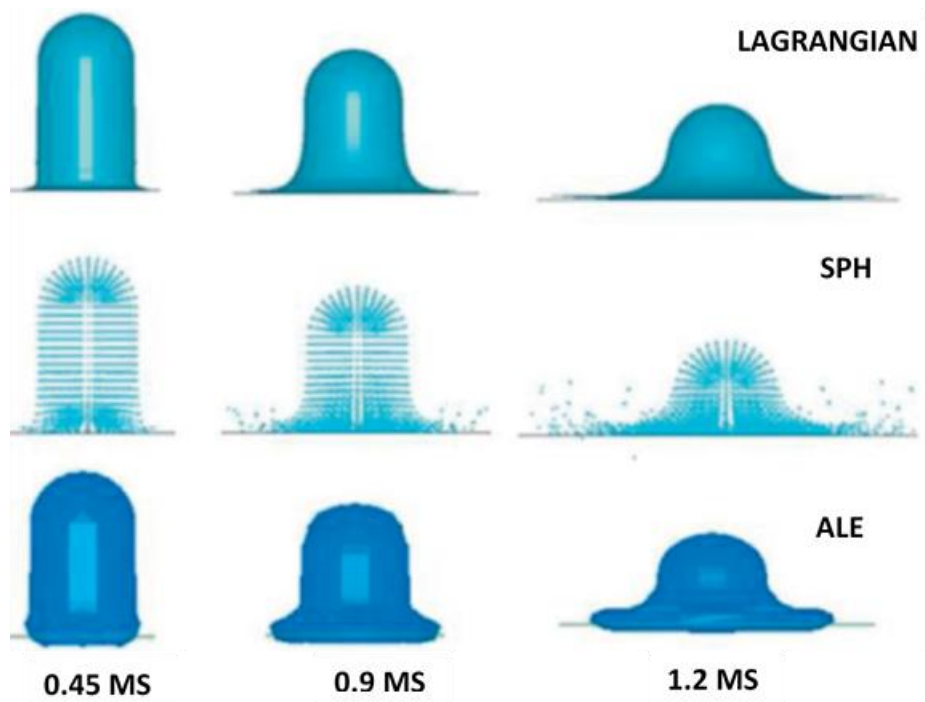
**Figure 8. Projectile Deformation at different time steps using Lagrangian, SPH and ALE
formulations. From: [4]**

In the work carried out by Lavoie [7], numerical models using ALE and SPH techniques were compared against experimental tests. Gel projectiles with 10 % of porosity were shot against steel rigid plates, which had piezo-electric carbon gauges in order to correctly measure the pressure exerted by the projectile, whereas the deformation patterns were captured using high-speed cameras. This study allowed validating the accuracy of the elastoplastic hydrodynamic formulation of the projectile used to build the numerical model (See Fig. 9).

It was found also in the work that the theoretical, experimental and numerical models were in good agreement, though it presented some discrepancies in the peak pressures. It is addressed that both ALE and SPH formulations conduced to similar results, each one with its own drawbacks. In the case of ALE, it was observed some loss of mass due to the not compliance of the minimal fraction of dense matter required inside an element between advections cycles, therefore not included in the calculation, subsequently presenting a reduction of the total energy in the system. Respect to the SPH method, it was observed a spurious reading for the pressure sensor, which still happens when more particles are added to represent the same body [7]. This work was the continuation of a previous study [6], where a similar analysis was performed including purely Lagrangian formulations. In this study, it was addressed the inability of such formulations in Soft Body impact simulations due mainly to the high distortion of these elements, which were subsequently deleted using erosion criteria, therefore causing a considerable loss of mass during the impact.
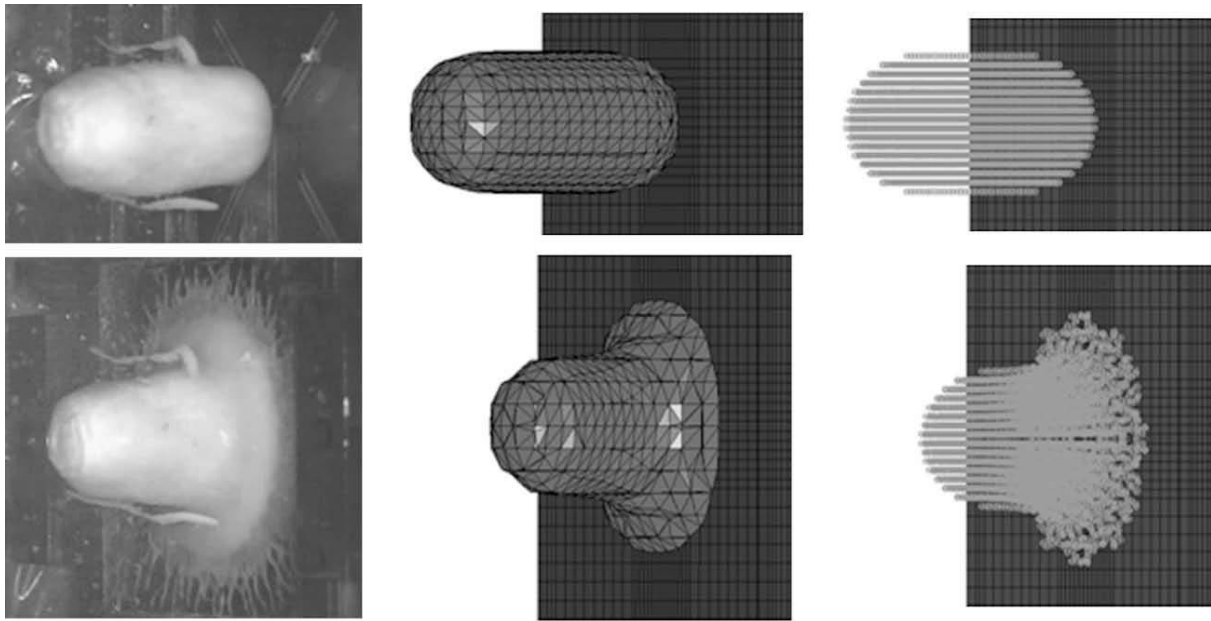
Figure 9. Comparison between different approaches for soft body impact events: Experimental, ALE and SPH (From left to right). From: [7]

It is stated also in this work [6] the limitations of ALE method for complex geometries in terms of computational costs, due to higher times in re-meshing between advection cycles compared to the SPH method, where no mesh exists. On the other hand, in Huertas work [8] was discussed that problems related to the pure Lagrangian formulation were not limited only to the loss of mass, but errors during the solving process due to negative volumes. He also made a comparison between Lagrangian, ALE and SPH method results for bird striking certification purposes, mentioning some difficulties related to ALE methods in its definition, such as the problems in defining an adequate mesh motion.

Moreover, in the work of Hedayati [9] is shown the importance of the impactor shape and its initial contact area in the magnitude of the peak pressure (Hugoniot). Different projectile shapes such as planar, rounded, ellipsoids and bird shaped projectiles were numerically studied, validating this way the high dependency of the Hugoniot pressure on the impactor frontal surface. Respect to the projectile initial velocity, it was addressed by Barber at al [10] in its experiments that this magnitude was much more important for the peak pressure than the size (mass) of the projectile.

Some other references for soft body impacts were also studied for the case of impact on plates made of elastoplastic materials such as the work carried out by Bo Wu [11], Welsh [12] and orthotropic materials formulations such as Horman [13], Heimbs [14] and Ericsson [15], but they will be explained deeper in later sections.

2.3. Impact on Fiber Reinforced Polymers (FRP)

The modelling of soft body impacts on Fiber Reinforced Polymers (FRP) has not been widely studied outside the aerospace industry. The anisotropic nature of these materials, combined with its complex failure modes, makes its numerical modelling even much harder. In the literature can be found several studies of impacts on composite structures, almost all based on Composite Laminate Theory, differing mainly in the failure theory and modeling techniques used. It can be said that Chang-Chang and Hashin are the most used failure criteria for taking into account the intra-laminar damage, whereas the inter-laminar damage is often modeled by implementing cohesive elements or Tiebreak contact between the composite plies.
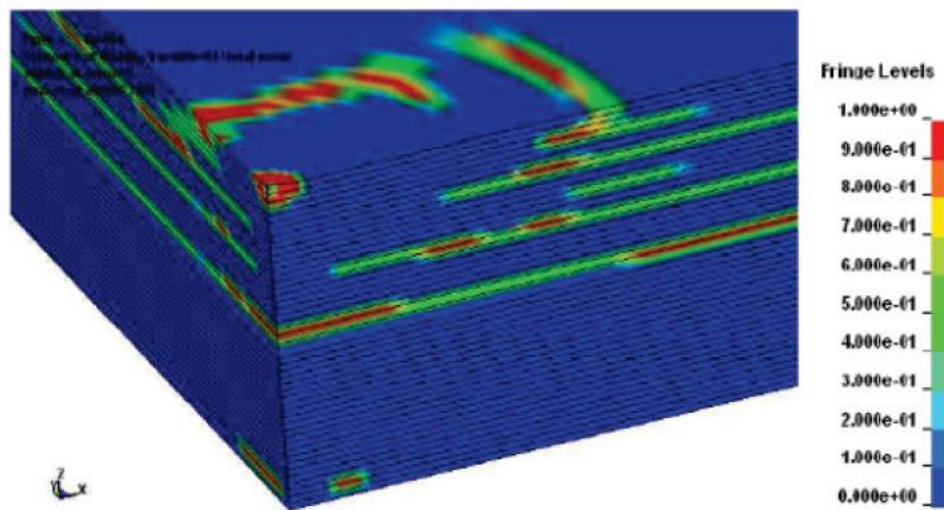
Figure 10. Delamination in a composite material using MAT 162. [16]
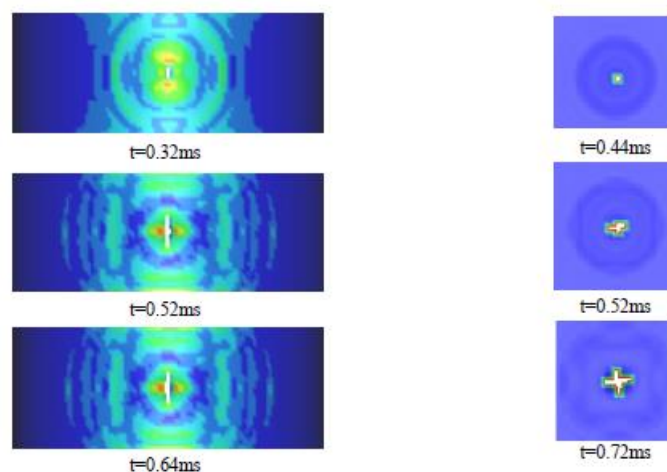
Figure 11. Development of perforation for a half ring (left) and a flat panel (right). [17]

In the work of Cheng [17], a simulation using the ALE method for impacts against composite plates is addressed and compared with experimental tests. The material model used in this work is MAT 58, implemented in LS-DYNA and suggested for fabrics modeling. The failure model is based on Hashin´s criteria, which includes four damage failure modes. However, delamination is not considered in this study, focusing mainly on the impact dynamics, contact forces, and penetration pattern after the impact.

It was observed in this work a good correlation in the results between the experimental and numerical simulations, where a gel cylinder with a radius of 70 mm and 127 mm length was impacted against a triaxial 0/+-60 CFRP laminate with 3.2 mm thickness. A Continuum Damage Mechanics (CDM) model was used in LS-DYNA (included in MAT 58) due to its capabilities in simulating the non-linear stress-strain behavior presented in braided composites, as well as its advantages concerning to fabrics modelling compared to MAT 54. The penetrations thresholds in both experimental and numerical tests agreed well, being between 149.5 and 154 m/s.

This investigation was taken even deeper by Staniszewski [18]. A complete fiber architecture modelling technique was implemented in his work, where the yarns were modeled using cells and sub cells, including this way a more accurate behavior of the composite response, although computationally more expensive. The author concludes that using this modelling technique, outputs such as damage size, shape and cracking of the laminate correlates very well with experimental tests. It also states that 45° orientations are more resistant to impacts than the other fiber orientations, which was expressed as well in the study presented in [19], where ±45° plies enhanced the impact resistance of aeronautical structures.
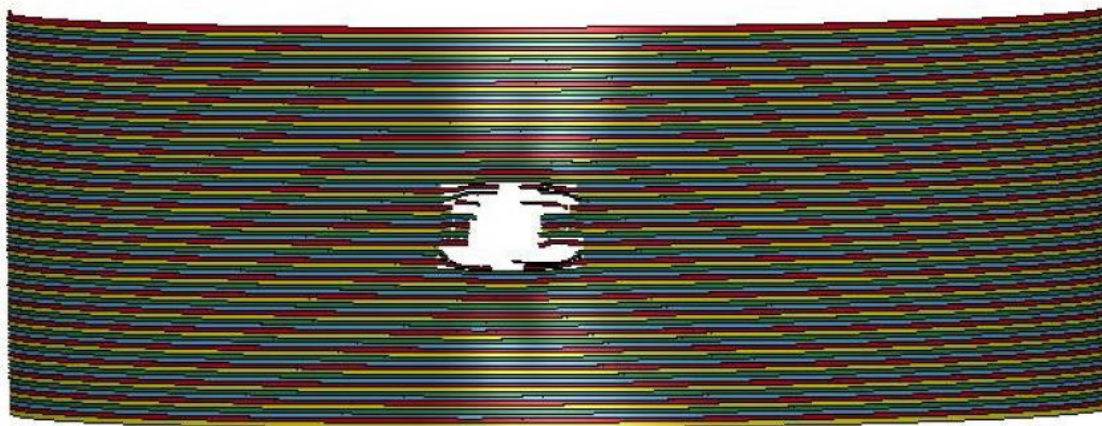
Figure 12. Deformation of a braided composite using Unit cell and Sub cell formulations. (Simulation of tri-axially braided composites). From: [18]

Furthermore, the works carried out by Heimbs [14], [20], [21] provide good insights about simulating these events. In the paper [20], intra-laminar and inter-laminar damages are studied in plates with compressive preload. Validations of the models are carried out first with rigid impactors against an unloaded plate, where a comparison against experimental test shows the accuracy of the numerical simulation developed. The intra-laminar failure is modeled using MAT 54 along Chang-Chang criteria, whereas the delamination is modeled using cohesive elements between different plies. After a sensitive analysis, the author found that the use of cohesive elements affects directly the plate bending stiffness, which will affect as well the intra-laminar failure modes. It is stated that using few delamination contact definition can lead to better results. (See Fig.13)
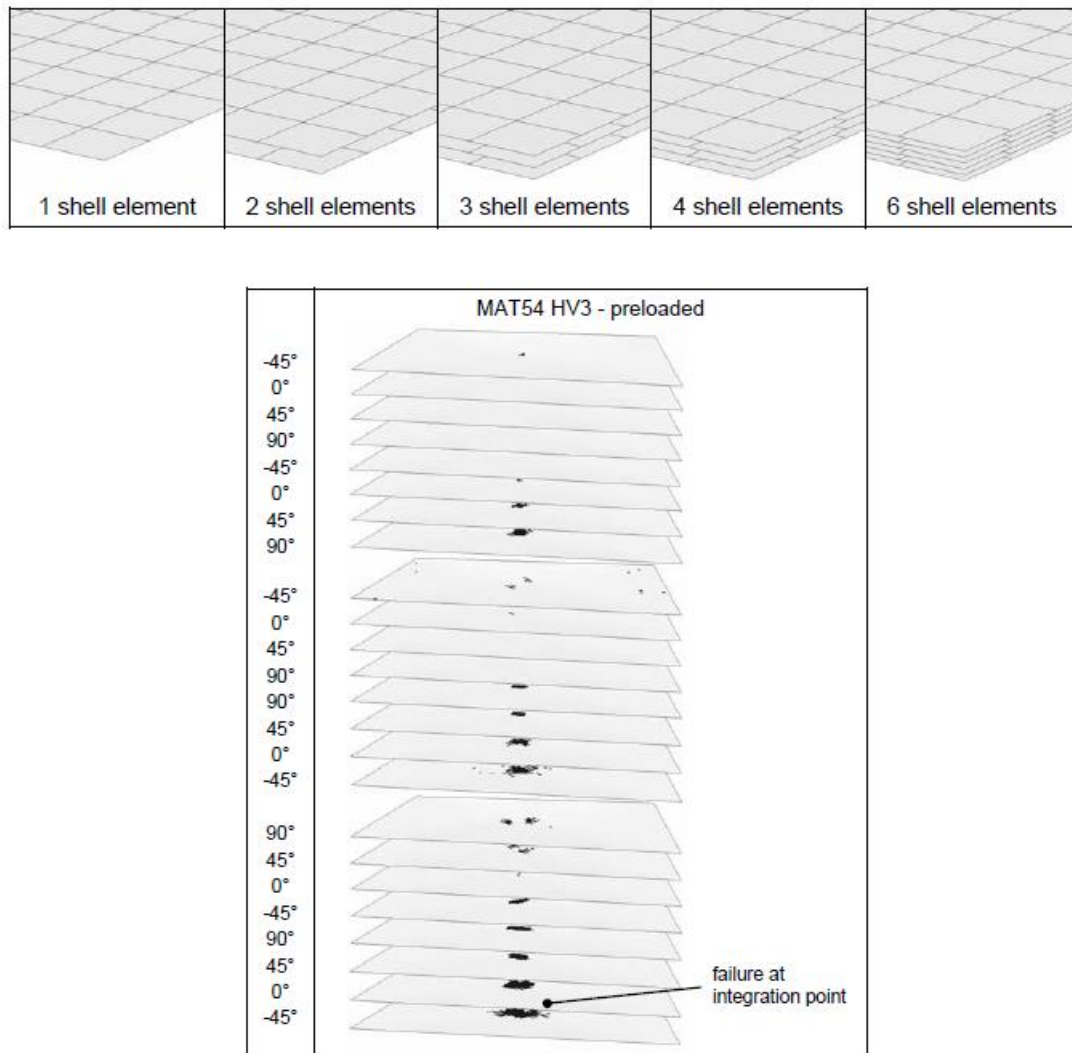
Figure 13. A composite laminate technique used for model delamination (upper) and extent of matrix tensile failure in preload plate (Lower) with two cohesive elements. From: [20]

Much of the research performed on the impact of composite materials has been oriented as well for developing analytical models that allow predicting the behavior of such structures. In the work performed by Kim [22], different failure modes were characterized according to the extent and type of damage, as it can be appreciated in Fig.14. An analytical model based on a global energy balance for predicting damage initiation was then developed while being built and validated by detailed numerical simulations.

The concept of Failure Threshold Energy (FTE) is introduced for characterizing the lowest kinetic energy required by an incoming elastoplastic projectile for causing damage in a composite material. One of the main conclusions of this study is that the damaged area does not always increase with the severity of the attack, and it was observed that inter-laminar failure, that is delamination, was always occurring before fiber rupture.
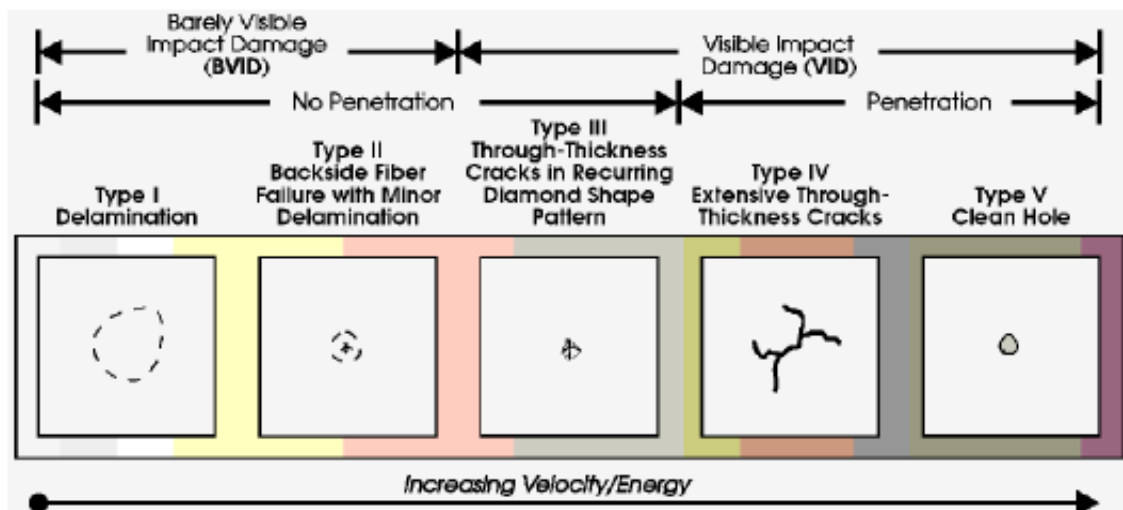
Figure 14. Failure modes observed experimentally for hail impact. From: [22]

On the other hand, in the research carried out by Kim [22], the main objective was to model the problem of structural response of a circular plate when subjected to impulsive loadings by using ordinary differential equations. This allowed obtaining accurate predictions of composites plate deflection whereas identifying the main parameters that govern its behavior when subjected to blast loads, although failure modes were not included.

The author exalts the difficulties related to the analytical modelling of the Fluid-Structure Interaction problem, especially when accounting for cavitation phenomena. However, FSI is included before and after of the first cavitation of the fluid during the blast. Because fully coupled FSI interactions can be only obtained by using numerical methods, the analytical models are compared with FEM simulations in order to validate its accuracy, being found to be

in good agreement. It is then proposed a series of non-dimensional charts in which a quasi-isotropic composite plate can be designed to sustain a defined maximum deflection just by using normalized input parameters such as plate radius, thickness and peak pressure.

3. PHYSICS OF SOFT BODY IMPACTS

When a soft projectile is impacted against a rigid plate, different energies transfer mechanisms are involved in a small fraction of time, in which the kinetic energy of the projectile is transformed on both plate and projectile deformations, as well as in a change in temperature of the collided objects. According to Wilbeck [5], when a projectile reaches the surface of a rigid plate, its frontal face is suddenly brought to rest, forming this way not only a stagnation pressure but a shock wave pressure inside the projectile. The compressive pressure of this shockwave is very high, and it is known as the Hugoniot pressure (See Eq.1).

$$P_{sh} = \rho V_{sh} V_{im} \tag{1}$$

$$P_{stag} = \frac{1}{2} \rho V_{im}{}^2 \tag{2}$$

As can be seen in Eqs .1 and 2, the Hugoniot pressure P_{sh} depends mainly on the impactor density ρ, shockwave velocity V_{sh} and impact velocity V_{im}, whereas the stagnation pressure depends only on the impact velocity and density, not in the object mass. However, it is important to note that the shock wave velocity depends as well on the impact velocity, making the equation nonlinear, which can be solved using the following relationship:

$$P_1 - P_2 = \rho_1 V_{sh} V_{im} \tag{3}$$

$$\frac{\rho_1}{\rho_2} = (1 - z)\left(\frac{P_2}{A} + 1\right)^{-\frac{1}{B}} + z(1 - q) \tag{4}$$

Where:

$$A = \frac{\rho_1 C_0{}^2}{4k - 1} \tag{5}$$

$$B = 4k - 1 \tag{6}$$

$$\frac{\rho_2}{\rho_1} = \frac{1}{1 - q} \tag{7}$$

Where ρ_1, ρ_2 are the densities of the medium before and after the impact, P_1, P_2 the pressures before and after the impact, C_0 the speed of sound in the medium, z the porosity and k an experimental constant. The parameter q depends on the ratio of densities ρ_1 and ρ_2, and it is found using a theoretical relationship shown in wilbeck´s work. [5]

The propagation of the shockwave inside the body is shown in the Fig.15. It can be appreciated that the shockwave not only travels in the longitudinal axis direction of the projectile, but it also causes radial waves which propagate toward the center axis (See C in Fig.15.), being the reason for which the problem cannot be treated in 1-D. When this transversal release converges with the longitudinal wave, the shocked region disappears completely and the stagnation regime will start to take place. The duration depends then on the time that the transversal release takes to go at point B (See Fig.15), which is denoted by Wilbeck as the critical time Cr.
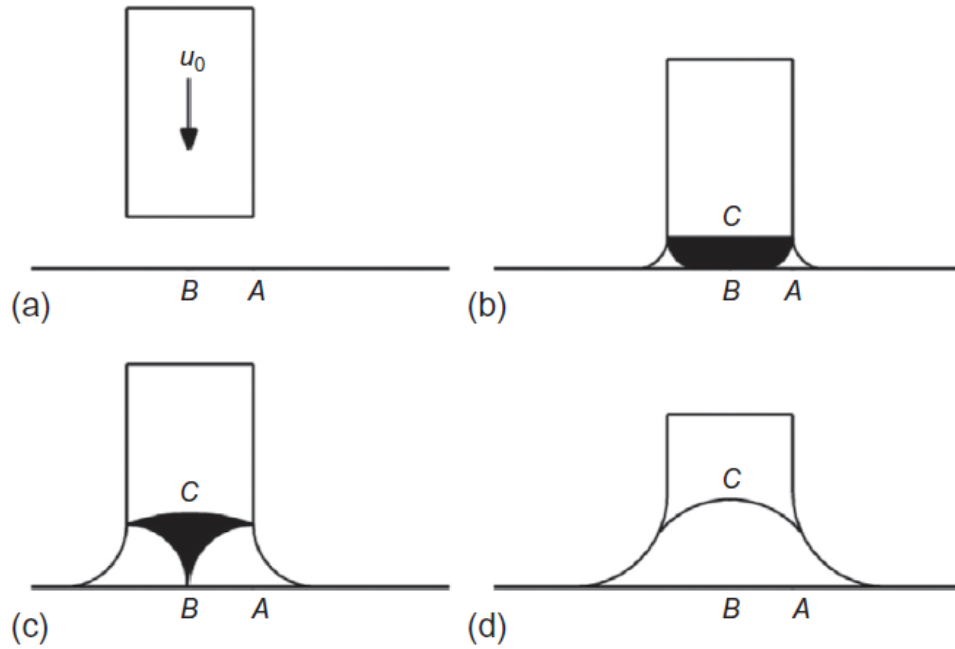
Figure 15. Shock and Release Waves in Fluid Impact. From: [4], [5].

It can be said then that the behavior of this shockwave depends highly on the L/D ratio of the impactor, due to the shockwave evolution process. Wilbeck introduces the critical ratio $(L/D)_c$ to characterize cylindrical impactors for different velocities. Hence, the L/D of the impactor should be always higher than the $(L/D)_c$ for a given velocity. This condition will assure that the radial release wave pressure will be merged with the longitudinal shockwave in some point before any reflection can happen. The critical length for a water cylinder can be seen in the Fig.16, and it is obtained by solving equation 8:

$$\left(\frac{L}{D}\right)_c = \frac{V_{sh}}{2\sqrt{C_r - (V_{sh} - V_{im})^2}} \tag{8}$$

Where C_r is defined as the speed of sound in the shocked region, which is equal to the isentropic pressure density curve slope in the Hugoniot state [5].
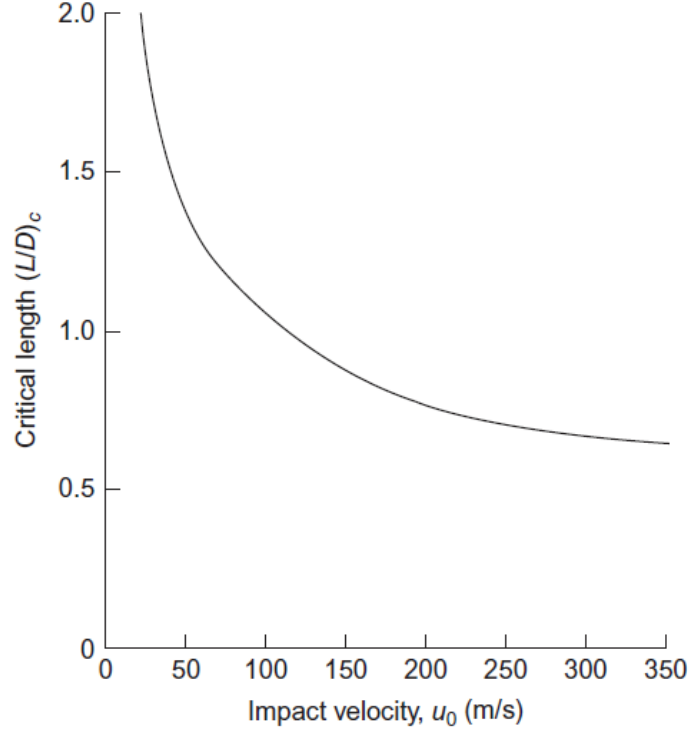
Figure 16. Variation of Critical Length with Impact Velocity for Water. [4], [5]

The time of an impact event depends entirely on the simple relationship of velocity, where L is the cylinder length. Normally, this time is in the order of milliseconds for standard gelatin impacts.

$$\Delta t = \frac{L}{V_{im}} \tag{9}$$

$$I = \int F.dt \tag{10}$$

$$I = P_{stag} \; x \; Element \; Area \; x \; \Delta t \tag{11}$$

The impulse of the impact is a good parameter to check the robustness of the model because the impact impulse can be easily approximated using the impact duration and the stagnation pressure P_{stag}. This way, the force obtained in a numerical simulation for a given element can be integrated to find the impulse and then compared to the theoretical value given in the Eq.11. A usual impulse profile, as well as the impact force along time for a gelatin impact are shown in the Figs.17 and 18.
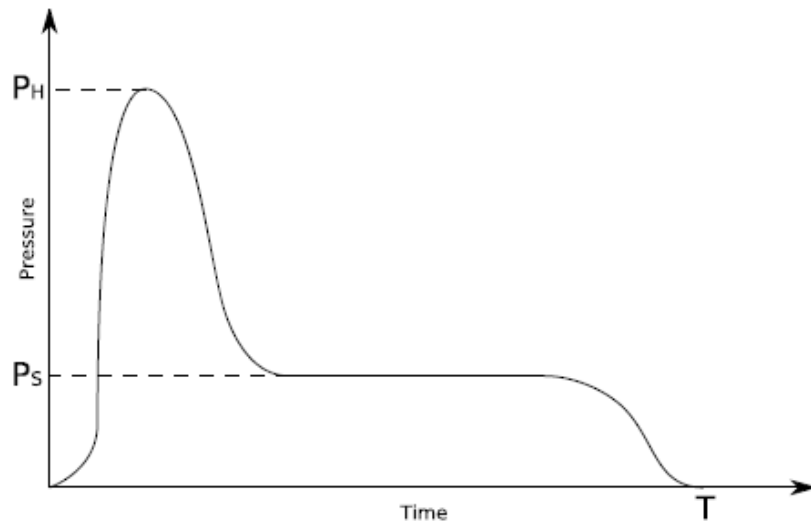
Figure 17. Expected pressure output for a hydrodynamic impactor. From:[23]
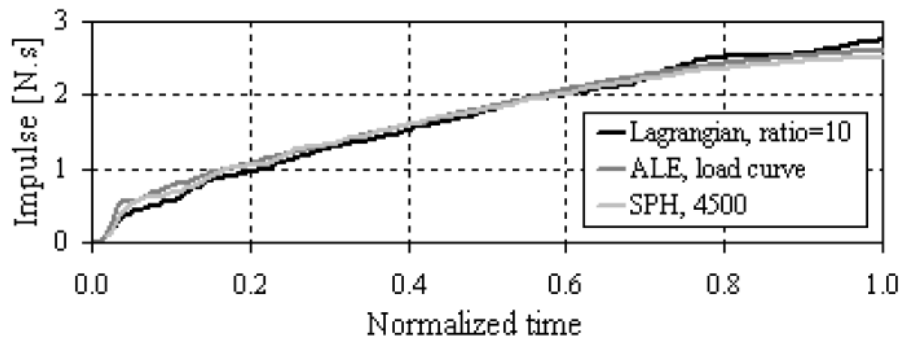
Figure 18. Impulse measured at the center of impact. From: [6]

However, this methodology needs to be modified for flexible targets, which is the case of the most structures found in Naval Engineering. Some modifications to the previous formulations are taken into account in Wilbeck's work, in which the Hugoniot pressure have the characteristic of not being equal in both impactor and target, being the formula for the Hugoniot pressure in the target as it follows:

$$P_H = \rho_P V_{sh(P)} V_{im} \left(\frac{\rho_T V_{sh(T)}}{\rho_P V_{sh(P)} + \rho_T V_{sh(T)}} \right) \tag{12}$$

As a quick reference, Wilbeck found that for some flexible targets impacted at high velocity, the Hugoniot pressure is reduced compared to the case of a rigid plate. It also remarks the influence of the target thickness in the reduction of the Hugoniot pressure [5].

Moreover, the geometry of the impactor highly influences the initial Hugoniot pressure as well as the pressure evolution. In the Fig.19 can be seen the distribution of pressure along a rigid plate at the peak impact pressure for different shapes, all with the same initial Kinetic energy, extracted using a FEM model in the work of Hedayati [4]. As it was expected, the highest pressure was recorded for the straight-ended cylinder, whereas it was highly diminished when using an ellipsoid. This behavior is very important when selecting the impactor shape, which is critical in composite materials because the Hugoniot pressure will initially induce matrix cracking.
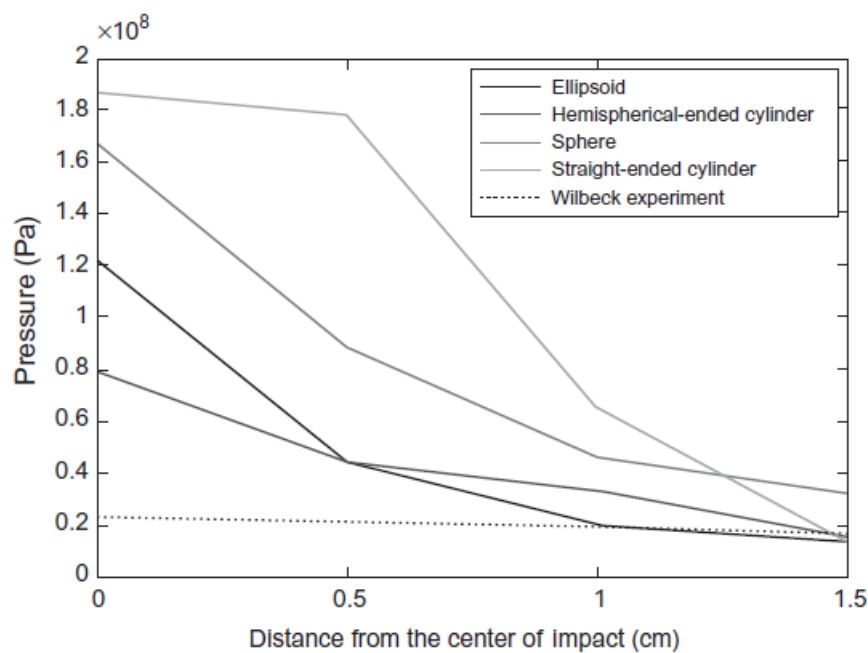
Figure 19. Distribution of peak pressure on the rigid target plate for different geometries. From: [4]

4. NUMERICAL MODELLING OF SOFT BODY IMPACTS

Soft body impact problems require robust numerical models where the mass, energy and momentum conservation laws for both fluid and solid structures are coupled by the means of a reliable Fluid Structure Interaction algorithm. Several numerical methods have been used in the past for modelling such events, being the most used ones the pure Lagrangian, Coupled Eulerian-Lagrangian (CEL), Arbitrary Lagrangian-Eulerian (ALE) and Smooth Particle Hydrodynamics (SPH).

In the past, the pure Lagrangian formulation was the most used due to its simplicity and low computational cost. In the Lagrangian scheme, both impactor and structure are models using Lagrangian elements. Material nodes are attached to the mesh nodes, the last ones following the movement of the material nodes causing big deformations on the mesh, therefore being not very useful in problems where large deformations are present (See Fig.20), as it is the case of soft body impact events.

In order to manage the mesh big deformations, CEL schemes were introduced to model such events, this time using a Eulerian mesh for modelling the impactor and a Lagrangian one for the structure, both coupled by the means of an FSI coupling algorithm either kinematic, contact or penalty based [24]. CEL schemes are able to correctly model the huge deformations suffered by both impactor and structure, although with a much higher cost due to the advection time step in the Eulerian scheme (See section 4.1), and the increase of mesh nodes required to define the entire domain for the impactor during the event.

Arbitrary Lagrangian Eulerian (ALE) methods were later used to model these events due to the advantages over CEL method. ALE could not be used before due to past limitations on the transport algorithms required for the state elements transport [24]. In fact, it can be said that Eulerian formulation is an ALE particular case where the mesh velocity is zero. This resides on the fact that in ALE formulations, three meshes coexist, one of them having an Arbitrary movement which objective is to smooth the deformation of the body elements, while following a pattern given by the user, saving this way computational cost in the sense that fewer elements are needed to define the Eulerian domain. A further explanation of this method is given in the following subsection.

The Smooth Particle Hydrodynamics (SPH) method was also included for modelling soft body impacts due to its numerous advantages in FSI modelling, where large deformations occur. In the SPH scheme, a number of discretized particles (Meshless scheme) with its own mass, velocity, and stress rate, changing according to the fundamental conservation laws, models the impactor domain. The typical partial equations derivations of these laws are changed to an integral formulation by the means of a smoothing kernel function. [25]
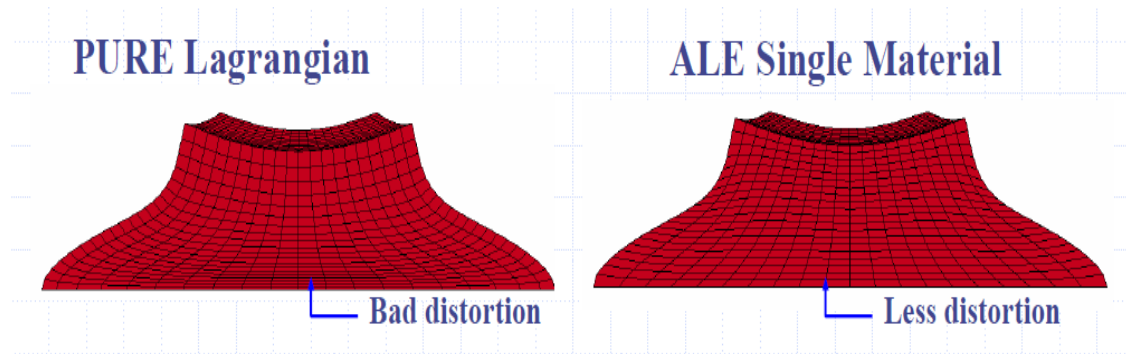
Figure 20. Lagrangian and ALE Schemes. From: [28]

The Lagrangian scheme, although is the fastest, is not able to simulate correctly the soft body deformations patterns. Numerical tuning needs to be performed against experimental tests in order to have accurate results in terms of strain and avoid problems related to the errors due to elements negative volumes and reduction of the time-step, which is critical for explicit formulation schemes [4]. In contrast, it was observed that the most appropriate methods for simulating such impacts are the ALE and SPH schemes in terms of computational cost and accuracy.

These both methods conduct to very similar results and computational cost when simple geometries are used [6], [26]. Even though, it is important to remark the following aspects:

- ALE is less adequate when complex geometries are taken into account, due to the increment of computational cost in the smoothing step of the ALE mesh. [24]

- ALE requires more physical and numerical controlling parameters than SPH, in both the contact definition and the user-defined motion of the mesh, requiring much more expertise from the user, especially for complex geometries. [4]

- SPH method, due to its particle nature, conduces to more "spurious" results than ALE, this being especially relevant when very fast pressure peaks are studied.[7]

- SPH is less expensive computationally than ALE, this being especially noticeable when complex geometries are used.

Considering that the geometries used in this study are simple enough, consisting just of a planar plate and a circular cylinder, either ALE or SPH methods can be used effectively. The selection of using ALE for this work is because ALE is able to capture a better deformation pattern of the impactor and present a more continuous behavior of the Hugoniot pressure, which will be later critical for the structure response, especially when studying damage in composites. Nonetheless, SPH methods can be used in future work in order to optimize the computational cost when models that are more complex are used.

4.1. ALE method

The ALE method is one of the most robust formulations used in Fluid Structure Interaction problems. As it was mentioned before, its formulation consists in the discretization of a domain in three meshes: a Eulerian, Lagrangian and Arbitrary meshes (See Fig.21), the last one being the main difference compared to the CEL formulations. The tasks performed during an ALE time step are given as follows [27]:

1. Perform a Lagrangian time step
2. Perform an advection step
      a. Decide which nodes to move.
      b. Move the boundary nodes.
      c. Move the interior nodes.
      d. Calculate the transport of the element centered variables.
      e. Calculate the momentum transport and update the velocity

As it can be seen in the previous list, the advection step has an important effect in both calculation time and accuracy, being the reason for why adequately smooth algorithms should be able to relax the mesh deformation in an optimal way. According to LS-DYNA manual, this advection step is in the order of 2 to 5 times the cost of the Lagrangian time step, and normally the advection of the element centered variables to the ALE mesh occurs when at least 20% of its volume is being transported, although the user can define this [27] .
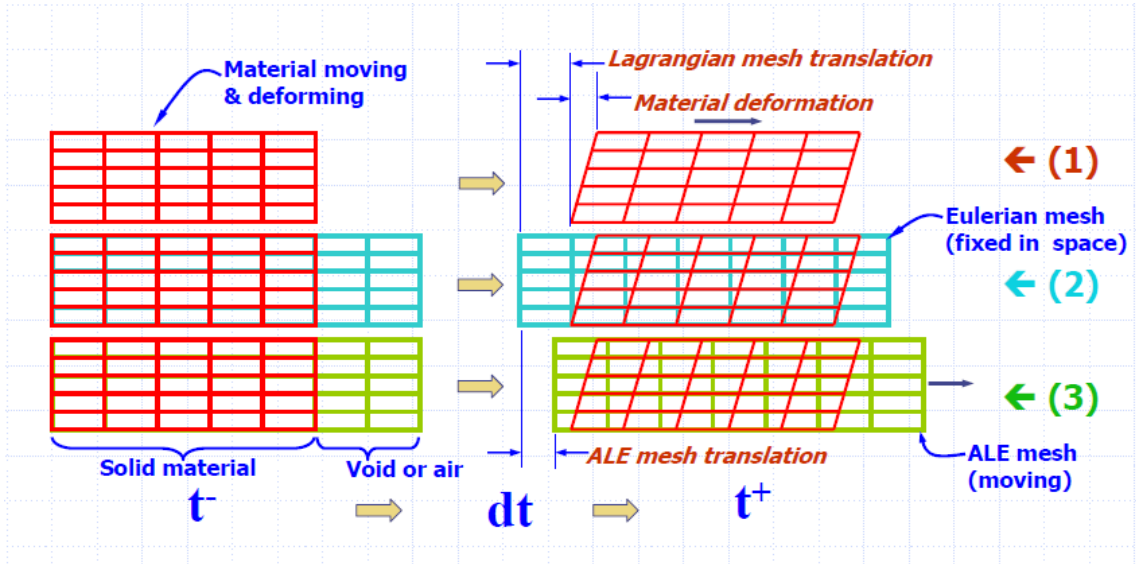
Figure 21. Movement of the meshes during an ALE step. From: [17]

The governing equations in the ALE method are expressed in a PDE formulation as it happens in the Eulerian formulation, but this time the ALE mesh velocity $w = v - u$ is included [24].

i)   Conservation of mass

$$\frac{\partial \rho}{\partial t} = -\rho \frac{\partial v}{\partial x_i} - w_i \frac{\partial \rho}{\partial x_i} \tag{13}$$

ii)   Conservation of momentum

$$\frac{\partial v}{\partial t} = -(\sigma_{ij,j} + \rho b_i) - \rho w_i \frac{\partial v_i}{\partial x_j} \tag{14}$$

With the stress tensor σ_{ij} described as:

$$\sigma_{ij} = -p\delta_{ij} + \mu(v_{i,j} + v_{j,i}) \tag{15}$$

iii)   Conservation of Energy

$$\frac{\partial E}{\partial t} = -(\sigma_{ij}v_{i,j} + \rho b_i v_j) - \rho w_j \frac{\partial E}{\partial x_j} \tag{16}$$

These equations can be solved in two different manners: one in which the fully coupled equations are solved, with the restriction that only a single material can exist in one element. The other way is using a method known as split operator, where the calculation is divided into two phases: first, a Lagrangian step is performed, in which the changes in energy and velocity due to internal and external forces are calculated. Subsequently, the advection phase is performed, where the advection of mass, internal energy, and momentum along the cells boundaries are computed. This last step was the ALE main limitation in the past, and the current limitation from applying it to very complex geometries, because deciding how the mesh nodes should move is not an easy task, and this is the job of the different smoothing algorithm [24].
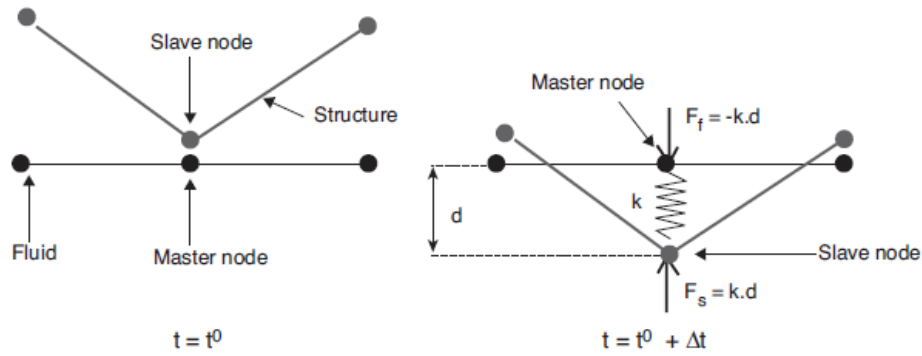
Figure 22. Sketch of contact algorithm. From: [24]

An important key point in FSI problems is the contact algorithm that is used at the interface between the fluid and the structure. The most common coupling algorithms are based on penalty factors, which are the most robust than constraint based coupling [24]. These algorithms, on contrast to the Kinematic contact where the momentum is conserved but not the energy, is based on a resisting force that is applied to slave nodes (which in the case of ALE is the Lagrangian structure).

$$F_s = -k.d \tag{17}$$

$$F_m{}^i = N_i.k.d \tag{18}$$

$$k = P_f.\frac{KA^2}{V} \tag{19}$$
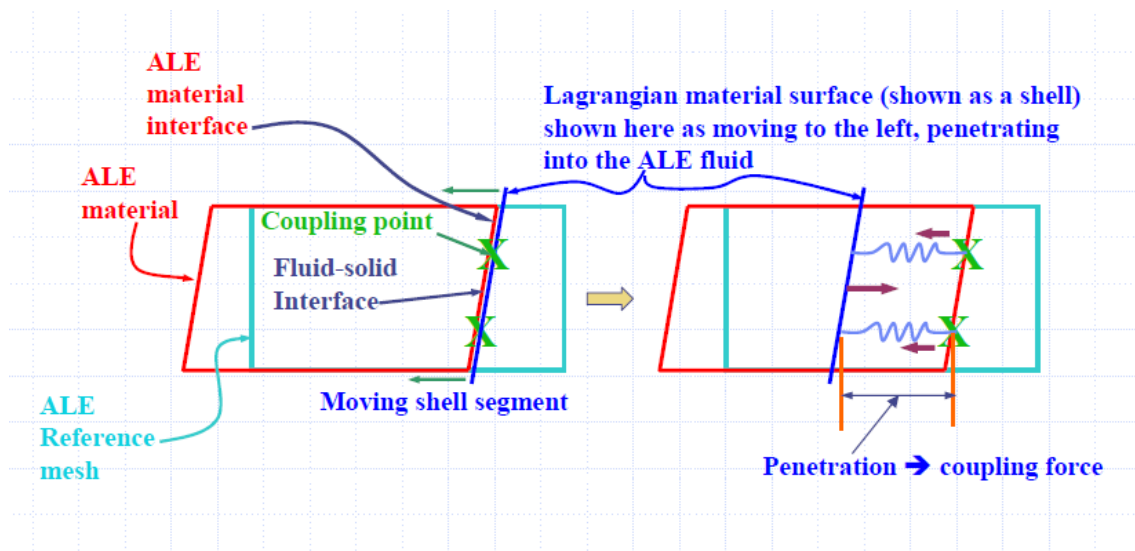
Figure 23. Diagram of ALE step and a penalty based contact algorithm. From:[28]

This force is proportional to the penetration through the master element, acting this way as a spring which stiffness depends mainly on the bulk modulus, the area, and volume of the master element (Eulerian). Then, it is multiplied by a penetration factor, which can be tuned by the user in order to enhance the correspondence with experimental tests (See Eqs.19 and Fig.22). This force is applied in both master and slave nodes in order to satisfy the equilibrium. The way for LS-DYNA to detect such penetrations is to define a number of coupling points for each Lagrangian slave element by the option NQUAD [29], which should be modified depending on the refinement of the Lagrangian mesh. It should be noted that the higher this value, the higher the computational time would be. In Fig. 23, the penalty factor concept is explained in a graphical manner.

5. FAILURE THEORY ON COMPOSITE MATERIALS

The failure behavior in composite materials has been a major research subject after these materials were introduced massively in aeronautical industry in the second half of the 20th century, being complex due to the orthotropic nature in its structural morphology, the variation of material properties through-thickness, presence of micro-defects and micro cracks, interactions occurring at the fiber-matrix interface, among others. The definition of an adequate failure criterion is highly important because that is the basis which designers use in dimensioning structural parts. Ideally, this limit depends mainly on the strength characteristics of a given material, which can be extracted from experimental tests following the procedures such as ASTM, ISO, etc. However, these strengths vary depending on the manufacturing process, fiber arrangement, curing cycle, and so on, which is even more critical considering that the material is usually manufactured during the building of the part.

In FRP, different failure modes can be found, started by one or a combination of the following mechanism [30]:

- Fiber Rupture.
- Fiber Matrix Debonding.
- Matrix Cracking.
- Fiber Buckling
- Delamination
- Fiber Kinking.

Damage on composite laminates is commonly initiated along the microscopic imperfections inside the resin (Micro-cracks or Micro-voids) and fiber-resin interface (Debonding), evolving then during the load cycles or the load evolution (in case of impact loading) into mesoscopic damage as matrix transverse fissures and local delamination. Later, they become macroscopic damages such as longitudinal cracks, delamination and finally fiber rupture (Fig.24). From an overall perspective, damage occurs as a combination of the different damage mechanisms along the individual plies, which interact between them in order to create overall damage inside the material [30]. Damage on composite is generally studied separately in two major groups, which in some failure criteria are joined forming hybrid damage criteria [31]:

- *Intra-laminar damage:* Refers to the damage occurred within a ply, including modes such as Fiber Rupture Buckling and Kinking, Matrix Cracking, Fiber Matrix de-bonding.

- *Inter-laminar damage:* Refers to the damage occurred within plies interfaces, such as delamination failures.

Many different criteria have been developed in the past for estimating the failure of a composite laminate, without a single criterion being adopted worldwide so far. In fact, at the beginning of 21st century, a campaign named World Wide Failure Exercises gave researchers a chance to apply its criteria on a rupture scenario of monolayer and laminates, which later were corroborated against experimental data. However, no criteria were able to give an accurate prediction for all the loading combinations [30], [32].
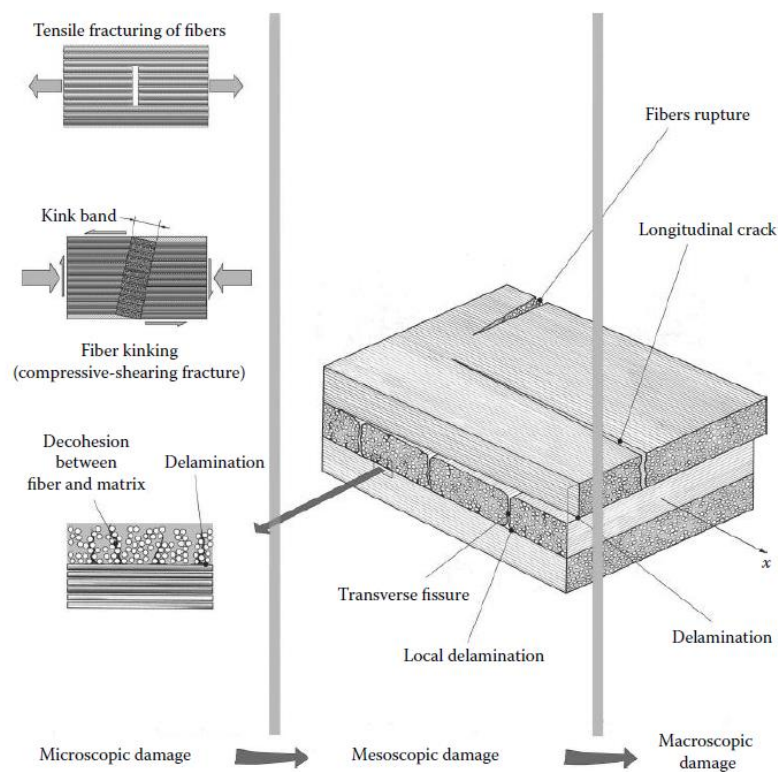
Figure 24. Different levels of damage in a laminate consisting of UD plies. From: [30]**.**

Due to the "laminated" nature of composite stacks, criteria models are built in such a way that exists [33]:

- **Failure Criteria not directly associated with failure modes**: a failure envelope is built for either a ply or a complete laminate for a coordinate system (σ_l, σ_t, τ_{lt}). Different approaches can be used such as linear or quadratic envelopes, which will differ in the end in the structural conservatism for each combination of loads. Tsai-Hill, Tsai-Wu and modified Tsai Wu are the most used criteria in this group.

- **Failure Criteria associated with failure modes**: failure predictions are obtained by progressive failure damage resulting from a combination of different failure modes such as Matrix Cracking, Fiber Rupture, Etc. The extension of damage for each mode can be traced, is the reason why the major part of numerical studies implements this type of criteria for analyzing composite structures. Sudden or continuum damage schemes can be found in this category. Maximum strain or stress, Puck, Hashin, Yamada and Chang-Chang criteria's are the most used in this group.

5.1. Tsai-Hill Criteria

This criterion is widely used in the industrial sector due to its high precision for determining the failure envelope for structural parts subjected to quasi-static loads. Its reliability is because its derivation comes from an energy distortion formulation for orthotropic materials, in the same manner as it is derived Von Mises criteria for metallic materials.

In Tsai-Hill formulation, the following assumptions are made [30]:

- The principal directions for stresses do not coincide with the orthotropic directions.
- Mechanical behavior of the material varies with the direction of the loading.
- When using FRP, the elastic limit is equal to the rupture limit, transforming it from a yield criterion to a rupture criterion.

For the case of Unidirectional Plies (UD), the following is given after derivation of the complete 3D expression:

$$\sigma_z = \tau_{lz} = \tau_{tz} = 0 \tag{20}$$

$$\frac{\sigma_l^{\;2}}{\sigma_l^{\;2}{}_{Rupture}} + \frac{\sigma_t^{\;2}}{\sigma_t^{\;2}{}_{Rupture}} - \frac{\sigma_l\sigma_t}{\sigma_l^{\;2}{}_{Rupture}} + \frac{\tau_{lt}^{\;2}}{\tau_{lt}^{\;2}{}_{Rupture}} < 1 \tag{21}$$

As can be seen in Eqs. 20 and 21, for obtaining the failure criteria in a 2D unidirectional ply, the out of plane stresses due to tensile, compressive and shear components are neglected. Failure occurs if the expression on the left hand side is greater than one. Care must be taken when input the $\sigma_{i_{Rupture}}$, because this value is different for tensile or compressive loads for both matrix and fiber.
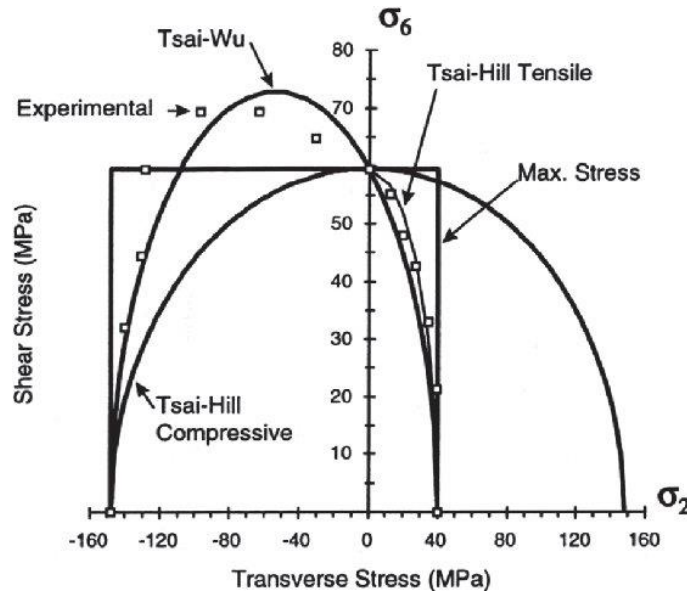
Figure 25. Different failure envelopes in σ_t-τ_{lt} plane compared against experimental tests. From: [34]

As can be appreciated in Fig.25 and 26, good results are obtained for both quadrants in the plane $\sigma_t - \tau_{lt}$ (Not too conservative but not dangerously underestimated either) in contrast of what happens with maximum stress criteria , that even when it is accurate for combination of transverse tensile and in-plane shear , it is dangerously optimistic for compressive and in-plane shear combination. For the case of $\sigma_l - \tau_{lt}$, the results in quadrants I and II are very accurate as well, but dangerously optimistic in quadrant III [30]:
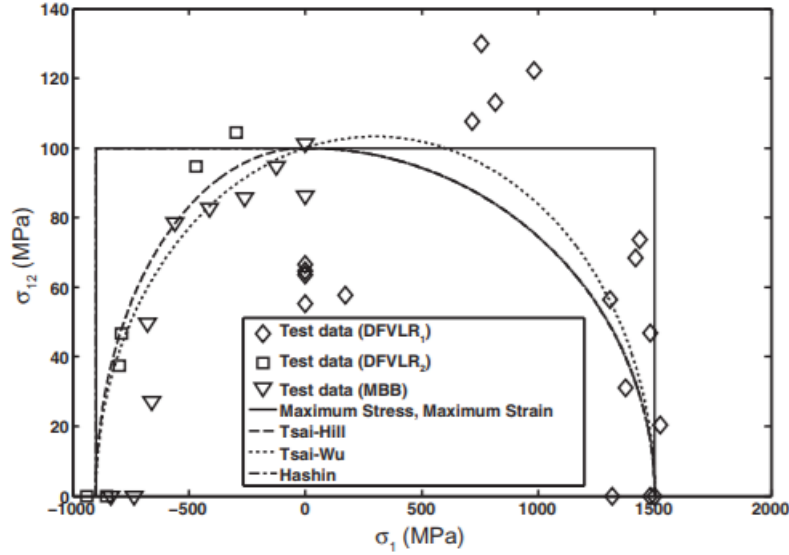
Figure 26. Comparison of failure criteria with test data for UD CFRP lamina. From:[35]

5.2. Chang-Chang Criteria

In contrast to what happens with non-failure modes criteria such as Tsai-Hill, the Chang-Chang criteria [36] separates and evaluates different failure modes occurring on the composite material. This allows tracing how the failure is developed on the composite, being of especially interest in fatigue studies as well as in dynamic crash events such as impacts or collisions. The strains are in a planar stress condition are derived as [37]:

$$\varepsilon_1 = \frac{1}{E_1}(\sigma_{11} - \nu_{12}\sigma_{22}) \tag{22}$$

$$\varepsilon_2 = \frac{1}{E_2}(\sigma_{22} - \nu_{21}\sigma_{11}) \tag{23}$$

$$2\varepsilon_{12} = \frac{1}{G_{12}}\tau_{12} + \alpha\tau_{12}^3 \tag{24}$$

Chang-Chang criteria are similar to the criteria proposed by Hashin [38], differing on the fact that Chang-Chang takes into account the nonlinear shear stress behavior of the ply by adding a parameter α as follows:

$$\bar{\tau} = \frac{\frac{\tau_{12}^2}{2G_{12}} + \frac{3\alpha\tau_{12}^4}{4}}{\frac{S_{12}^2}{2G_{12}} + \frac{3\alpha S_{12}^4}{4}} \tag{25}$$

The Chang-Chang criteria distinguish between the different type of failures in the matrix and fiber through the following conditions [37]:

MODE I: Fiber tension (Rupture)

$$if\ \sigma_{11} > 0\ then\ e_f{}^2 = \left(\frac{\sigma_{11}}{X_t}\right)^2 + \beta(\bar{\tau}) - 1 \begin{cases} \geq 0\ Failed \\ < 0\ Elastic \end{cases} \tag{26}$$

If failed, then $E_1 = E_2 = E_{12} = \nu_{21} = \nu_{12} = 0$

MODE II: Fiber Compression (Fiber buckling and kinking)

$$if\ \sigma_{11} < 0\ then\ e_c{}^2 = \left(\frac{\sigma_{11}}{X_c}\right)^2 - 1 \begin{cases} \geq 0\ Failed \\ < 0\ Elastic \end{cases} \tag{27}$$

If failed, then $E_1 = \nu_{21} = \nu_{12} = 0$

MODE III: Matrix Tension (Matrix Cracking)

$$if\ \sigma_{22} > 0\ then\ e_m{}^2 = \left(\frac{\sigma_{22}}{Y_t}\right)^2 + \bar{\tau} - 1 \begin{cases} \geq 0\ Failed \\ < 0\ Elastic \end{cases} \tag{28}$$

If failed, then $E_2 = \nu_{21} = 0 \ \rightarrow G_{12} = 0$

MODE IV: Matrix Compression (Matrix cracking under transverse compression + shearing)

$$if\ \sigma_{22} < 0\ then\ e_d{}^2 = \left(\frac{\sigma_{22}}{2S_c}\right)^2 + \left[\left(\frac{Y_c}{2S_c}\right)^2 - 1\right]\frac{\sigma_{22}}{Y_c} + \bar{\tau} - 1 \begin{cases} \geq 0\ Failed \\ < 0\ Elastic \end{cases} \tag{29}$$

If failed, then $E_2 = \nu_{21} = \nu_{12} = 0 \ \rightarrow G_{12} = 0$
$$X_c = 2Y_c \ \rightarrow \ \text{for 50\% fiber volume}$$

Furthermore, when using fabrics, tension and compressive modes in the Y direction are formulated in the same manner as the modes I and II in the unidirectional case, this time using Y_t and Y_c for including the strengths of the fabrics in the Y direction, and the matrix failure criterion depends purely on the in-plane shear deformation as follows:

MODE V: Matrix failure criterion for fabrics

$$e_f{}^2 = (\bar{\tau})^2 - 1 \begin{cases} \geq 0 \ Failed \\ < 0 \ Elastic \end{cases} \qquad (30)$$

It is important to remark that the parameter β refers to a weighting factor for the shear term in fiber mode. It can be noticed then than when using $\alpha = 0$ and $\beta = 1$, the original Hashin criteria is obtained. For the cases where $\beta = 0$, the maximum stress criterion is used, which according to LS-DYNA manual [37], corresponds better to experimental values. However, its limitations in each quadrant need to be taken into account by analyzing the combination of stresses in the element (See Fig.26). These values α and β are not easy to define. The first one can be found performing shear-strain measurements, and normally it is within a range of 0- 0.5. On the other hand, the parameter β needs to be manually tuned according to experimental tests, and it is within a range of 0-1 (0.5 is recommended initially by Tabiei [39]).
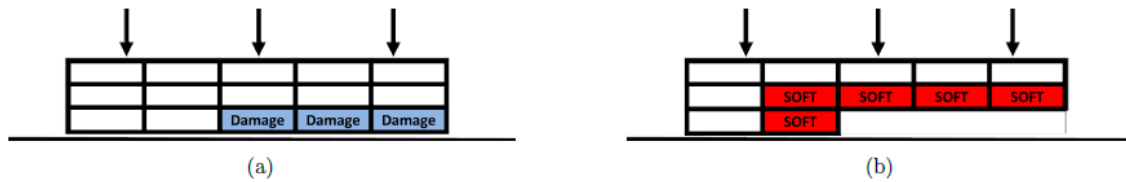
Figure 27. Element degradation due to Crashfront algorithm. From: [40]

According to LS-DYNA Theory manual, this criterion is implemented in such a way that when all the through thickness integration points fails in both fiber and matrix modes in a single element, the element is deleted. After this deletion, the surrounding elements become part of a "crash-front" area, in which their strengths can be reduced by using the set up parameters SOFT, TFAIL and PFL (See Fig.27). This means that each integration point of an element is either damaged or undamaged, being different then from the Continuum Damage Model (CDM), like the one implemented in MAT 58, where a smooth damage transition is performed [37]. This is important to remark because when post-processing the results, the element values for each failure mode between 0-1 are just an indicative of the how many gauss points have failed inside the element. A reduction of strength parameters is performed for "crashfront" elements only if the function is activated. Element deletion can be controlled as well by the means of deletion by Time Step with TFAIL parameter.

FIBER FAILURE MODE   **MATRIX FAILURE MODE**
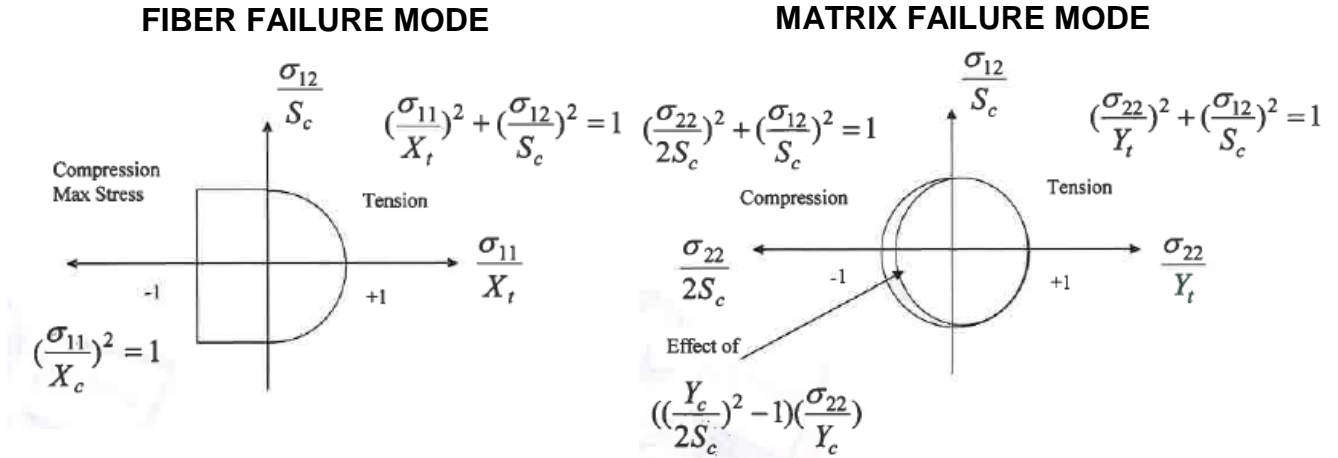
Figure 28. Chang-Chang failure envelopes for different failure modes. From: [39]

A further explanation of Chang-Chang model in LS-DYNA is found on Feraboli et al work [41], where the additional Strain Based Limits criteria for failure is explained after a single element analysis of the model was carried out (See Fig. 29). These strains are defined in order to limit the failure of a ply as an additional restriction to Chang- Chang stress basis, due to the complex deformation pattern of the composite. This work proposes a theoretical way to find such strains based on the Hooke law limit (strain rupture for each direction). Subsequently, the material model is transformed into an elastoplastic behavior as it can be seen on Fig.30.
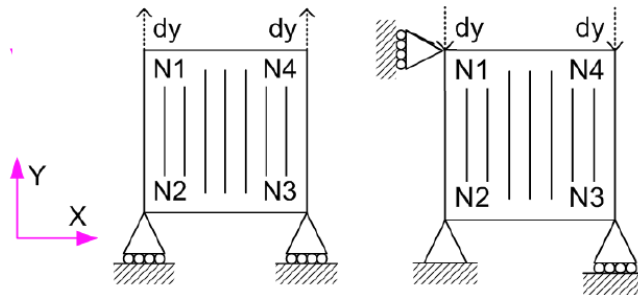
Figure 29. Schematic of a Single element MAT 54 simulations for tension (Left) and compression (Right) From [41]**.**

If DFAIL (in any direction) strain is used, the element stops carrying the further load after Chang Chang criteria are reached, maintaining itself in a constant stress state until the limit strain value of DFAIL is reached, the moment where the integration point fails. Although this is not true for the case of composites where a sudden failure it is presented, several works [14], [41], [42] have addressed an adequate correlation with experimental tests by including these limits. For UD tapes and fabrics on impact events, the failure begins as matrix cracking. According to this model, the element will stop to receive any more load in the transverse

direction (for UD´s) when reaches the transverse strength, but it will keep this maximum load stress until fiber rupture happens (here the importance of limiting the strain), consequently deleting the element. This was corroborated later in the simulations, where huge element deformations were obtained without any deletion due to this "artificial plasticity" of the matrix.
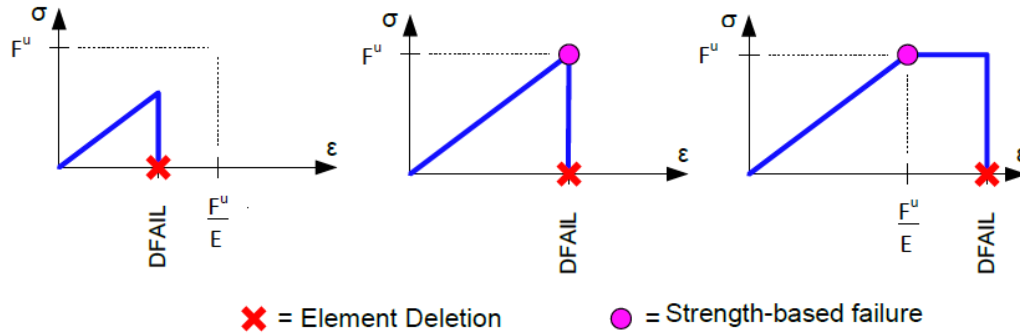
Figure 30. Three basic stress-strain behaviors dependent on MAT 54 failure strains. From: [41]

On the other hand, if DFAIL parameters are not known (as they are extracted from experimental tests), a parameter called Effective Failure Strain (EFS) can be set in order to constraint the strain of the element just by knowing its maximum strains using Hooke laws. Then, the program compares it using the following relationship:

$$EFS = \sqrt{\frac{4}{3}\left(\varepsilon_{11}^2 + \varepsilon_{11}\varepsilon_{22} + \varepsilon_{22}^2 + \varepsilon_{12}^2\right)} \qquad (30)$$

In the Figs. 26 and 31 can be appreciated different failure envelopes for CFRP and GFRP laminas, including Tsai-Hill, Maximum Stress –Strain and Hashin Criteria. As it was discussed previously, it can be seen that although Tsai-Hill criteria are the most accurate and less dangerous, it does not allow studying the different failure modes. The Maximum Stress/Strain criteria is a good approximation for the initial setting of a model, which will need to be tuned after experimental tests in order to enhance the results, avoiding thereby the "optimistic" envelope in the case for both GFRP and CFRP, for which Hashin envelopes seem to fit better in the case of CFRP . For GFRP, the Maximum Stress and Hashin criteria coincide in the same envelope for the $\sigma_1 - \sigma_{12}$ plthe ane, but still the nonlinear terms need to be tuned in order to avoid again an optimistic envelope. Tsai Wu criteria seems to fit better in this load condition.
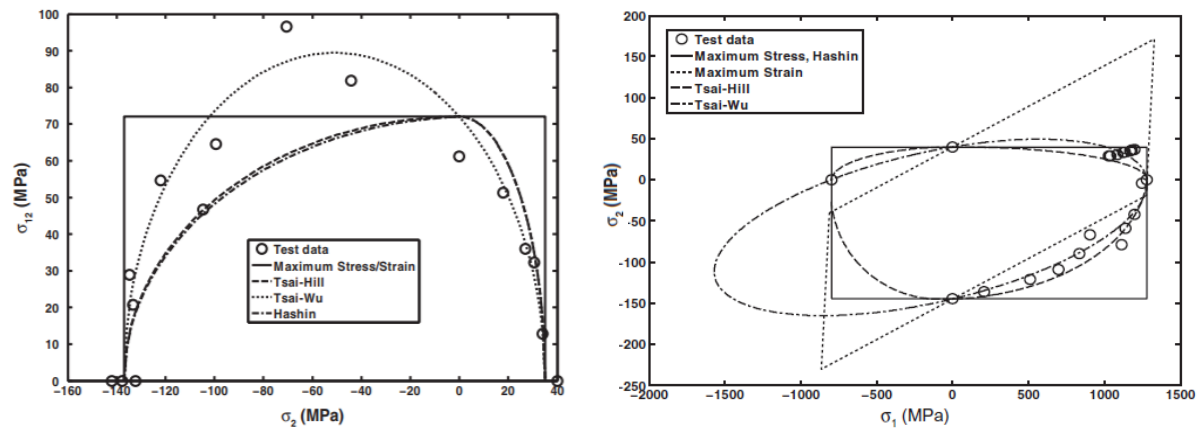
Figure 31. Comparison of failure criteria for E-glass/Epoxy UD lamina for different stress states. From: [35]

6. COMPOSITE MODELLING TECHNIQUES IN LS-DYNA

There are several ways to model composite laminates in LS-DYNA, and their difference relies on the type of elements used, as well as the type of damage which needs to be model. A laminate stack can be model either using (See Fig.32):

- Single Shell approach along through thickness integration points.
- A stack of Shell elements (2D elements).
- A stack of Solid elements (3D elements).

Each approach has its own advantages in computational cost and accuracy (See Fig.32). The fastest one in terms of computational cost is the Single Shell approach. In this model, the elastic behavior and intra-laminar failure modes can be studied, but this model is not able to model inter-laminar damage modes such as delamination. For the other approaches, the inter-laminar failure can be model by using either Cohesive elements or Tie-break contacts (See section 6.3) between plies. These last methods are much more expensive computationally, being especially true for the case of brick elements. Moreover, an exhaustive additional tuning work needs to be performed for these cohesive layers or contacts, complicating, even more, the implementation of these approaches in industrial scenarios, where simplicity and low computational cost are often required. On the other hand, these elements seem to artificially reduce the bending stiffness of the laminates, for which different techniques such as stacking discretization have been performed by different researchers [20].
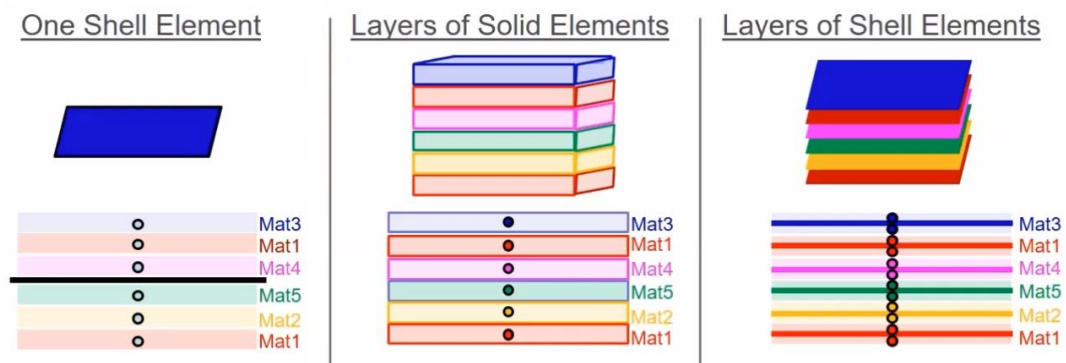
Figure 32. Different techniques used for modelling composite materials. From: [43]

In LS-DYNA library can be found different materials models, which are used to model orthotropic materials, as can be seen in the Fig.33. The difference between these material models relies on the approach used to take into account the type of failures and some additional physical effects, such as hardening by fast strain rates. The use of each material model depends as well on the kind of element used to discretize the laminate, as it can be seen in Fig.32. It was found in the literature that the most used model for simulating Soft Body Impacts is MAT_ENHANCED_COMPOSITE_DAMAGE (MAT 54), which presents a pure intra-laminar failure formulation for shell elements, where both unidirectional and fabrics can be used. The failure model of this material is based on Chang-Chang criteria (See section 5.2), which can be changed to Tsai-Wu (for matrix failure), Hashin or Max Stress/Strain depending on some parameters defined in the material card (See Fig.34).

On the other hand, MAT_LAMINATED_COMPOSITE_FABRIC (MAT 58) is used for modelling laminates composed entirely by fabrics. Again, the failure formulation is pure intra-laminar, with the difference that a Continuum Damage Model (CDM) is introduced, making a "smoother" transition by including an area degradation model caused by the initiation of cracks [37].

	Element	Failure criteria	Comments
*MAT_022: COMPOSITE_DAMAGE	Shell, Tshell, Solid	Chang-Chang	No fibre compression failure Simple brittle model No crash front algorithm
*MAT_054/55: ENHANCED_COMPOSITE_DAMAGE	Shell, Tshell, Solid	54: Chang-Chang 55: fibre:Chang-Chang matrix: Tsai-Wu	Improvement of MAT_022 Crash front algorithm Minimum stress limit factor
*MAT_058: LAMINATED_COMPOSITE FABRIC	Shell, Tshell (1,2)	Modified Hashin. Three different failure criteria: 1. multi-surface, 2. smooth failure surface, 3. faceted failure	Smooth stress-strain relation Non-linear shear behaviour Minimum stress limit factor Exponential softening
*MAT_059: COMPOSITE_FAILURE_MODEL	Shell, Tshell, Solid, SPH	Modified Hashin	Similar to MAT_054 Crash front algorithm Minimum stress limit factor
*MAT_158: RATE_SENSITIVE_COMPOSITE_ FABRIC	Shell, Tshell	Modified Hashin	Same as MAT_058 Rate sensitive
*MAT_261: LAMINATED_FRACTURE_DAIMLER_ PINHO	Shell, Tshell, Solid	Pinho: Considers the state of the art Puck's criterion for inter-fibre failure	Physical based failure criteria Continuum damage model Linear softening evolution based on fracture toughness
*MAT_262: LAMINATED_FRACTURE_DAIMLER_ CAMANHO	Shell, Tshell, Solid	Camanho: Considers the state of the art Puck's criterion for inter-fibre failure	Physical based failure criteria Continuum damage model Bi-linear/linear softening evolution based on fracture toughness

Figure 33.Composite material models available in LS-DYNA and limitations. From: [43]

Material models such as MAT_COMPOSITE_MSC(161) and MAT_COMPOSITE_DMG_MSC (162) were developed by third party companies, aiming to include inter-laminar damage formulations on solid elements while reducing computational times, as well as creating new post-processing history variables which allow the designer to post-process better and faster the obtained results. It should be noted that inter-laminar damage can be modeled using shell or solid formulations along MAT 54 and MAT 58, but the damage is not captured by a specific formulation inside these failure models but rather on the overall behavior of the cohesive element or tiebreak contact included between the plies.

6.1. Mat 54: Enhanced Composite Damage

In the Fig.33 can be observed the card required for MAT 54. The material constitutive parameters are defined for the main orthotropic directions, except the Poisson ratio in the out of plane direction, which is not considered in shell formulations.

Figure 34. Material 54 input card on LS-DYNA. From: [44].

The AOPT refers to the material axis option, where the coordinate systems for the material is defined as vectors, nodes or predefined coordinate systems. The parameter CRIT defines whether Chang-Chang or Tsai Wu criteria for matrix failure mode will be used. The parameters in blue refer to the ply maximum strengths which can be found after experimental tests, and those in red refer to the strain limiting criteria which were discussed previously (See Fig.36). The damage factors for the "crash-front" algorithms are shown in green, where tuning work needs to be performed in order to correlate well against experimental tests.

Moreover, the ALPHA and BETA parameters correspond to the shear weighting factors for Chang-Chang criteria that were discussed in Section 5.2. Some additional cards can be used to take into account the degradation of the material strengths after the maximum stress is reached (Ex. SLIMIT), it can be seen in Fig.36. Again, this parameter needs to be defined after a tedious tuning work when correlating numerical to experimental results. Additionally, the LAMSHT flag was turned on in order to consider the non-uniform shear stress through the thickness, which is very important when modelling laminates with different materials or sandwich structures [37].
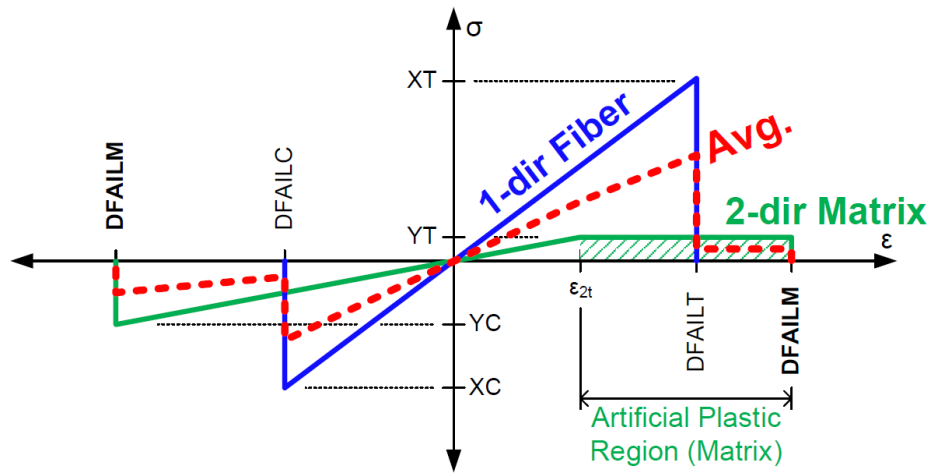
Figure 35. Material 54 average behavior (Including failure strains). From: [44].
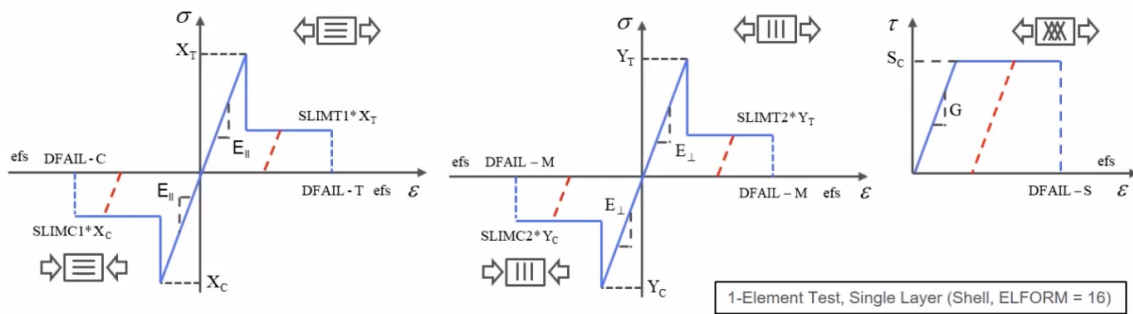
Figure 36. Effects of degradation models SLIMIT on MAT 54. From: [43].

6.2. Composites Coordinates Systems in LS-DYNA

It is important to distinguish between the different coordinate systems in composites analysis in order to select correctly the measure reference for both strains and stresses because several coordinate systems are used inside the program and this can lead to a wrong interpretation of results when they are not fully understood. LS-DYNA has the option to plot the results in each one of these coordinates, which can be changed in the DATA_BASE_EXTENT_BINARY card. The Material Coordinates System (MCS) flag was activated for the simulations performed in this work in order to obtain the results in the material reference frame, making the results easier to understand and post-process. This is especially critical in complex geometries, where the results in the global coordinate system and in the material one highly differ. The program assumes that the angle between the element and material coordinate remains constant during the simulation in order to make the transformation of the Cauchy stress tensor through the transform matrix, which is not true in the case of highly warped elements [39].

Layer 45°
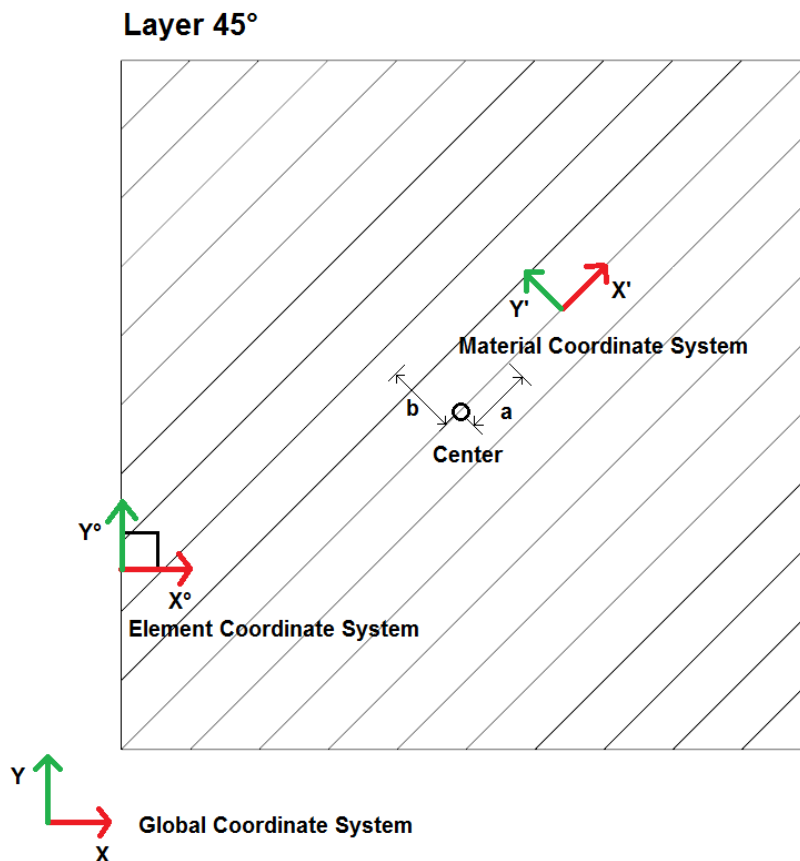
Figure 37. Coordinates systems used in LS-DYNA for composites simulations.

In the Fig.37 can be appreciated the different coordinates systems: Global, Element, and Material respectively. This means that for each integration point, the coordinate system will change according to the fiber orientation (which was defined previously in AOPT option), being always the X direction parallel to the fiber direction for each ply, while Y direction being perpendicular to the fiber. It is important to remark that 3-D plots fringe components and all history variables will be shown in the MCS in this work.

6.3. Inter-laminar failure modelling techniques

Inter-laminar failure is still one of the main challenges in composites modelling. Analytical models along FEM has been used to model such phenomena, being the most preferred the so-called hybrid failure models, where failure criteria are used to predict damage initiation, and then an approach based on fracture mechanics is used for predicting the evolution of damage [31]. Delamination usually occurs between layers with different fiber orientations in highly loaded laminates, especially on impact events where the inter-laminar stresses (out-of-plane normal and shear stresses) exceeds the mechanical strength through-thickness of the laminate.

One of the main reference work in inter-laminar failure formulation was presented by Ladeveze in 1993 [45], which is based on fracture mechanics and includes the effects of inter-laminar fracture toughness in different modes, known as energy release states (G_I, G_{II}). Here, the laminate is modeled in such a way that an interface is created between layers, being this the mechanism of transfer for the stress and displacement within the different plies (see Fig.38).

This approach is used in the work of Johnson [46] for modelling soft body impact on aeronautical structures, where an extensive material testing was compared against the model of Ladeveze using cohesive elements, finding good correlation between this model and experimental tests. The model of Ladeveze was used later to create the mixed mode de-cohesion elements which were implemented in LS-DYNA in the material model MAT_262. [31]
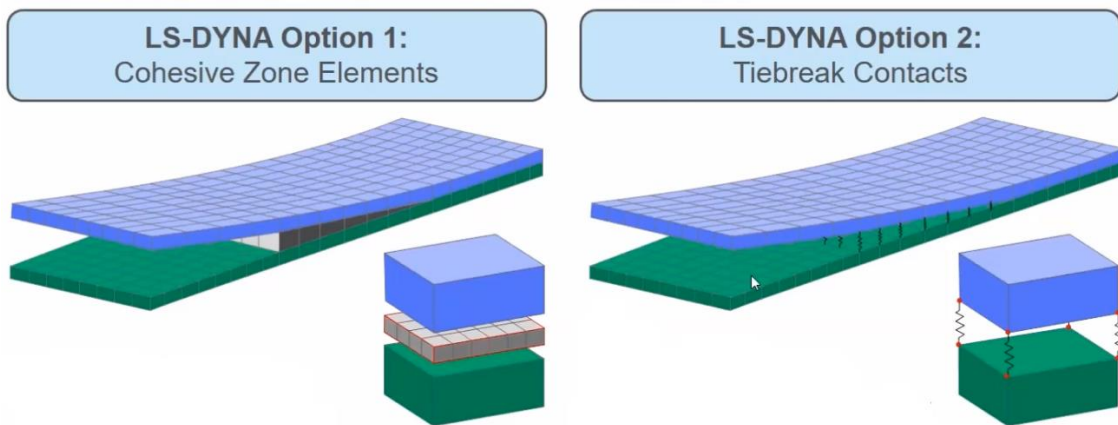
Figure 38. Techniques used for modeling delamination on Composites. From: [43]
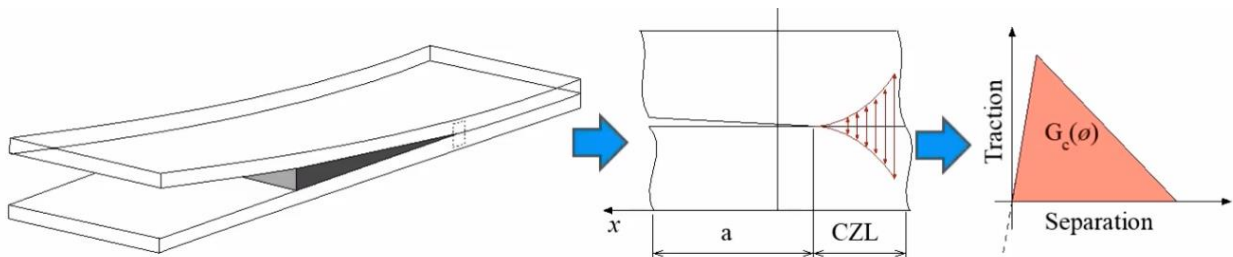
Figure 39. Energy release state used in cohesive element formulation for modelling delamination. From: [43]

As it was mentioned previously, a Single Laminate Approach cannot be used for modelling numerically delamination. Instead, the stack of shells or solids is used where the cohesion is made with either cohesive elements or tiebreak contacts (See Fig.38). In the first approach, a layer defined with a cohesive material model is used between plies, whereas in the second approach the interface between them is modeled using an especial contact between nodes. Although with both methods similar results are obtained [43], cohesive elements are preferred due to the higher resolution of its results and the fact that element post-processed information can be extracted, on the contrast of what happens with tiebreak contact, where only nodal values can be post-processed. Even though, it has to be considered that the use of cohesive elements requires a bigger effort in terms of initial setting and includes an additional mesh that needs to be studied in terms of sensitivity.

Although some methods for inter-laminar damage were studied in the present work, none of them was used because a quick and simple method for studying damage initiation in composites was desired, according to the objectives of project SUCCESS. Inter-laminar failure modeling, although is closer to reality, presents big disadvantages in terms of computational costs, parallel increasing the complexity of the model.

7. SOFT BODY IMPACT NUMERICAL MODEL

7.1. Impactor Model

One of the main challenges in soft body impact simulations is to build an adequate material model for the impactor due to its hydrodynamic nature. In most of the cases, the projectile is defined as a water projectile and its density is calibrated to account for the effects of porosity [47]. In the literature survey, it was found that two kinds of material models accompanied by an Equation of State (EOS) are often used, the last one correlating the pressure with the density:

MATERIAL DEFINITIONS LS-DYNA
- MAT_NULL
- MAT_ELASTIC_PLASTIC_HYDRO

EOS DEFINITIONS LS-DYNA
- EOS_LINEAR_POLYNOMIAL
- EOS_GRUNEISEN

The coefficients used in these EOS are highly important because they will characterize the behavior of the fluid during the impact according to the state variables of the fluid, therefore affecting the pressure distribution along the plate area. The physical properties used in the material models are usually the same than those of water.

The material model used for the present simulation is MAT_ELASTIC_PLASTIC_HYDRO along an EOS_LINEAR_POLYNOMIAL. Such model was chosen because the material allows the projectile to behave as an elastoplastic material when the pressure exerted on it is low, and be governed by a pressure-volume relationship like a fluid governed by the EOS when the pressure increases to very high values. [47]

The parameters used in the present work can be seen in Fig.11 for both material and EOS. These values were implemented successfully in the work of Lavoie [47], as well as in the work performed by Horman in [13]. Although some of these parameters do not correspond exactly to water properties, they have been used widely in the literature after an extensive tuning work by different authors, proving to have good behavior respect to experimental results for capturing an adequate deformation pattern of the impactor, thus having a good agreement in the pressure profile.

```
*MAT_ELASTIC_PLASTIC_HYDRO
$#     mid          ro           g         sigy          eh          pc          fs       charl
         9    950.02.000000E9     20000.0      1000.0      -90000         0.0         0.0
$#    eps1        eps2        eps3        eps4        eps5        eps6        eps7        eps8
         0.0         0.0         0.0         0.0         0.0         0.0         0.0         0.0
$#    eps9       eps10       eps11       eps12       eps13       eps14       eps15       eps16
         0.0         0.0         0.0         0.0         0.0         0.0         0.0         0.0
$#     es1         es2         es3         es4         es5         es6         es7         es8
         0.0         0.0         0.0         0.0         0.0         0.0         0.0         0.0
$#     es9        es10        es11        es12        es13        es14        es15        es16
         0.0         0.0         0.0         0.0         0.0         0.0         0.0         0.0


*EOS_LINEAR_POLYNOMIAL
$#   eosid          c0          c1          c2          c3          c4          c5          c6
      1511         0.0         0.0    0.02.93000E10         0.0         0.0         0.0
$#      e0          v0
         0.0         0.0
```

Figure 40. MAT model and EOS parameters used for the impactor, SI units (Kg-m-s)

The MAT_NULL model along an EOS_GRUNEISEN was used initially in the simulations, based on the parameters given in [11]. However, it was discarded later due to some contraction behavior of the elements inside the body a few decimals of milliseconds after the impact (Fig.42). Even though, the pressure profiles between both models agreed well. The parameters used for these material models can be seen in the Figs. 40 and 41. The physical properties of water were used for defining the material of the impactor, as it was mentioned before.

```
*MAT_NULL_TITLE
Mat for Projectile
$#     mid          ro          pc          mu       terod       cerod          ym          pr
         2       950.0      -90000     8.94e-4         1.1         0.8         0.0         0.0
*EOS_GRUNEISEN_TITLE
EOS for projectile
$#   eosid           c          s1          s2          s3       gamao           a          e0
         2      1480.0        1.92           0           0         0.1         0.0         0.0
$#      v0
         0.0
```

Figure 41. MAT model and EOS Alternative for modeling the impactor properties.
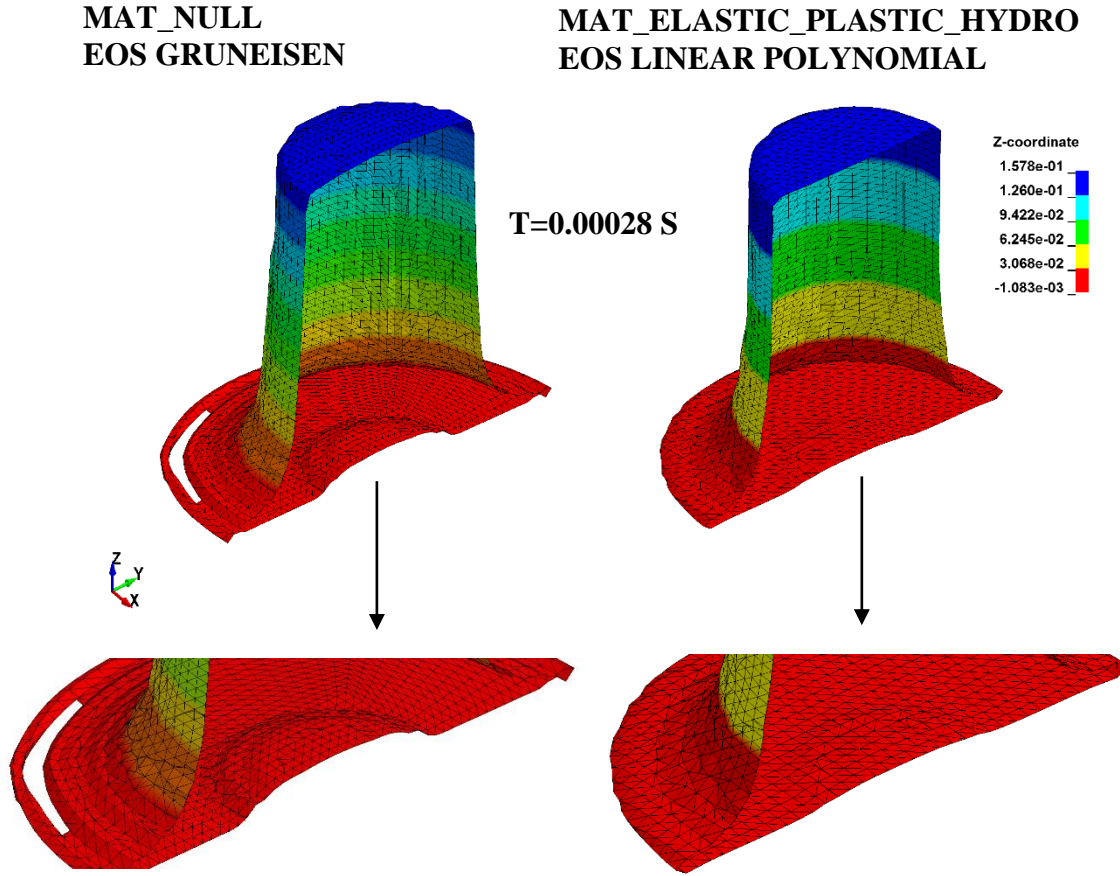
Figure 42. Deformation patterns of soft impactors with different material models. V = 116 m/s

In MAT_ELASTIC_PLASTIC_HYDRO effective yield stress is used as a function of the plastic strain suffered by the impactor, as it can be seen in the Fig.43. This curve can be either defined by a formulation depending on the plastic hardening modulus of the material, or either by defining a set of points, used when the material behavior is known by experimental testing. In the present work, the model was defined using the plastic hardening modulus E_h used in previous works for birds-strike modelling [47] , but which can be found normally using the Eqs.31 and 32. For the yield stress relation, the following formulations are implemented in LS-DYNA:

$$\sigma_y = \sigma_0 + E_h \bar{\varepsilon}^p + (a_1 + p a_2)\max[p, 0] \tag{31}$$

$$E_h = \frac{E_t E}{E - E_t} \tag{32}$$

Where E_t is the tangent modulus, σ_0 the initial yield stress, a_n coefficients related to pressure hardening phenomena (not used in this work) and $\bar{\varepsilon}^p$ the effective plastic strain which is in terms of the plastic deviatoric stress tensor [37].
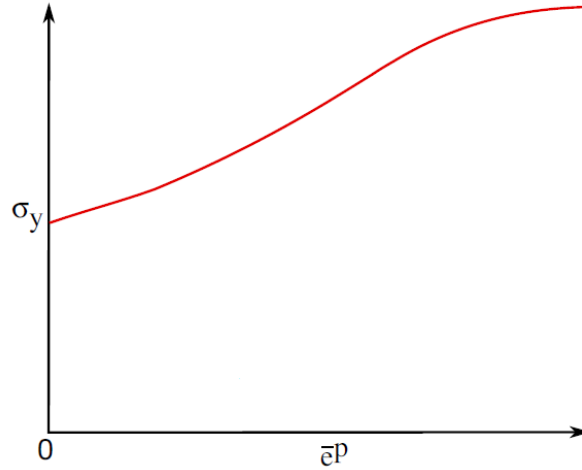
Figure 43. Effective yield stress versus effective plastic strain curve. From: [LS-DYNA manual]

7.2. Rigid Plate Model

The definition of a rigid element in LS-DYNA is performed by invoking the card MAT_RIGID (See Fig.44). This material is used often in numerical modelling to simulate accurately and efficiently some phenomena like tooling (for manufacturing applications) or even in some elements such as connections in order to simplify complex FEM models. When solving a numerical model with rigid materials, the software bypasses rigid elements when making calculations, therefore the files on history variables are not saved, subsequently making the calculation very efficient from the computational point of view. It can be observed as well that young modulus E and Poisson ratio ν are required for defining this material. Realistic values of these properties are suggested by LS-DYNA manual because they are used for determining sliding interface parameters when this kind of element interacts in the contact definition.

This kind of elements are used often in Soft Body Impact simulations in order to calibrate the impactor pressure against the theoretical values or experimental results, which can differ highly depending on the assumptions for the compressibility, porosity, bulk modulus, among other properties of a given projectile (See Section 3).

```
*MAT_RIGID
Mat for plate
$#     mid        ro         e        pr         n    couple         m     alias
         3  7800.02.00000E11      0.29       0.0       0.0       0.0
$#     cmo      con1      con2
         1         7         7
$#lco or a1       a2        a3        v1        v2        v3
       0.0       0.0       0.0       0.0       0.0       0.0
```

Figure 44. Card in LS-DYNA for defining a rigid material.

7.3. Elastoplastic Plate Model

Defining an adequate elastoplastic model is a hard task due to the highly non-linear behavior that occurs in the material when it exceeds the yield point, this being especially true when the strain rates are high, which is the case of soft body impacts. In numerical modeling, it is a usual practice to define such materials in terms of the real true stress-strain curve, discretized as a set of points and then entered into the software. However, this curve is not always known, is the reason why some simpler cost-effective models are used to take into account plasticity. Plasticity is a wide and complex subject, which requires a big mathematical and physical effort for both explain it and develop it. As it is not the objective of this master thesis, only a brief explanation of the plasticity model used will be performed in this section.

Through this work, some numerical simulations were performed for impacts on metals such as steel and aluminum in order to validate the model in a simpler way before implementing composite materials. Laminates validation against experimental results is hard not only due to the complex damage modes but also due to the limitations in the use of instruments to measure internal damage such as X-RAYS or C-SCANS.
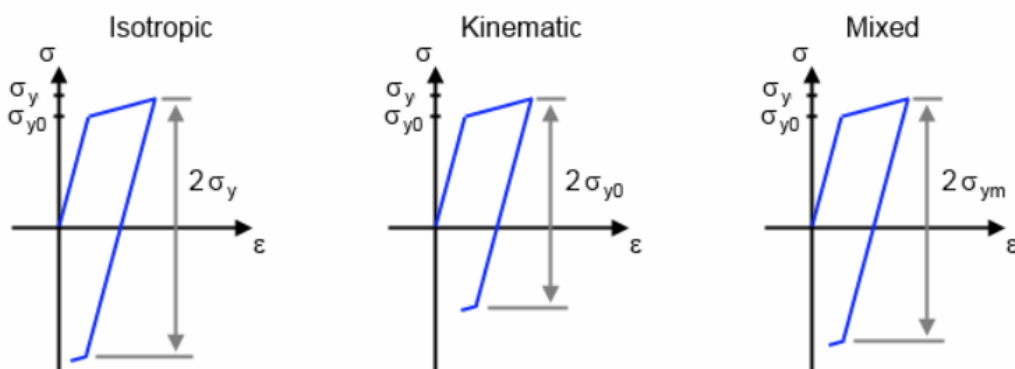
Figure 45. Stress-strain relation for uniaxial loading in three different cases for metal hardening. From: [50]

The material used in this work to represent an elastoplastic behavior was MAT_PLASTIC_KINEMATIC. In this material, a characteristic tangent modulus E_t is used for modelling the plastic zone as an averaged linear behavior (See Fig.46), representing then the stress strain curve by a bilinear model. Additionally, strain rate effects can be included as additional cards in this model, whereas the material hardening can be treated in a kinematic (See Fig.45), isotropic or averaged behavior by defining a factor β (do not confuse with shear weight factor defined in Section 5.2). The selection of the hardening model is especially important in fatigue analysis, due to degrading effects of hardening in tension and compression during the load cycles. Since this is not the case for Soft Body impacts, this parameter will not influence the plate response.

On the other hand, the tangent modulus E_t will govern the material behavior when the yield stress has been reached. The strain is calculated in a very similar way as it is performed for the impactor model, with the difference that this time the deviatory stiffness will be higher as it is a solid element [37].
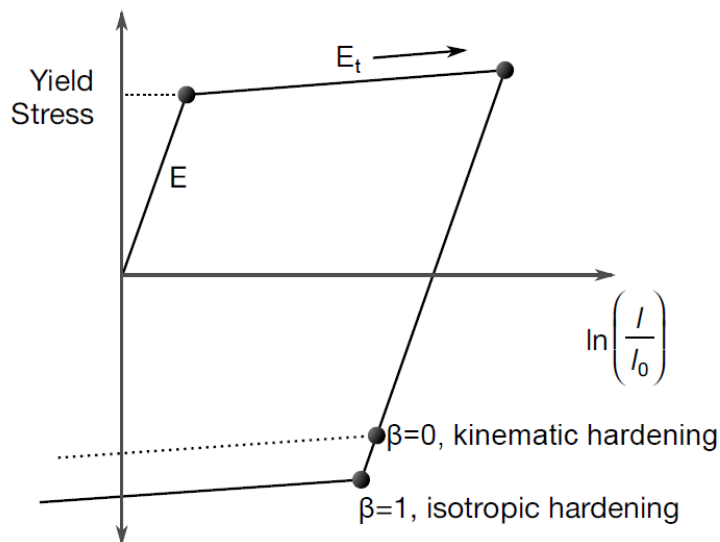
Figure 46. Elastoplastic behavior for either Kinematic or Isotropic hardening for uniaxial tension specimen. From: [37]

The tangent modulus varies in a nonlinear way after the yield stress is reached. This modulus can be taken into account analytically in terms of the Ramber-Osgood equation (See Eq.31), where some additional constants are added for including the non-linear behavior depending on the material. A bilinear transformation of the true stress-strain graph can be implemented as well by using as Tangent modulus E_t the so-called strain hardening modulus, which considers the behavior between the yield and ultimate strength points of the material as linear (Fig.47). It is usual as well to find the values of E_t in the design codes in terms of percentages of the Young Modulus E, usually being between 0 and 10% of the young modulus [48].
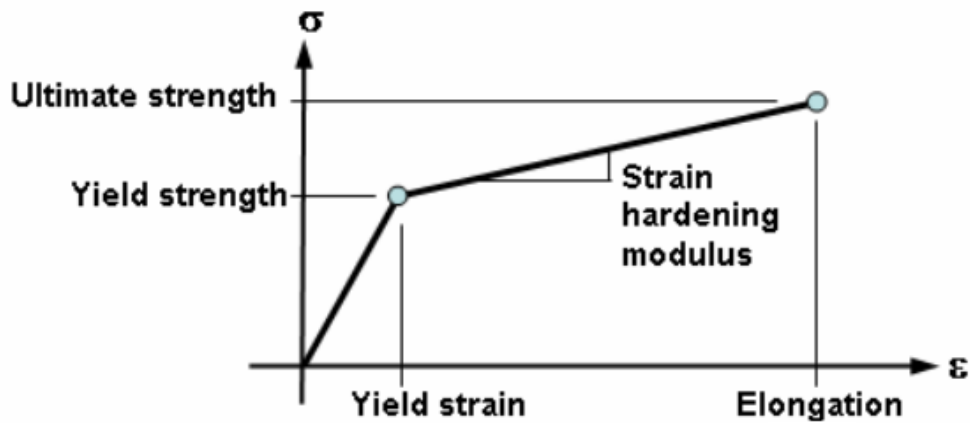
Figure 47. Bilinear stress-strain relation of an elastoplastic material model
From: [48]

8. NUMERICAL MODEL VALIDATION

8.1. Case 1- Rigid Plate Impact: Lavoie´s Model

As a first approximation, the impact of a rounded gel projectile against a rigid plate was simulated in order to set some parameters and validate the material model used to describe the impactor. The work performed by Lavoie was used as a reference to compare the obtained results, due to its good agreement with experimental tests [7].
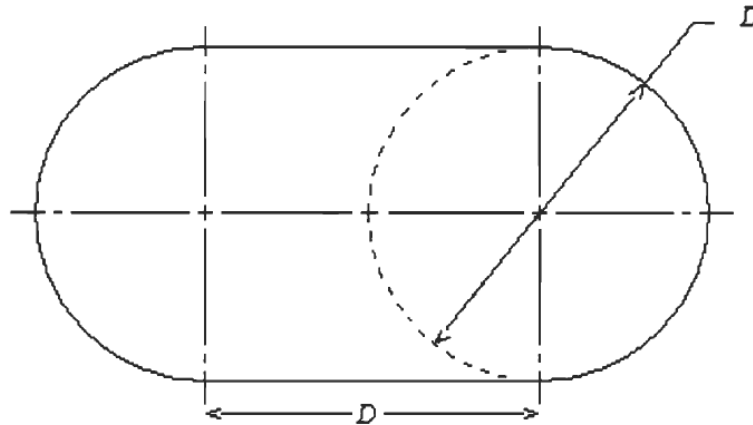
Figure 48. Geometrical parameters of Gel Impactor. From: [7]

The plate was defined as a rigid plate by assigning it MAT_RIGID properties along a Belytschko-Tsay shell formulation. Several pressure gauges were placed on the center of the plate to record the pressure history of the impact, being later averaged in order to obtain results with no mesh dependency. Different ALE mesh sizes were built in order to study the mesh size sensitivity. The projectile was defined inside the ALE mesh by using a volume fraction delimited by a shell, which had the dimensions of the impactor used by Lavoie (See Fig.48).

The initial velocity of the projectile was 116 m/s (with a mass of 1 Kg), although different velocities were simulated in order to check the coherence of the model. During the setting of these simulations, the parameters that influence most the stability and results of the simulations were identified. These parameters are mainly related to the contact defined in the CONSTRAINED_LAGRANGE_IN_SOLID card, which is the contact card definition used in ALE impact simulations. These are:

CONSTRAINED_LAGRANGE_IN_SOLID
- NQUAD
- MCOUP
- PFAC
- FRICMIN
- DAMP
- PLEAK
- TSSFAC

CONTROL_ALE
- All the parameters in this card. It controls advection cycles and conditional operations.

CONTROL_BULK_VISCOCITY
- All the parameters in this card

MAT_ELASTIC_PLASTIC_HYDRO
- Density

EOS_LINEAR_POLYNOMIAL
- All the parameters in this card (for the correct modeling of the shockwave and Hugoniot pressure)

ALE MESH SIZE
- Affects mainly the simulation time and the Hugoniot pressure magnitude.

PROJECTILE SURFACE MESH SIZE
- Affects mainly the simulation time and the Hugoniot pressure magnitude.
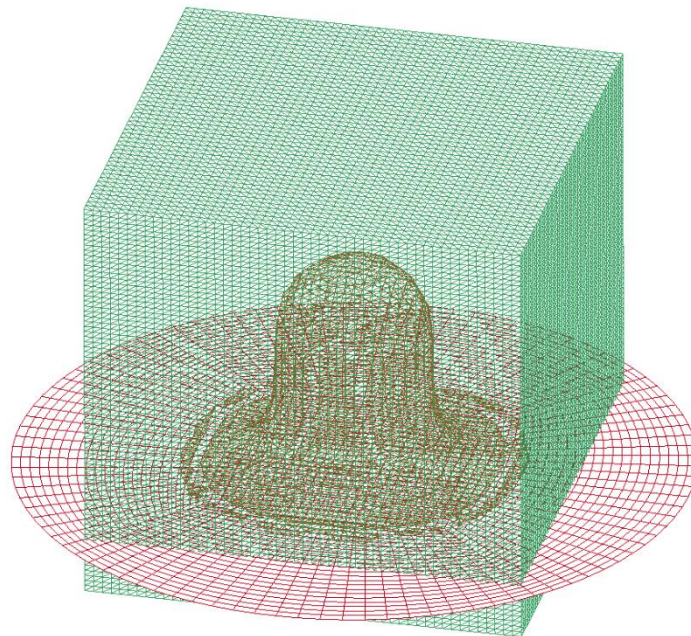
Figure 49. ALE mesh diagram of the impactor and rigid plate.

The numerical properties of the model can be appreciated in Tab.1. It has to be remarked that different boundary shells to initiate the volume fraction of the impactor in the ALE mesh were tested in order to reduce the computational time of the simulation, which was increasing exponentially when the geometry was discretized in more elements. When dealing with volume fraction, care must be taken for the definition of the boundary mesh: it must be fine enough to model correctly the curvature of the impactor face, but coarse enough to not increase too much the simulation time. LS-DYNA presents some default geometries for this initialization that enhance automatically this operation, but it is limited to simple geometries such as a straight cylinder, square shapes or spheres.

The deformation patterns of both projectile and ALE mesh for 116 m/s impact can be seen in the Fig.50. It can be appreciated also in this figure the motion of the ALE mesh along the impact, which captures the deformation of the projectile by using an automatic mesh motion, defined by the mass weighted average velocity in the ALE mesh, implemented in LS-DYNA using the ALE_REFERENCE_SYSTEM_GROUP card. It has to be noted that the definition of this movement is made in order to reduce computational cost compared to a Eulerian case, being the reason why the mesh must have as fewer elements as possible while not deforming too much during the impact event. This could induce later negative volume errors or time step reductions, which can collapse the entire simulation.
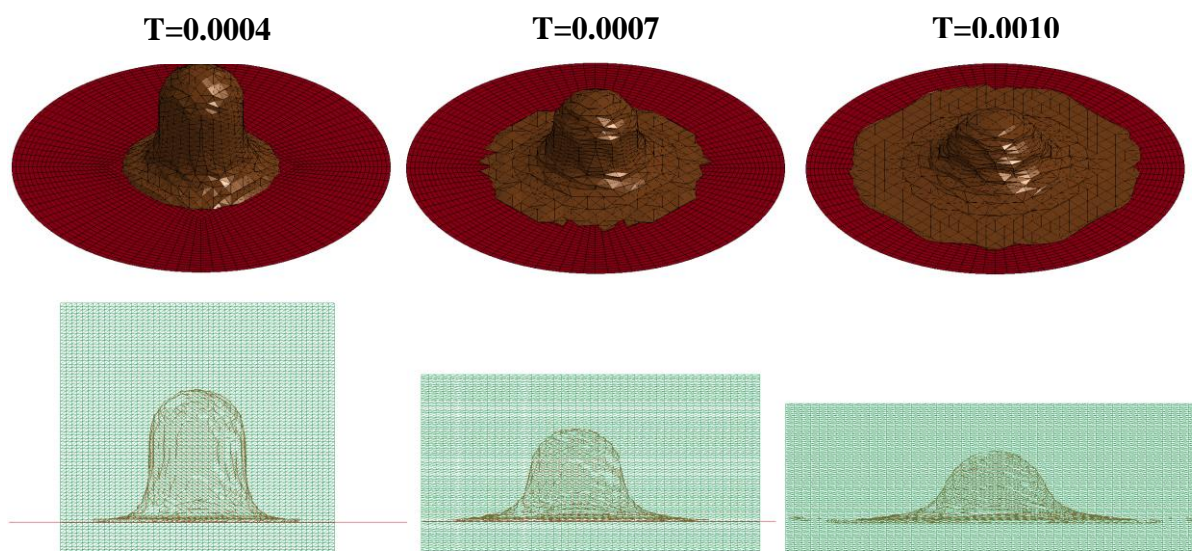
Figure 50. Deformation pattern of the impactor (Upper) and ALE mesh (Lower) at different times (S).

Table 1. Numerical model parameters: Impact against rigid plate.

PLATE DIMENSIONS		
Diameter	Φ=400	[mm]
		[mm]
Thickness	1.625	[mm]
IMPACTOR DIMENSIONS		
Diameter	93	[mm]
Length	186	[mm]
Density	950	[Kg/m³]
Mass	1	[Kg]
Impact Face	Rounded	[N/A]
MESH PARAMETERS		
Type of Mesh	Dimensions[mm]	# Elements	Element Size
ALE Mesh	200x200x300	Variable	4-8 mm
Boundary Shell	= to Impactor	181	Variable
Plate Shell	Φ=400	2784	Variable
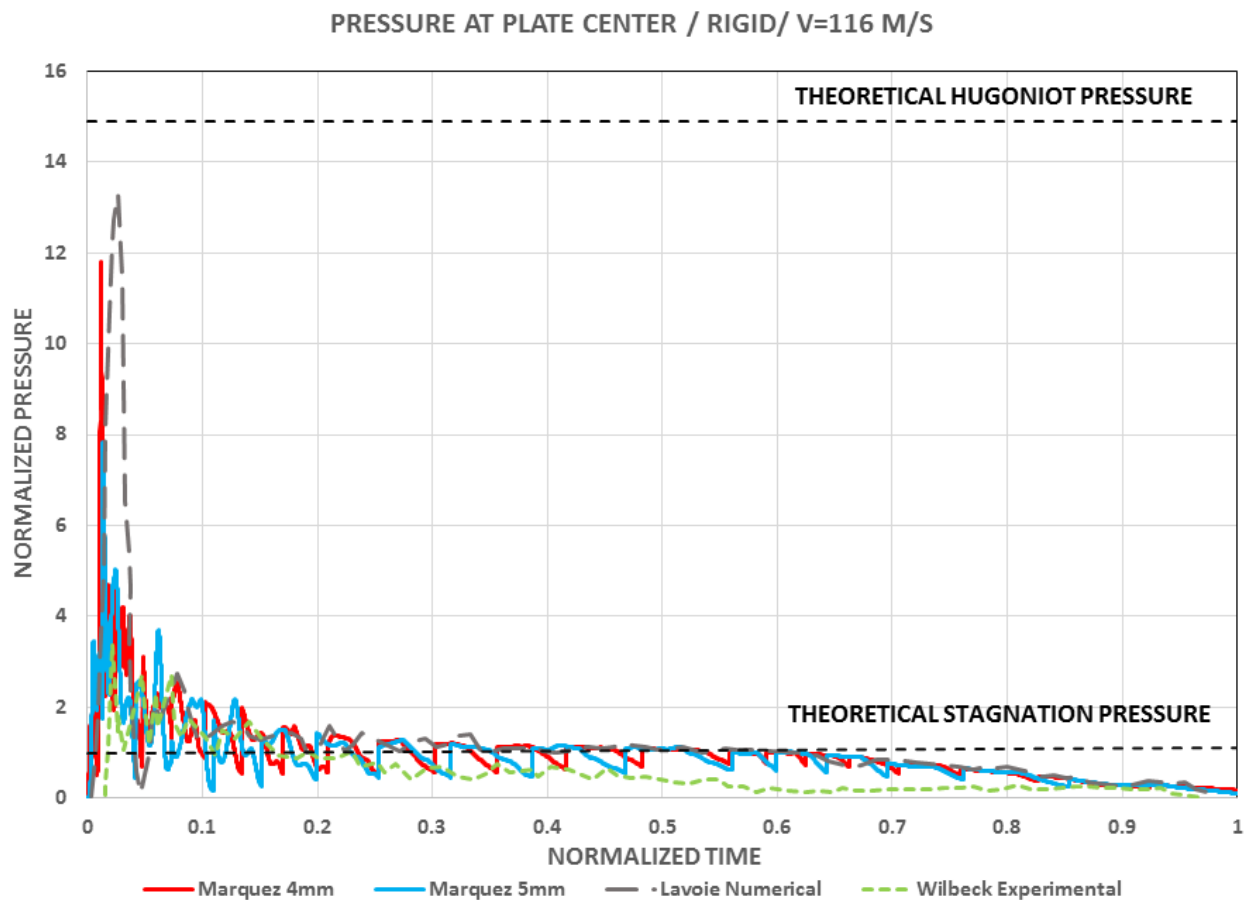
Figure 51. Pressure profiles recorded at the center of the Rigid Plate.

In Fig.51 is shown the Normalized pressure obtained for the ALE impactor case, compared with the results of Lavoie [7] and the experimental formulation of Wilbeck [5]. The overall behavior of the pressure was similar to the theoretical one, having a sudden rise in pressure at the beginning of the impact due to the shockwave generation, after which the pressure decreases up to a steady regime (See Section 3) while the remaining mass is completely crashed. It can be appreciated that the rigid target model developed in this work is in good agreement with Lavoie´s work, presenting a difference only of 8% on the Hugoniot Pressure. In contrast, the theoretical Hugoniot pressure is about 20% higher, while the Stagnation pressure difference is less than 0.1% when compared with Lavoie. However, this difference in pressure resides on the fact that meshes are highly sensitive to CONTACT parameters, which must be calibrated for each mesh, as well to the pressure differences between elements, which varies for round projectile impacts due to the projectile curvature model. Compared to Wilbeck´s experiments, the initial peak pressure does not agree in magnitude, which is explained by the fact that in his work, there were several issues related to the pressure gauges.

It was observed during the simulations that the Hugoniot Pressure increased when the mesh size was decreased, having especially good results with a 4 mm ALE mesh, being more accurate compared to Lavoie's results and the theoretical impulse calculation shown in the Fig.51.
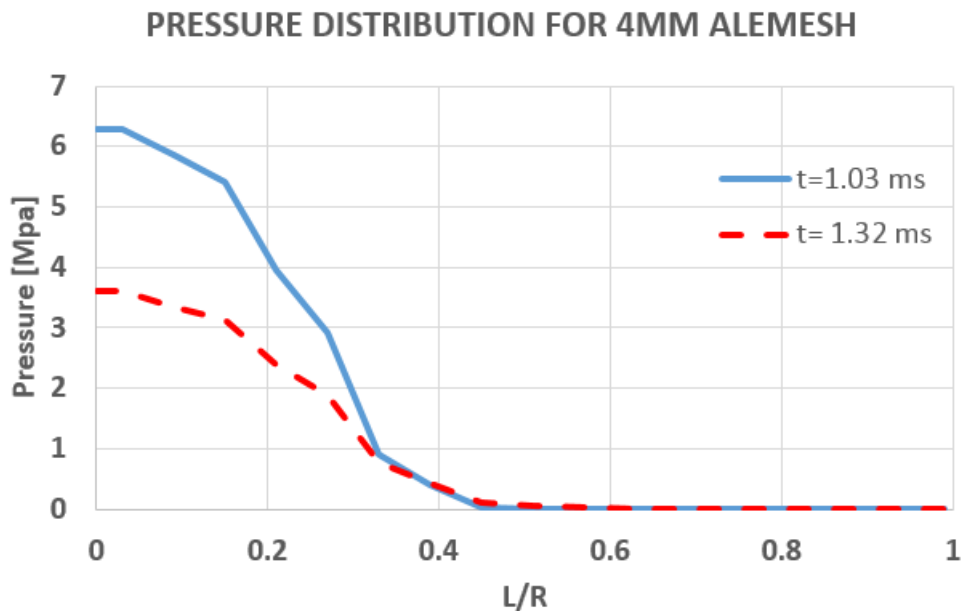
Figure 52. Pressure distribution along the plate radius for a 116 m/s impact.

The pressure distribution shape for different moments during the impact after the Hugoniot pressure phase is shown in the Fig.52. These shapes correlate to the Bell shape profiles analytically described by Wilbeck [5], and its magnitude correlates with the ones obtained by Lavoie for the 100 m/s case [7]. It is interesting to note that for this case, the pressure is reduced to zero at the same location in the plate for different instants, defining this way a pressure zone in the structure, which will be very important when studying the initiation of damage when composite structures are used.

This behavior can be appreciated again in Fig.53, where different meshes under the same initial and contact conditions were tested. The overall tendency is similar: they all reach the same P_{stag}, but presents high variations in the Hugoniot pressure. The finer the mesh, the higher the Hugoniot pressure, therefore increasing the impulse. The transition between the Hugoniot pressure peak and stagnation pressure becomes noisier when the mesh becomes coarser.
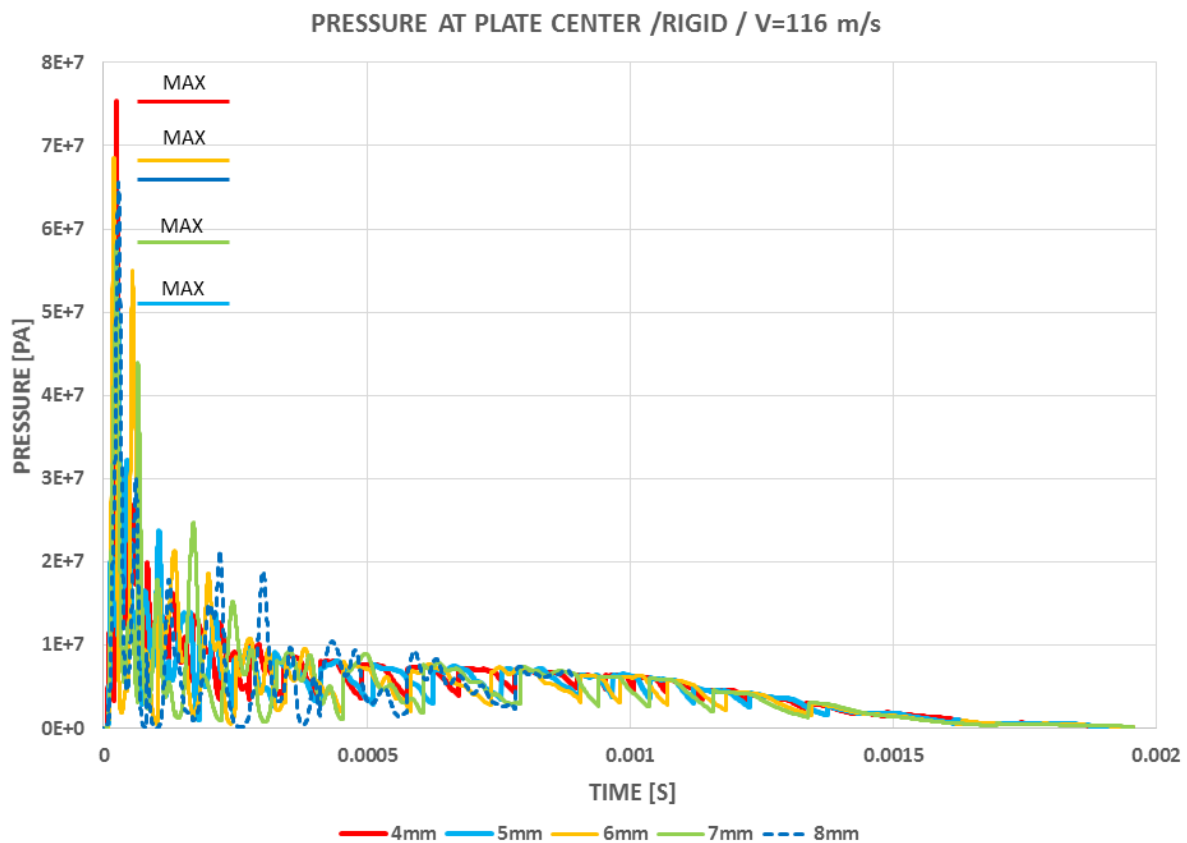
Figure 53. Pressure profiles at the center of the plate for different ALE Mesh Sizes.
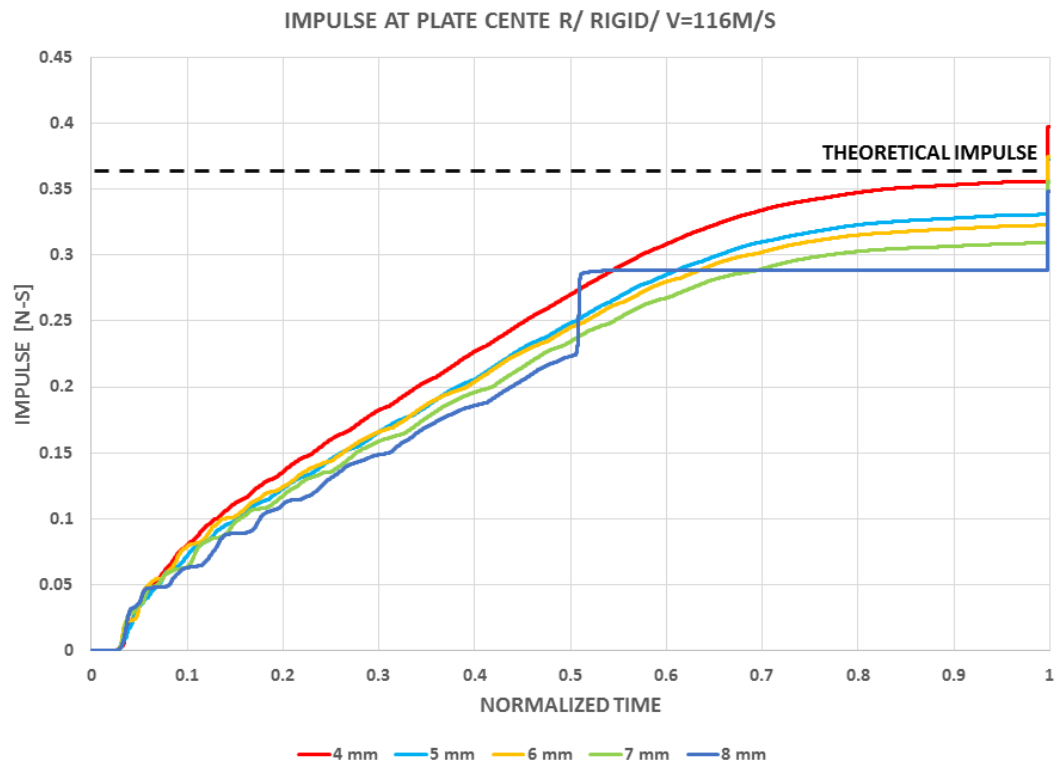
Figure 54. Impulse profiles at the center of the plate for different ALE Mesh Sizes.

It can be concluded then that a 4 mm ALE Mesh is enough to model soft projectiles with similar dimensions, although finer meshes can be used sacrificing some additional computational resources. It must be noted that when using 8 mm mesh, some numerical instabilities are observed in the center elements of the plate at t=0.5 (See Fig.54), but this seems not to affect the pressure received by the plate, subsequently its response. Care must be taken when defining the CONTACT parameters, which for ALE cases are found in the CONSTRAINT_LAGRANGIAN_IN_SOLID card, especially the number of coupling points defined (NQUAD), the contact type (CTYPE) and the penalty factor used (PFAC), which in the literature review was observed that a user defined curve is preferred in most of the cases.

The energy profile of the simulation with the 4 mm mesh can be observed in the Fig.55. In the beginning, the energy starts as pure kinetic energy from the projectile ($K=1/2MV^2$), which is converted though the simulation in internal energy inside the projectile (deformation), being reduced through time due to loss of mass during the impact (mass outside from the ALE mesh). As expected, the plate does not receive any kinetic or internal energy due to its rigid behavior. It can be appreciated that the energy absorbed by projectile deformation is very low compared

to the one that will be absorbed by the plate when an elastoplastic or damage model is implemented. When performing elastoplastic simulations, care must be taken in order to set adequate Hourglass energy in case of observing that the under integrated shell elements are suffering from this numerical instability. In the case of composite shell damage models, this instability will be avoided by using fully integrated elements.
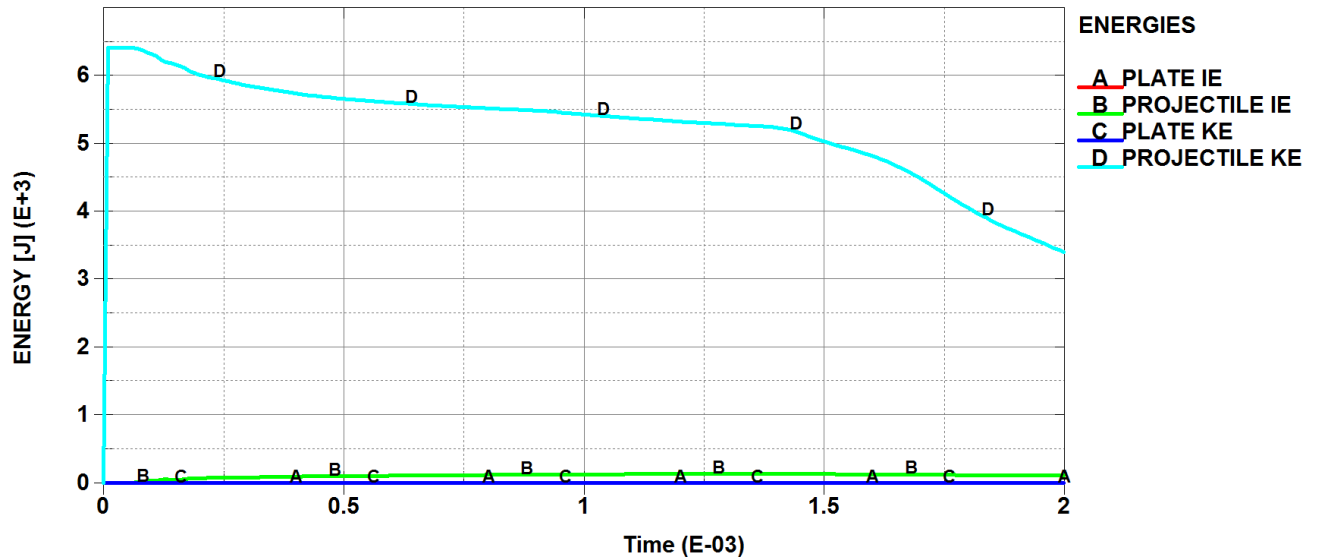
Figure 55. Energy profile for a soft body impact on a rigid plate.

8.2. Case 2- Elastoplastic Plate Impact: Bo Wu numerical Model

Once the gel impactor model was validated in the rigid model, the next step was to simulate the impact of the projectile against an elastoplastic material, in this case, aluminum. The reference chosen to compare the results was the work carried out by Bo Wu [11] because it was hard to find another reference for this material where the deflection profile and Von Mises stresses were given in the same report.

Table 2. Elastoplastic properties for the aluminum model.

Properties	Value	Units
Density	2780	[Kg/m3]
Yield Stress	345	[Mpa]
Young Modulus	71	[Gpa]
Poisson ratio	0.303	[N/A]
Tangent modulus	690	[Mpa]

For modeling the aluminum plate, a MAT_PLASTIC_KINEMATIC behavior (See Section 7.4) and Belytschko-Tsay formulation with 7 integration points through the shell thickness were used. Metal hardening was assumed isotropic (as discussed in the previous section, this will not affect the results). Again, a sensitivity study was performed in order to check the robustness and consistency of the numerical model. Therefore, some additional parameters needed to be set in addition to the ones mentioned in the previous section:

PLATE SURFACE MESH SIZE

- Affects mainly the simulation time and the plate response (Deflection, Von Misses stresses, plastic deformation. etc...)

MAT_PLASTIC_KINEMATIC

- All the parameters in this card, as explained in Section 7.4.
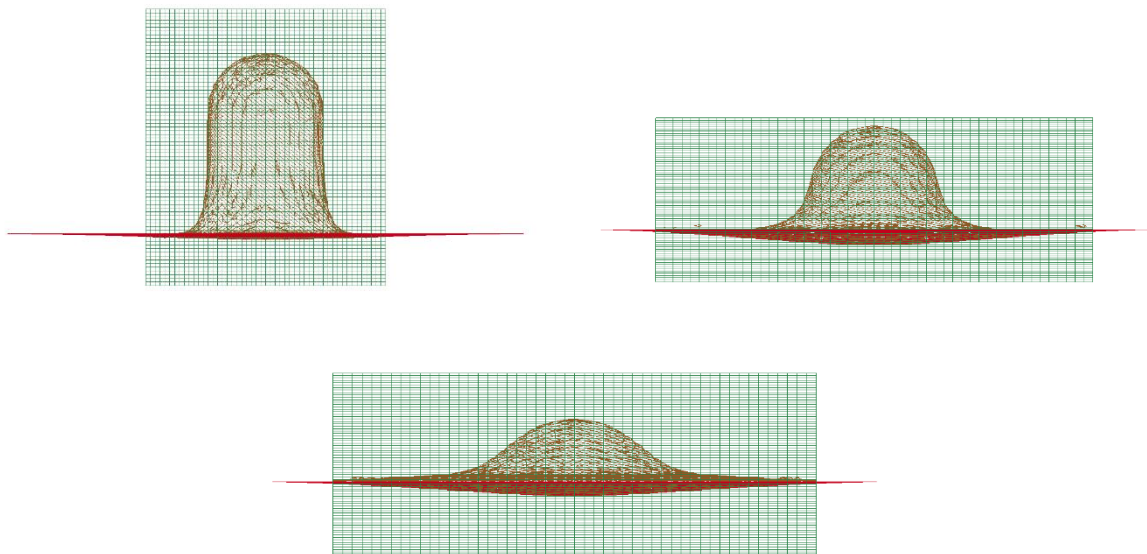
Figure 56. Deformation pattern of ALE mesh in the elasto-plastic model.

The squared plate with the dimensions shown in Tab.3 was clamped along its four edges. The impactor face was again rounded, with an initial velocity of 120 m/s for which a decrease in the Hugoniot Pressure is expected due to the flexibility of the target, even when the velocity this time is 4 m/s higher compared to the rigid case (See Section 3). In Bo Wu´s work, the plate was discretized with 2500 shell elements, and the impactor was build using Smooth Particle Hydrodynamics (SPH), is discretized in 29365 particles evenly distributed with a space of 4 mm [11].

Table 3. Numerical model parameters: Impact against an elastoplastic plate.

PLATE DIMENSIONS			
Width	500	**[mm]**	
Length	500	**[mm]**	
Thickness	14	**[mm]**	
IMPACTOR DIMENSIONS			
Diameter	114	**[mm]**	
Length	228	**[mm]**	
Density	950	**[Kg/m3]**	
Mass	1.82	**[Kg]**	
Impact Face	Round	**[N/A]**	
MESH PARAMETERS			
Type of Mesh	**Dimensions [mm]**	**# Elements**	**Element Size**
ALE Mesh	200x200x300	31613	4 mm
Boundary Shell	= to Impactor	222	Variable
Plate Shell	500 x500	Variable	Variable

In Fig.57 are shown the results obtained with the elastoplastic aluminum model. All the simulations were performed using the same parameters and the same ALE mesh (4 mm), varying only the aluminum plate mesh. The results obtained were satisfactory: the deflection obtained for the plate with the different plate meshes were very similar to the Bo Wu´s results. It is important to remark that in the paper [11] was stated that a 10 mm mesh was used for the simulation. However, the result that fitted the most with the reference data was the 20 mm mesh, which could be explained by the use of a quadratic criterion for the elements, although the authors do not explicitly mention it.

The Von Mises distribution for different time steps agreed very well. It can be observed in Fig.58 that although the magnitude of the VM distribution is a little higher for the simulation performed in this work (for 4 mm mesh), the general contours are in good agreement. This can be due to the small differences on the stress waves magnitude caused by the differences in the impactor modelling techniques because the response in terms of plate deflection correlates with an error less than 2%.
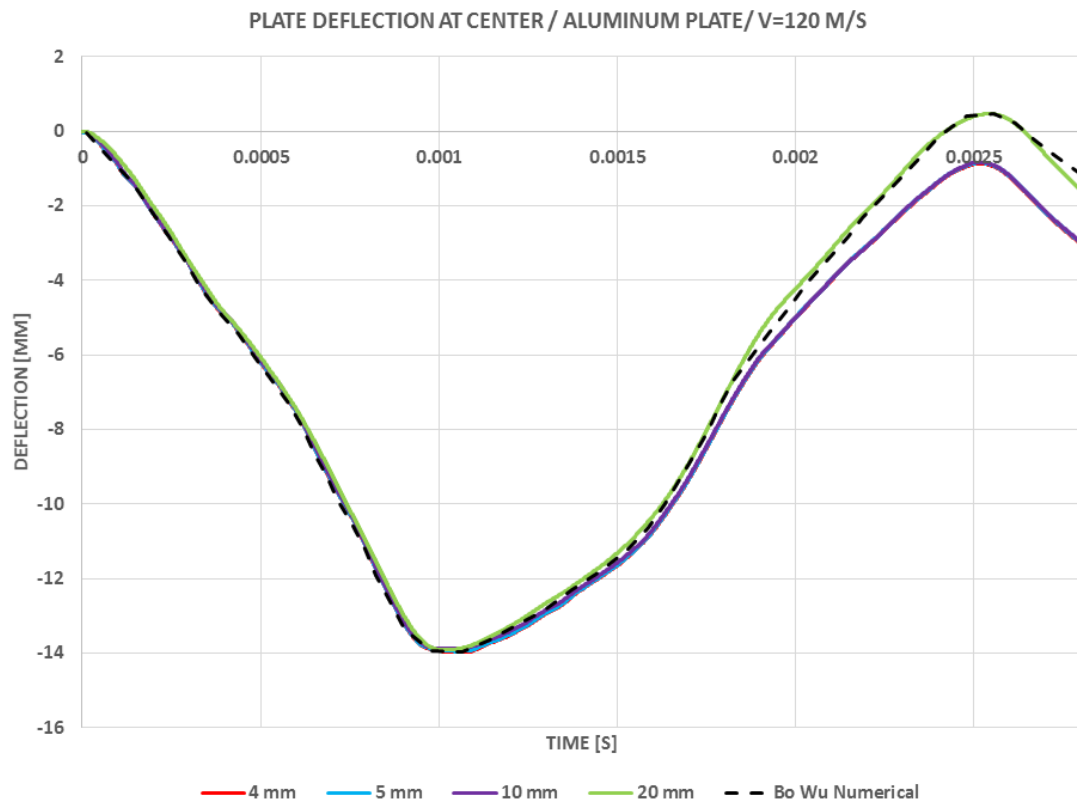
Figure 58. Deflection at the center of the plate, elastoplastic material model for aluminum.
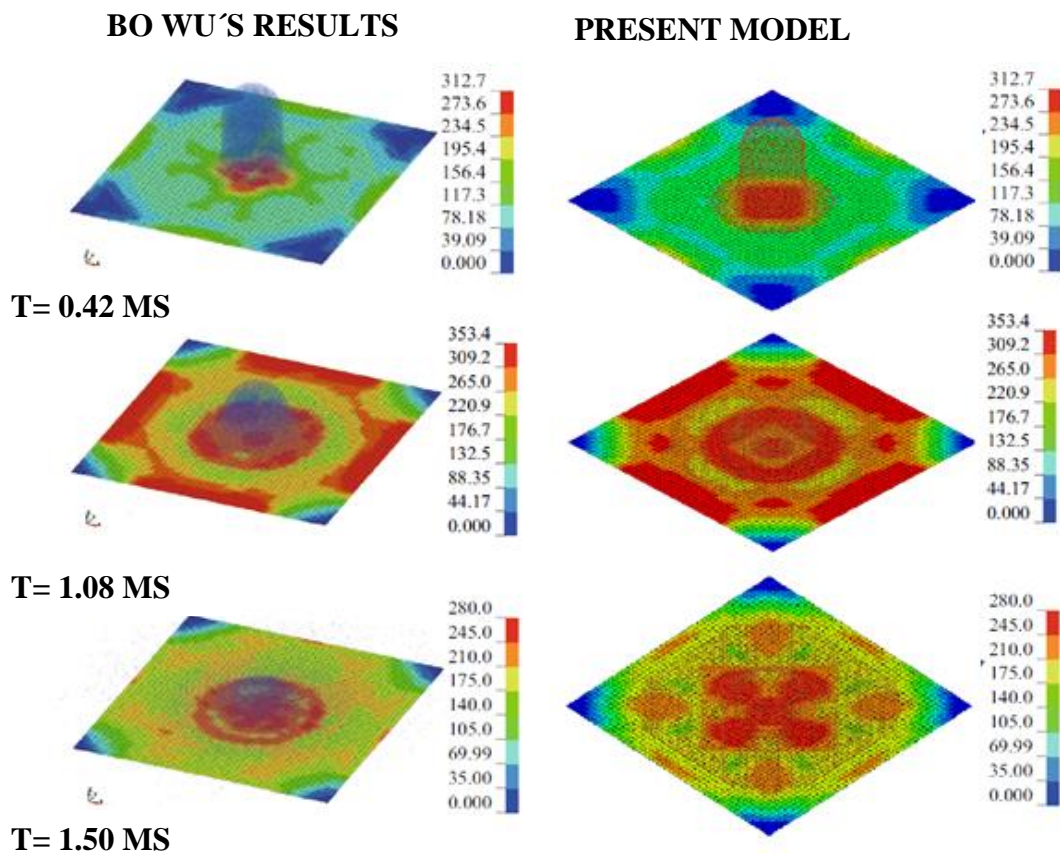
Figure 57. Von Mises stress comparison of the aluminum plate model for different times. Bo Wu's results (Left) and present study results (Right). From: [11]

Furthermore, the pressure profiles for different plate meshes are shown in Fig.59. It is interesting to observe that similar behavior, compared to the rigid plate sensitivity analysis, is obtained: the Hugoniot pressure increases when the plate mesh is refined (in the rigid study, the ALE mesh was the one changed). Moreover, it can be observed that all the Hugoniot pressures are far lower than the rigid plate case, even when the projectile mass is almost the double and the velocity is higher, which is in accordance with Wilbeck´s theory where the Hugoniot pressure is highly affected by the flexural properties of the target.

A more chaotic pressure profile is observed for the elastoplastic case, which was expected due to the flexural behavior of the plate. It was found that a 4 mm mesh for the plate (as it is for the ALE mesh) is suitable for modelling soft body impact events on elastoplastic cases. This time, the stagnation pressure is higher than the theoretical value for all meshes but the 20 mm one. It has to be remembered that Eqs. 1 and 2 only apply for rigid targets, discarding this way flexural response effects.
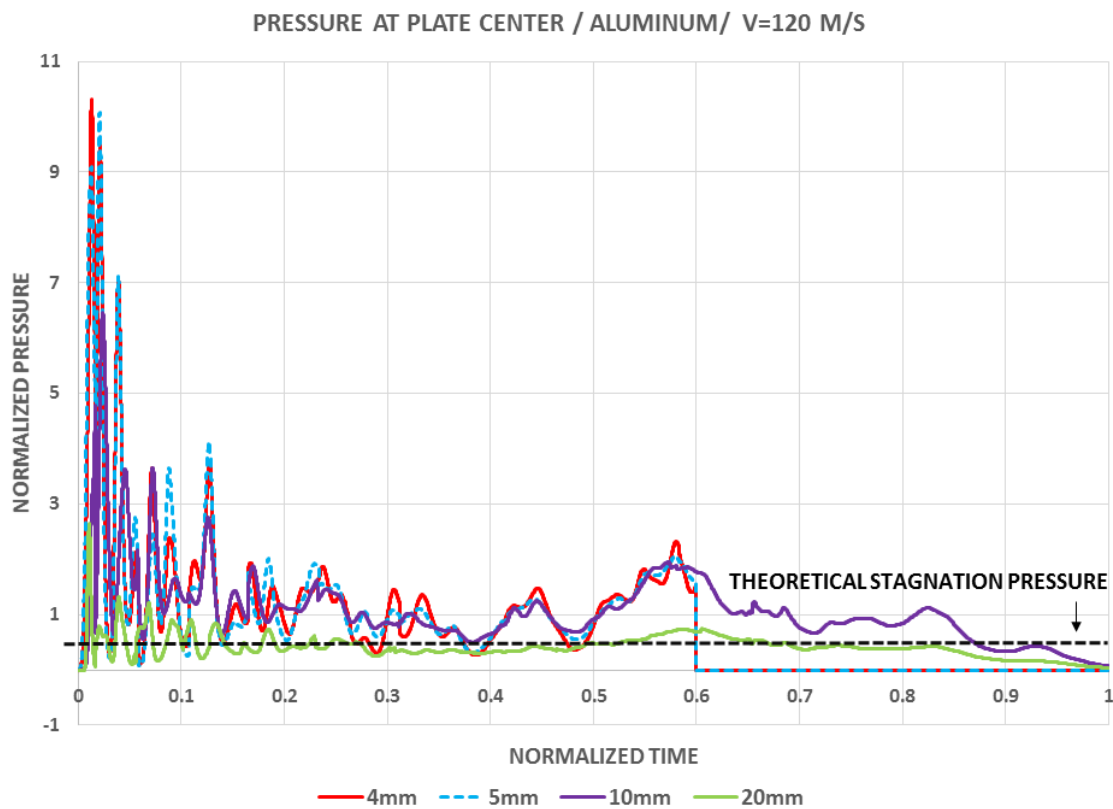
Figure 59.Pressure profiles for different Plate Mesh Sizes in an elastoplastic model.
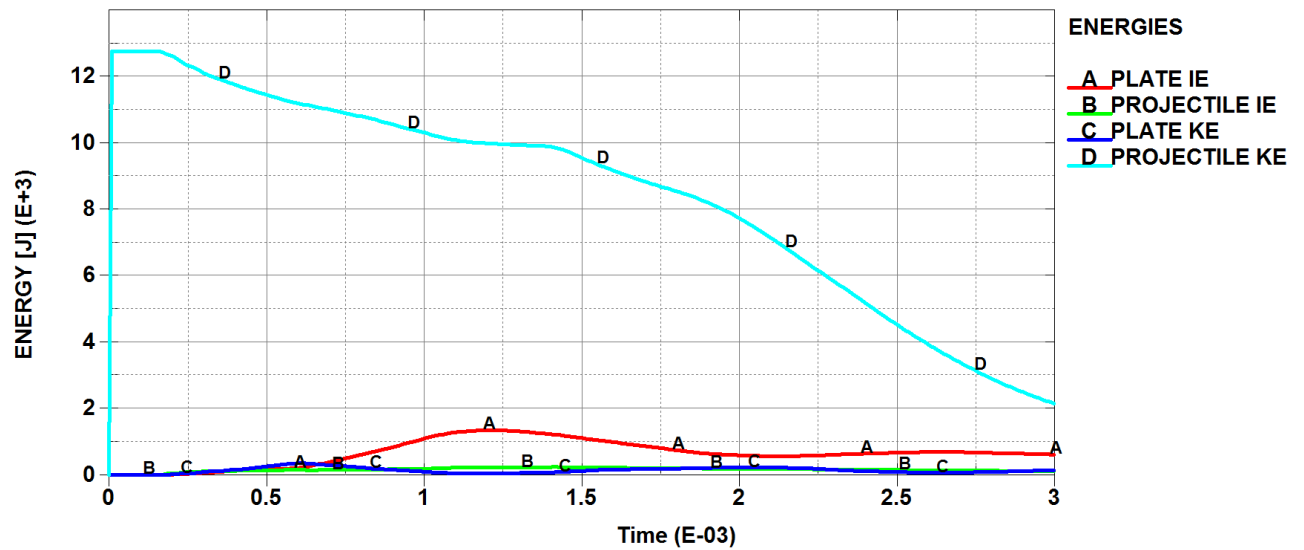
Figure 60. Energy profile for a soft body impact on an aluminum plate.

The energy profile for the elastoplastic model (See Fig.60) is in agreement with the one obtained for the rigid plate impact. This time, the energy is being dissipated by the plate deformation as IE energy, having as result some effective plastic strain at the end of the impact. However, the energy absorbed by the plate, in this case, is just about 9% of the impact energy, which is the behavior for very stiff plates, in this case, caused by having a high thickness (= 14 mm).

8.3. Case 3- Elastoplastic Plate Impact: Welsh Experiment

The accurate results obtained with the model developed in this work compared to the Bo Wu's report were very satisfactory having in mind that in the last one, two different numerical approaches were performed, finding them in good agreement. Nevertheless, the lack of comparison against experimental data was a concern for the validity of the current model, is the reason why it was decided to compare it against experimental tests found in the literature. Subsequently, the work performed by Welsh [12] was found to be ideal to test the numerical model of this work.

The tests developed in Welsh work consisted on the impact of both chickens and gelatin projectiles against an aeronautical grade aluminum (Aluminum 6001-T6 grade). The plates with the characteristics shown in Tab.5 where bolted in rigid steel support with a hole of 16 Inches of diameter. The 1.5 Kg projectiles were fired at 152 m/s to the target plate using the cannon gas set up shown in Fig.61, where the maximum deflections were extracted using high- speed cameras.

Figure 1. AEDC Bird Impact Range, S3.
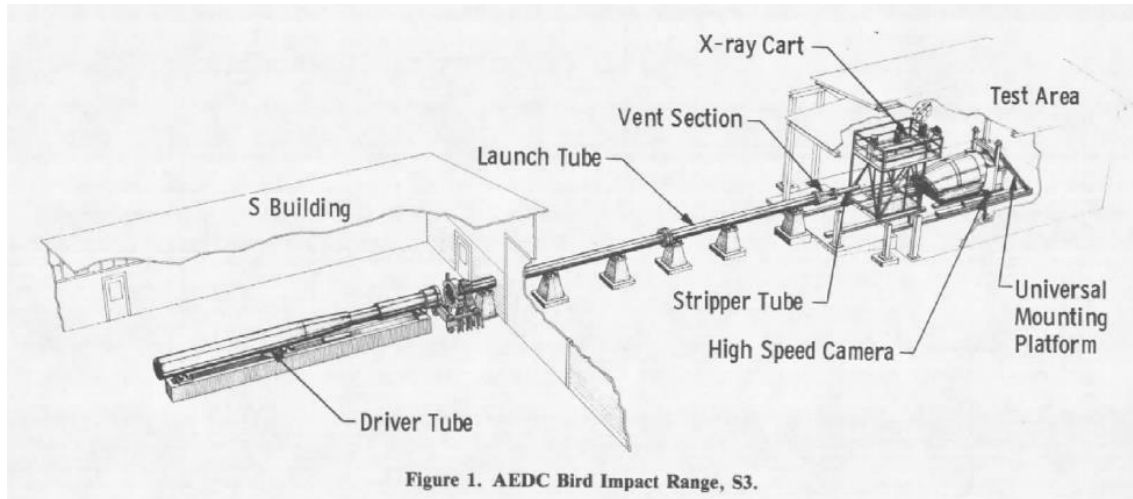
**Figure 61. The experimental scheme used in the Cannon gas experiments performed by Welsh.
From: [12]**

The LS-DYNA model was build based on both ALE and plate mesh sizes obtained in previous
sections, as well as the same MAT_PLASTIC_KINEMATIC model parameters, just differing
in the aluminum mechanical properties, which were changed in order to be in accordance with
the tested material. The gel impactor used in the experiments was planar, being easier to model
it in LS-DYNA by using a default shell boundary, used to define straight cylinders geometries.
Moreover, the plate was modeled as a 16 inches circle clamped along its perimeter (See model
properties in Tab.4).

Table 4. Numerical model parameters: Impact against the elastoplastic plate, Welsh model.

PLATE DIMENSIONS			
Diameter	Φ=16″	[in] [in]	
Thickness	6.35	[mm]	
IMPACTOR DIMENSIONS			
Diameter	101.6	[mm]	
Length	203.2	[mm]	
Density	950	[Kg/m³]	
Mass	1.54	[Kg]	
Impact Face	Planar	[N/A]	
MESH PARAMETERS			
Type of Mesh	Dimensions [mm]	# Elements	Element Size
ALE Mesh	200x200x300	197676	4 mm
Boundary Shell	= to Impactor	Default	Default
Plate Shell	Circular Φ=16″	2784	Var. 4-6mm

Table 5. Elastoplastic Aluminum 6061-T6 Properties used in the numerical model.

Aluminum 6061-T6 Properties	Value	Units
Density	2780	[Kg/m^3]
Yield Stress	276	[Mpa]
Young Modulus	68.9	[Gpa]
Poisson ratio	0.33	[N/A]
Tangent modulus	1000	[Mpa]

The maximum deflection found for the gel impact was 33.3 mm (corresponding to Shoot 5 in Welsh test [12]). The maximum deflection obtained with LS-DYNA model was about 37 mm, later converging in 33 mm as the final plastic deformation, which was measured by plotting the displacement along Z-axis for four central nodes. In Welsh work, there is no final deformation data, reason why the results cannot be compared directly. However, considering than the results in the maximum deformation differs only by 8%, it can be said that the model presents a good level of accuracy in both impact pressure modelling and the plate elastoplastic response.

For the energy profile, this time the energy absorbed by the plate as plastic deformation is much higher than the previous case, being almost 28%. Some kinetic energy is dissipating in terms kinetic energy (7.1%), projectile deformation (6%) and the rest is still carried by projectile mass which is being expelled as small debris after the impact.
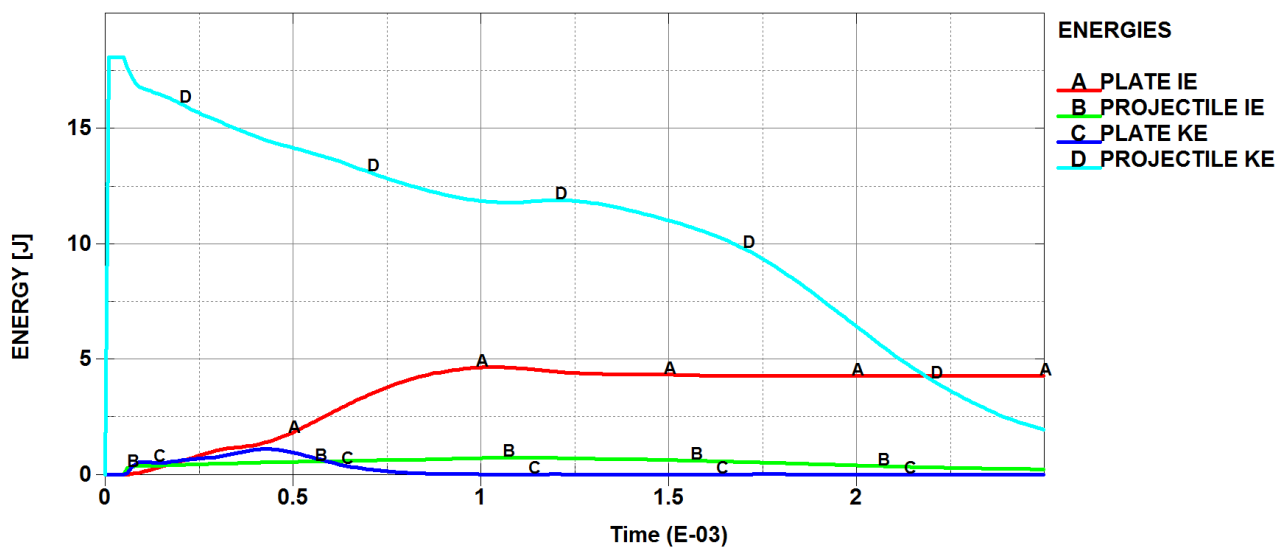
Figure 62. Energy profile for a soft body impact on an aluminum plate. Welsh experiment.
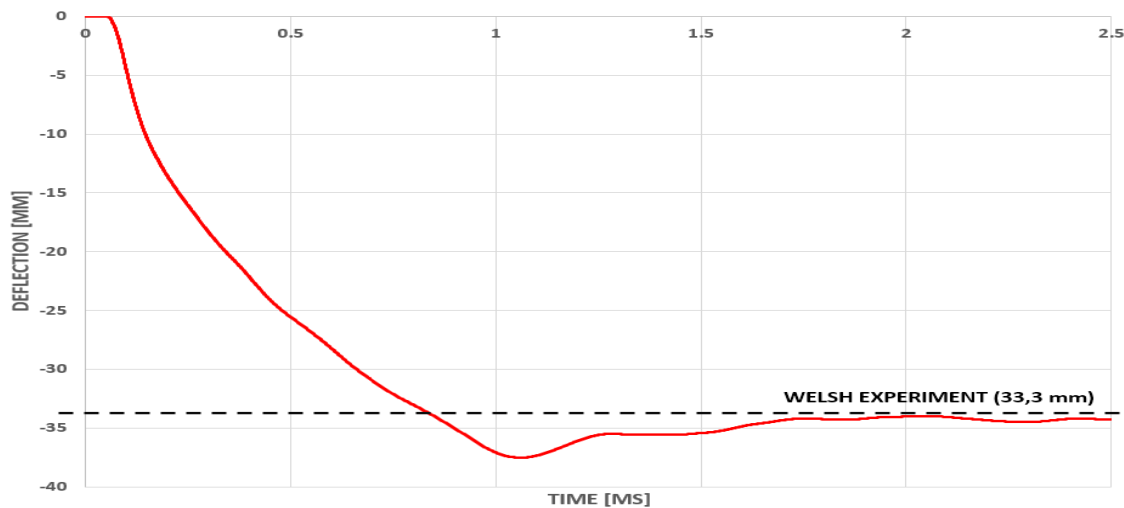
Figure 63. Deflection of the Aluminum plate in LS-DYNA and Welsh Experiment.

In the Fig.64 can be appreciated the Von Mises stresses contours of the aluminum plate 0.0025s after the impact (deformed impactor in gray). The maximum stresses go from the edges to the center due to the clamped conditions of the plate. At the end of the simulation, large plastic deformations are obtained.

These results, combined with the sensitivity analysis performed for both Rigid and elastoplastic impact cases, give confidence on the impactor model implemented in LS-DYNA, which will be used from further on to study the impact on composite materials.
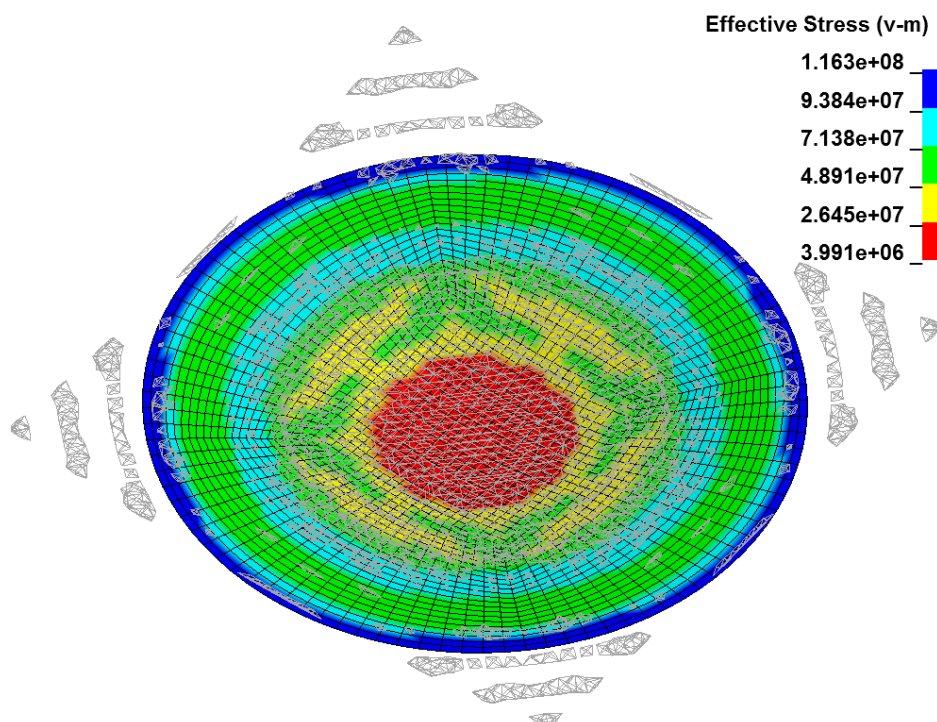
Figure 64. Aluminum Von misses stress state at 0.0025 s after impact.

8.5. Case 4- High Velocity Composite Plate Impact: Heimbs´s Model

The LS-DYNA model implemented built up to now was used subsequently for studying the behavior of composite plates when the velocity was increased up to values of 160 m/s using a straight cylinder soft impactor. Another work carried out by Heimbs was used to build and compare the present model [14]. In this paper, high velocity impacts of pre-stressed composites plates were studied including both intra-laminar and inter-laminar damage, the last one modeled using cohesive elements along the thickness, whereas the round-faced impactors were modeled using Lagrangian and Eulerian formulations.

This study was supported by experimental tests carried out by DLR Stuttgart Gas Cannon test facility, where C-Scan and Micrograph images of the laminate were taken prior and after the impacts. It is addressed that both experimental and numerical results are in good agreement, for both Lagrangian and Eulerian impactor models, remarking that both of the models tend to overestimate the initial contact pressure (Hugoniot Pressure) as compared to other studies [14]. An autoclave cured prepreg plate with the materials showed in Tab.6 was placed on a jig; clamping its short edges meanwhile the long edges were simply supported (same boundary conditions as the low velocity impact). Six strain gauges were placed on the back face of the laminate as it shown on the Fig.65
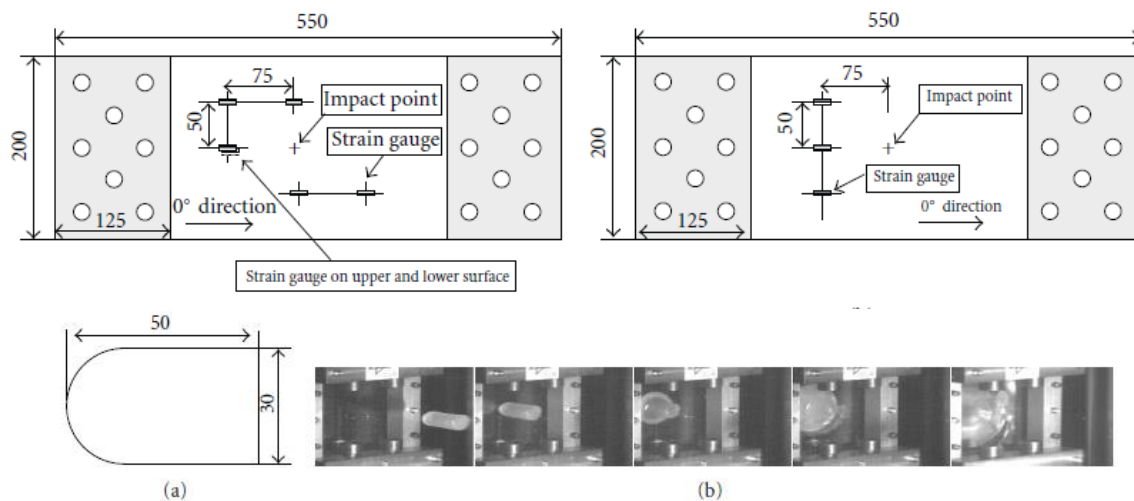
**Figure 65. Experimental arrangement of Heimbs Experiment. Dimensions are given in mm .
From: [14]**

After a sensitivity analysis carried out by the author for modelling both plate and impactor elements, as well as varying the number of cohesive interfaces along the thickness, the model using the properties shown in Tab.7 was selected.

These parameters were also used for building the current model in LS DYNA, with the main difference relying on the fact that cohesive elements were not considered again. For having an idea, the simulation increasing of time using cohesive elements can be in the order of 22 times, when 16 cohesive layers are used to simulate a laminate with similar dimensions and mesh characteristics [14]. The current simulation time is about 75 minutes when using an ALE impactor, and near to 35 minutes when using a rigid impactor.

Table 6. Plate characteristics and properties of the model tested by Heimbs.

PLATE CHARACTERISTICS		
Width	200	**[mm]**
Length	300	**[mm]**
Thickness	1.625	**[mm]**
Boundary Conditions	Short Edges (Clamped)	
	Long Edges (Simply Supported)	
Material	CFRP T800S/M21 PREPREG	
Stacking sequence	**[45/90/-45/45/-45/0/90/0/-45/45/-45/90/45]**	
MATERIAL PROPERTIES		
ρ	1580	**[Kg/m^3]**
E_{11}	172000	**[Mpa]**
E_{22}	10000	**[Mpa]**
G_{12}	5000	**[Mpa]**
ν_{12}	0.3	**[Adi]**
X_T	3039	**[Mpa]**
X_C	1669	**[Mpa]**
Y_T	50	**[Mpa]**
Y_C	250	**[Mpa]**
S_{LT}	79	**[Mpa]**
ALPHA	0	**[Adi]**
DFAILM	0.1	**[mm/mm]**
DFAILS	0.03	**[rad]**
DFAILT	0.017	**[mm/mm]**
DFAILC	-0.0135	**[mm/mm]**

The experiments carried out in this work [14] showed that for low energy impacts 140J-160J (velocities between 90-100 m/s) the plates did not suffer almost any damage, in contrast with what is shown in the Fig.66, where the numerical simulations show several Matrix Cracking due to tension in the different layers of the plate.

Table 7. Mesh parameters and information for all the objects in the model.

Item	Heimbs	Present Model
# Elements Impactor	1600 (3 mm)	2392 (2.5 mm)
# Elements Plate	9600 (2.5 mm)	9600 (2.5 mm)
# Cohesive layers	2 (1 mm)	0
Intra-laminar Damage	Yes	Yes
Inter-laminar Damage	Yes	No

In the Fig.66 can be seen the comparison between Heimbs Eulerian model and the ALE Present model for each ply (1 to 13). It is important to remark that Heimbs results consider a pre-stressed plate in tension, which includes two cohesive layers. It is stated in this work that tensile preloads increase the matrix cracking (MC) damage compared to the non-pre-stressed plate, but the cohesive elements will reduce it compared to the pure intra-laminar model due to the energy absorbed by these elements. This discussion is important to compare both cohesive and pure intra-laminar models showed in Fig.66, in which the damage propagation and location was similar for all the layers, changing only in magnitude.
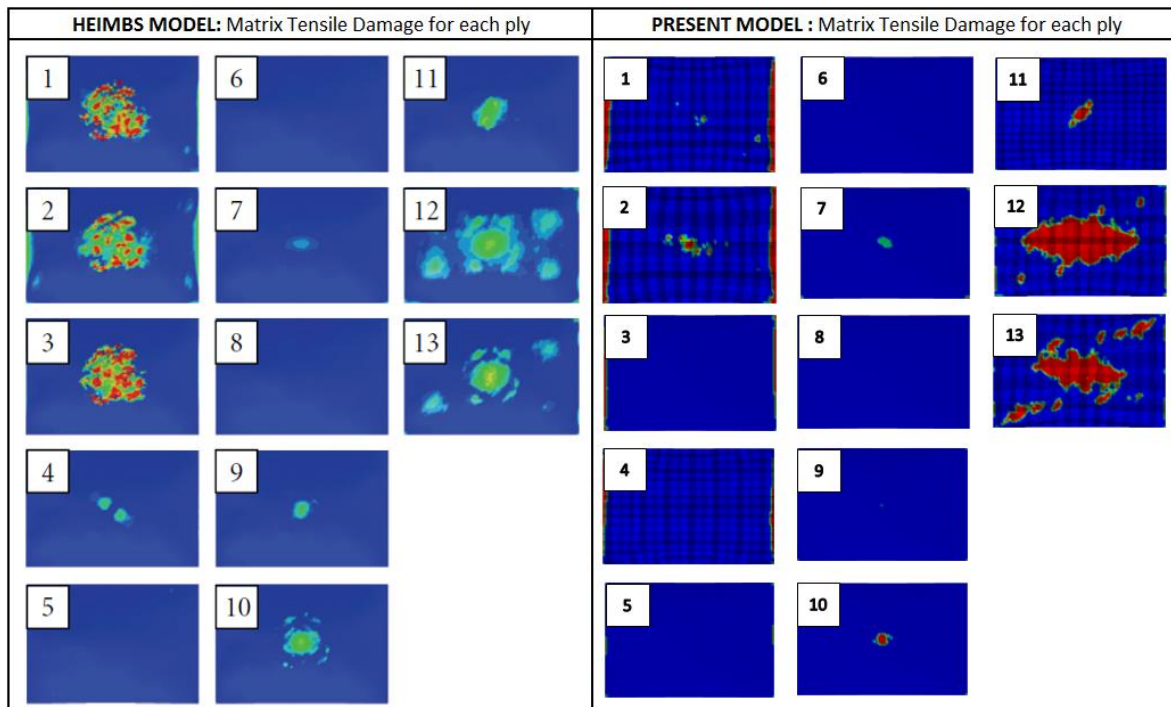
Figure 66. Matrix Failure due to tension. Comparison between Heimbs results (left) and Present Model (right) for a 100 m/s impact.
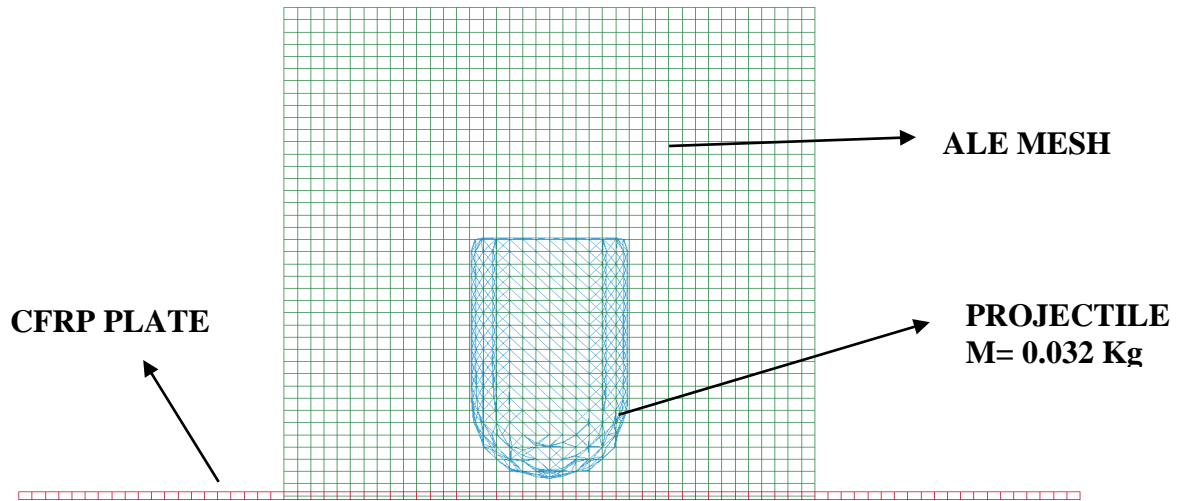
Figure 67. Mesh Diagram for a soft body high velocity impact.

Furthermore, when comparing the first three layers, it can be seen that the damage is concentrated at the center of the plate meanwhile in the present model it is concentrated at the clamped edges. This difference can be attributed to the fact that no crash-weakening algorithm is being used in the Present Model, as well as the presence and interaction of the cohesive layers. On the other hand, we should expect higher Matrix Cracking damage with respect to Heimbs model because the energy is being dissipated entirely by intra-laminar damage, as it was addressed in the low velocity impact simulation, subsequently affecting the bending behavior of the laminate. This is corroborated in Fig.68, where the maximum deflection of the present model is 20% higher compared to Heimbs, which is acceptable having in mind that this difference is about 2 mm.
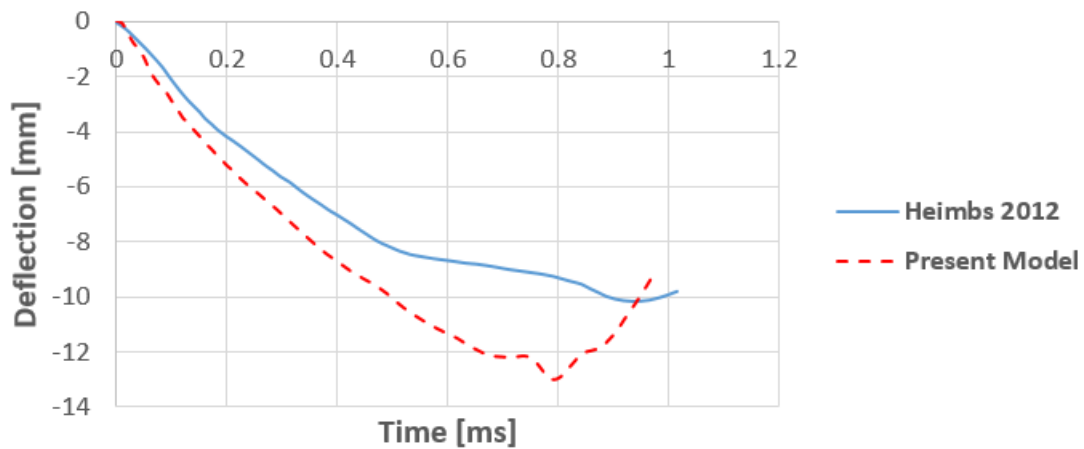
Figure 68. Maximum deflection comparison between Heimbs and Present model.
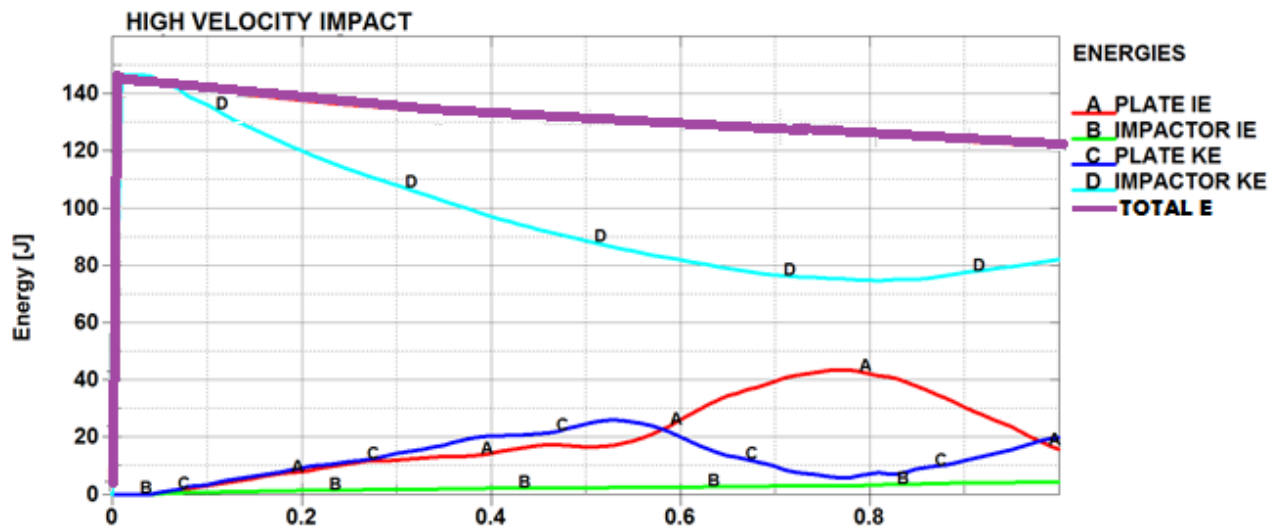
Figure 69. Energy profiles for both impactor and plate during a high velocity impact.

The energy levels in the simulation can be appreciated in the Fig.69. It is observed that almost all the kinetic energy of the impactor is transformed in the plate Internal energy into matrix yielding and damage; some are transferred to the plate movement in terms of kinetic energy and a small part is absorbed by deformation of the impactor. However, when summing these energies (Fig.69) can be observed a loss of energy of almost 30J (near 20%). This lost is attributed to the deletion of some projectile mass after the impact in form of small debris that goes out of the ALE mesh, as well as some mass loss between the advection cycle algorithm (See Section 4.1).

From the previous results, we can conclude that the present model correlates very good even for the cases of high velocity impacts with soft impactors, with some discrepancies in terms of deflection that probably comes from the assumption of neglecting inter-laminar damage. Nevertheless, the model is a good approximation for the preliminary simulations prior to the experimental tests, which can help to establish roughly some parameters such as elastic, matrix cracking and fiber rupture limits, as well as strain rates and overall times response.

Some assumptions and limitations of the present model are summarized as follows:

- The Present Model does not take into account Inter-laminar Damage. This parameter plays a key role in reality due to the energy absorption mechanism by delamination of the plate. For this reason, the model will overestimate the Intra-laminar damage, therefore increasing the laminate deflection and leading to conservative results.
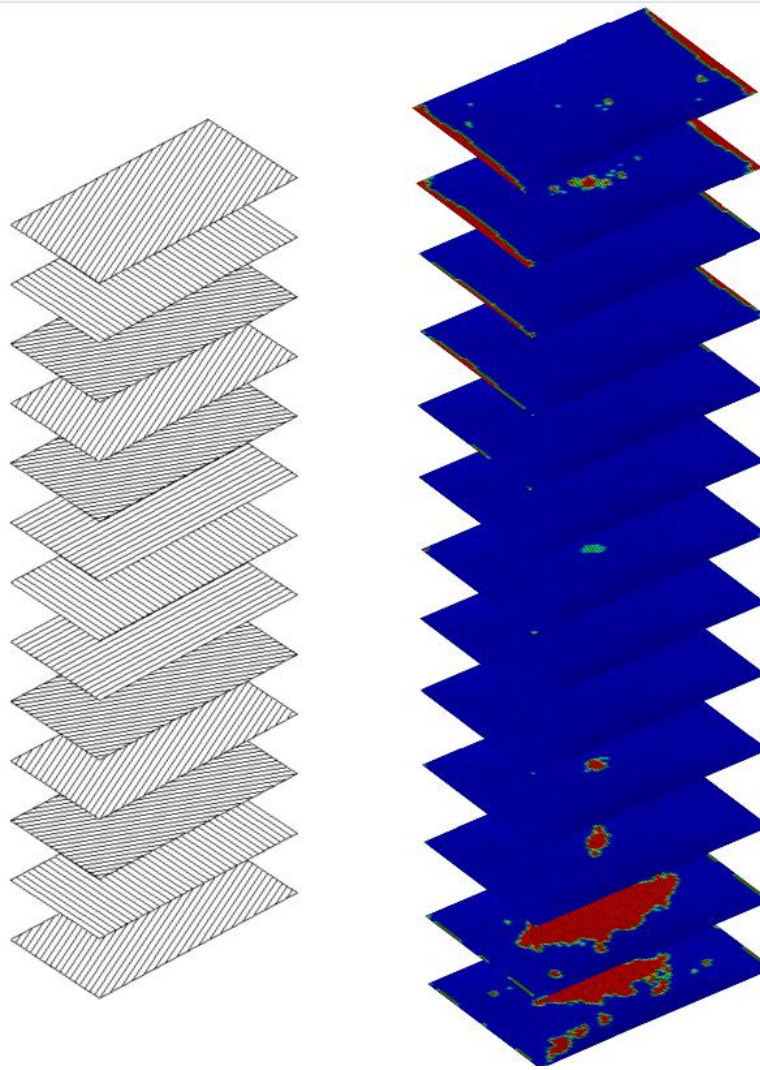
Figure 70. Fiber orientation at each ply (Left) and matrix cracking after impact (Right)

- Chang-Chang criterion is being used to model the damage in the plate. However, because this model relies only on a stress-based criterion, some additional strain based criteria need to be defined in order to accurately model the element failure. These parameters will need to be calibrated after experimental tests.

- Unidirectional tapes and fabrics can be modeled using MAT 54, although for fabrics it seems to be more suitable use MAT 58. This last model requires even more parameters that need to be tuned after experimental tests, which makes it more complex than MAT 54. It is advisable that for modeling fabrics accurately in the first phase of the project, an equivalent laminate composed of unidirectional plies is used.

- Hardening phenomenon due to strain rate effects is neglected.

- The model takes into account the non-uniform shear strain through the thickness of the plate, which is especially correct when sandwich structures are simulated [37].

- The nonlinear behavior of the shear-strain curve of the material, as well as its coupling in the correction parameter included in Chang-Chang, is not considered. α =0, β =0.

- Care must be taken when post post-processing the stress and strains due to different reference coordinate systems used in LS-DYNA. The stresses values in this report are given in the Material reference frame.

- Fully integrated shell elements are used to model the composite layers, each one defined by one integration point. In the work carried out by Sone Oo [49], approximate results are obtained using these elements at a low computational cost in the case of underwater explosions. Nevertheless, other shell formulations such as Belytschko-Tsay are required when delamination is accounted for, which will be more expensive computationally even though they are composed of under integrated elements.

- An accurate Hugoniot pressure is vital for obtaining good results in this model. As it was seen in a previous section, this variable is highly susceptible to the projectile geometry, initial contact area, density, meshing parameters, and velocity. This pressure will create the first matrix cracking and delamination, both evolving along the entire impact.
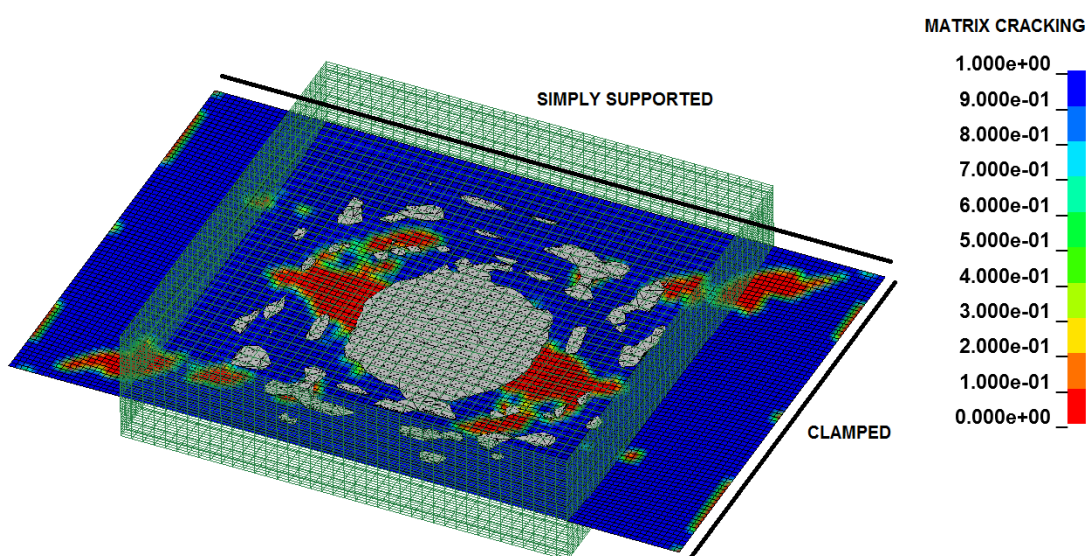
Figure 71. Matrix cracking in the back-ply at 1ms after the impact of a 32 g projectile at 100 m/s.

9. EXPERIMENTAL SET-UP SIMULATIONS

Once the model was validated against numerical and experimental tests found in the literature at both low and high velocity impacts, the experimental set-up, which will be held at Clément Ader Institute in Toulouse, was modeled numerically trying to recreate it as accurate as possible. As it can be appreciated in the Fig.72, a rigid back plate with a hole in its center, over which the composite plate will be placed, composes the model. The projectile is build using an ALE mesh, the composite plate is composed of fully integrated Lagrangian elements and the back plate is composed of under-integrated Lagrangian elements with rigid properties. In the experiments, the plate will be freely placed on the rigid back plate, being the reason why a back plate was modeled instead of defining initial boundary conditions along the edge of the plate.

Both geometrical and mesh properties of the objects are shown in Tables 8 and 9. The mesh characteristics were defined according to a previous sensitivity analysis (See Section 8) and the gravity inside the model was neglected, as well as the nonlinear shear behavior in the orthotropic ply mechanical properties. Three different laminates, two made of CFRP and one of GFRP, were tested (See Appendices) at different velocities ranging from 20 m/s up to 120 m/s. For each one of these velocities, two projectiles with different masses (0.37 and 0.75 Kg respectively) were impacted as it is shown in Table 9. This allowed observing the response of the different laminates when changing the impactor mass, in order to decide which mass should be used for capturing the damage transition phases as well as possible. Additionally, a rounded projectile impactor was tested so the changes in the Hugoniot pressure could be compared.

Table 8. Mesh properties of the objects in the Experimental Set-up simulations.

Item	Plate	Back Plate	ALE MESH
Width [mm]	400	500	250
Length [mm]	400	500	250
Thickness or height [mm]	5.76	2	200
Other dimension	N/A	φ =360 mm (hole)	N/A
# of Elements	10000	270	192200
Element size [mm]	4	25 approx.	4
TOTAL NUMBER OF ELEMENTS			202470

Table 9. Projectiles properties used for the experimental set-up simulations.

Item	Projectile A	Projectile B
Impact face	Planar/round	Planar
Diameter [mm]	100	100
Length [mm]	100	50
L/D	1	0.5
Mass [Kg]	0.75	0.375
Density [Kg/m^3]	950	950
# of elements*	7184	3592

Figure 72. Soft body impact arrangement: Experiment and numerical approaches.
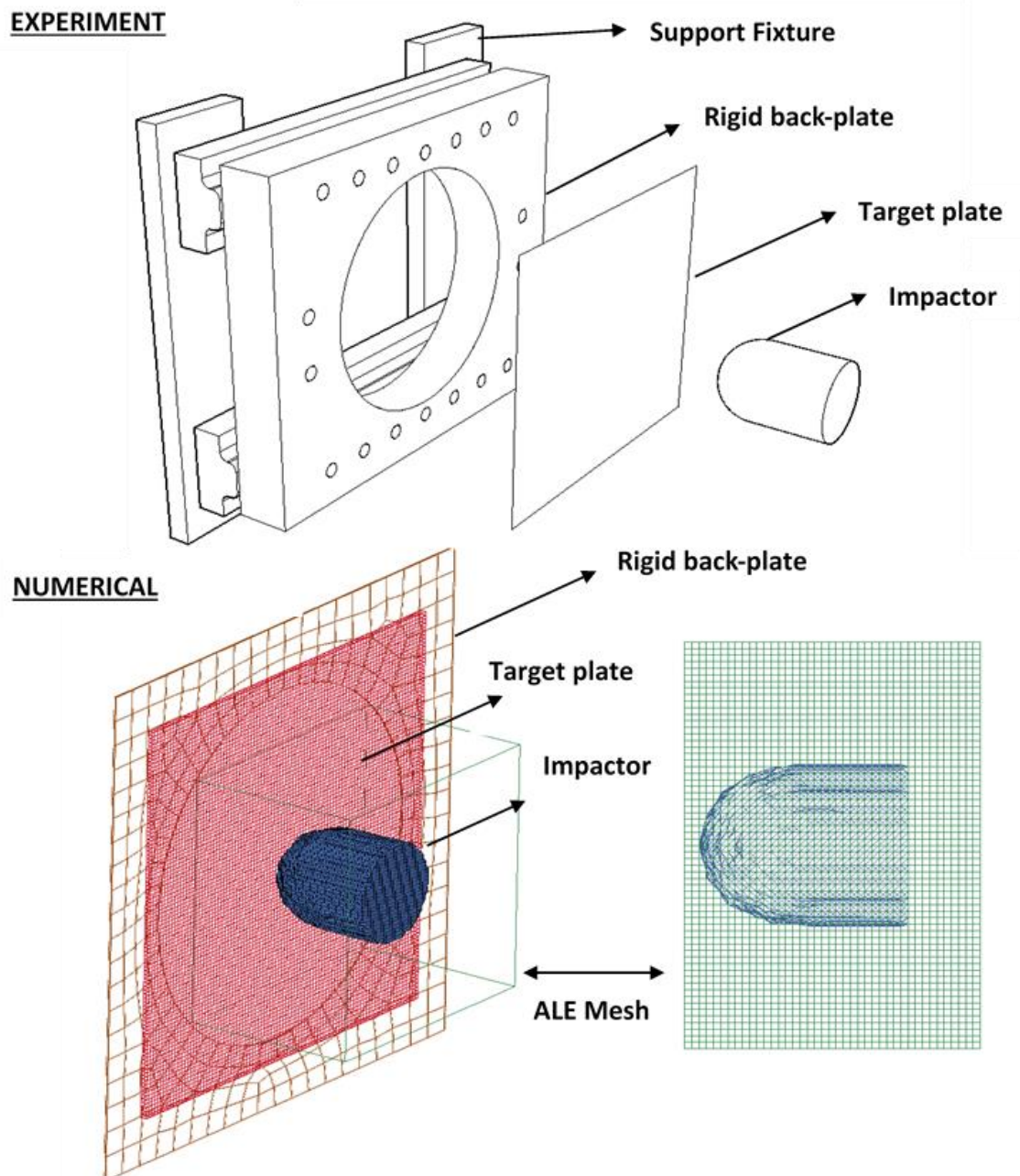
The assumptions of the present model are listed as follows:

- The impactor is modeled as an elastoplastic hydrodynamic governed material, with its properties and equation of state similar to the water.

- The Hugoniot pressure at the center was measured by using 16 ALE sensor at the center of the plate for the planar projectile, and four in the rounded projectile simulations.

- Fully Integrated shell elements along a single shell approach are used for modelling the composite laminate.

- Intra-laminar degradation is the only energy dissipation mechanism for damage inside the composite plate.

- The nonlinear shear behavior of the UD ply is neglected. The Shear strength (SC) is the maximum value of the linear part.

- Weighting shear term in tensile fiber mode for Chang-Chang criteria is 0. This means that fiber rupture is governed by the maximum stress criterion.

- Chang-Chang criterion is used for matrix failure.

- No strain failure criteria (DFAIL) is used.

- No softening reduction factor in crash front elements is used.

- No time step criterion for element deletion is used.

- No softening for fiber tensile or compressive strength after matrix compression failure is used (FBRT or YFAC).

- All the strain and stresses are given in the Material Coordinate System. (Stress X is in fiber direction and Strain Y is perpendicular to fiber).

- No Effective failure strain (EFS) for element deletion is used.

- No minimum stress after integration point failure is used (SLIMIT). That is, the stresses go to zero immediately after failure.

- Lamination theory for considering changes in shear strain through the shell when different materials are used is considered. This is especially important for sandwich simulations (LAMSHT).

- Fabrics are modeled using TWO WAY FLAG in MAT 54. Initially, their strengths were obtained by using the first ply criteria in a two UD equivalent laminate. This led to very conservative results and it was later changed by modelling it as equivalent UD plies.

9.1 Impact with 0.75 kg rounded face projectiles

A set of simulations were performed using a rounded face impactor with a mass of 0.75 kg, in order to see its effects on the Hugoniot and stagnation pressures, therefore comparing the damage evolution of the composite plate against the planar impactor cases (See Appendices 15.4).

For defining other shapes than cylindrical or spherical, an additional mesh must be created, which will act as the boundary inside the ALE mesh for creating the projectile, subsequently applying an operation defined as volume fraction inside the mesh composed by the fluid properties defined for the projectile. The main disadvantage of this operation is that the mesh of this shell boundary highly increases the calculation time when big refinements are employed. In fact, this mesh only needs to be refined enough in order to capture adequately the geometrical shape, but in the end, what will influence the projectile behavior is the ALE mesh size.

The configuration of this experimental set-up is the same as in previous cases and the same laminates are tested. This time, an additional UD equivalent GFRP laminate, for modelling laminate #3, is tested in order to improve the results that were obtained in for planar impactor cases, where fabric properties were used.

In Fig.73 are shown the results in terms of maximum deflection at different velocities for impactors with a mass of 0.75 Kg. It can be observed for the CFRP laminates that some changes in the plate response become noticeable after 40 m/s. The Matrix Cracking initiation was delayed for both laminates until 40 m/, compared to the planar case in which started at 30 m/s. Fiber Rupture also got delayed for both CFRP laminates, from 40 to 50 m/s for laminate #1, and from 80 to 120 m/s for laminate #2.
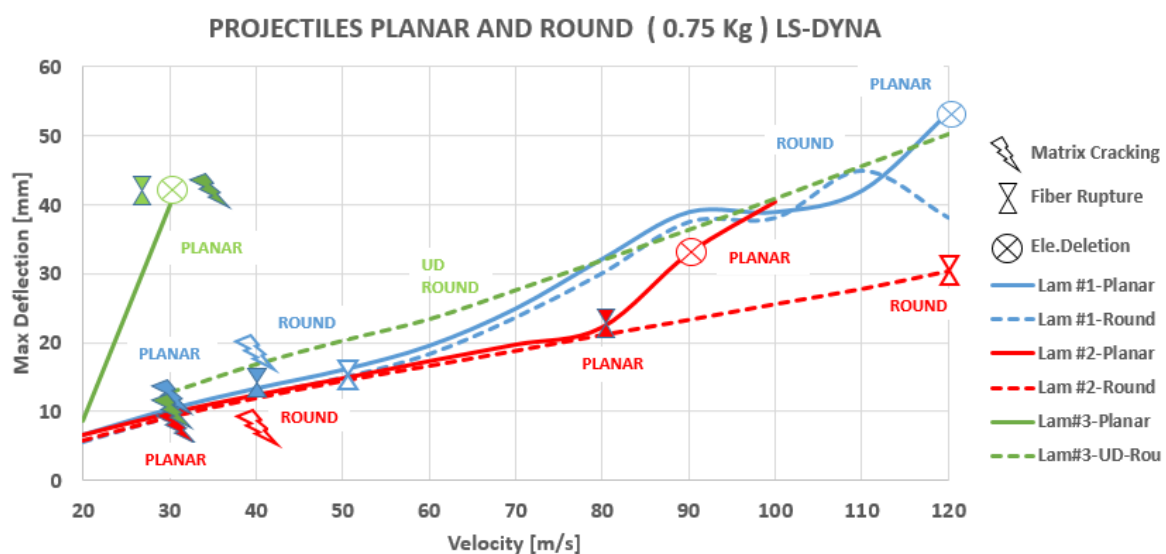
Figure 73. Maximum deflection and damage modes of laminates subjected to the impact of a 0.75 kg planar and rounded faced projectiles.

In fact, the stiffness of laminate #2 was unaffected up to 120 m/s, highly improving the response of this laminate in terms of increasing the damage initiation/velocity interval, which is critical for setting adequately the gas cannon experiments. The Element Deletion for both laminates also was delayed, not being reached in an interval between 20 and 120 m/s. However, large deformations in the fabric plies were observed in laminate #1 for velocities above 110 m/s, therefore causing some numerical instabilities.

For the UD GFRP laminate (Lam#3-UD Rou), the results highly improved with respect to the previous fabric model. The laminate presented an almost linear behavior in terms of maximum deflection and velocity, being less stiff than the CFRP laminates as expected, even when it was almost 3mm thicker. No Fiber Rupture occurred in this laminate (more strain is allowable for fiberglass materials) but in the Matrix Cracking contours, it was observed that all the layers were almost full of cracks for velocities above 80 m/s, which means that delamination has probably occurred at these impact velocities.

In the Fig.74 is shown the percentage of plies damaged by either Matrix Cracking or Fiber Rupture for all the laminates. It is very noticeable how the damage was delayed for all the laminates by almost a threshold of 10 m/s, and more than 40 m/s for laminate #2 for the initiation of Fiber rupture. For the GFRP laminate, Matrix Cracking occurs in all layers after 60 m/s, and when velocities are above 80 m/s, the cracked area becomes more than 80% of the damaged area of each ply.
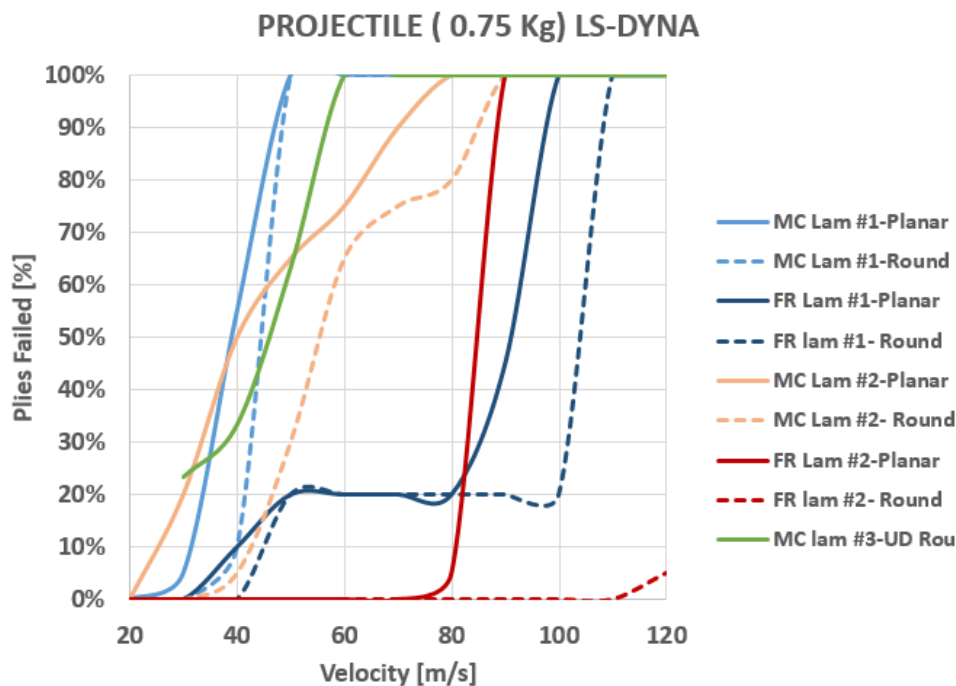
Figure 74. Percentage of plies failed for different damage modes after the impact of a 0.75 kg planar and round faced projectiles.

On the other hand, the Fig.75 shows the pressure comparison for the rounded projectile, which was extracted from four ALE sensors located at the center of the plate. As expected, the Hugoniot pressure was reduced almost by half just by changing the impact face geometry for all the velocities tested (from 20 to 120 m/s), whereas the stagnation pressure was almost the same for both cases.

This decrease in the Hugoniot Pressure is the reason why the Matrix Cracking and Fiber Rupture thresholds were delayed, as well as the damaged area reduction for all the plies at a given velocity. These results are in accordance with the theoretical formulations explained in Section 3, supporting and validating the fact that the damage progression inside the composite material depends highly on the Hugoniot pressure, which depends on geometrical parameters and velocity rather than the mass of the incoming projectile. It is advisable for the experimental tests to use rounded projectiles instead of planar ones if a wider damage threshold is desired, which needs to be decided depending on the cannon gas capabilities.
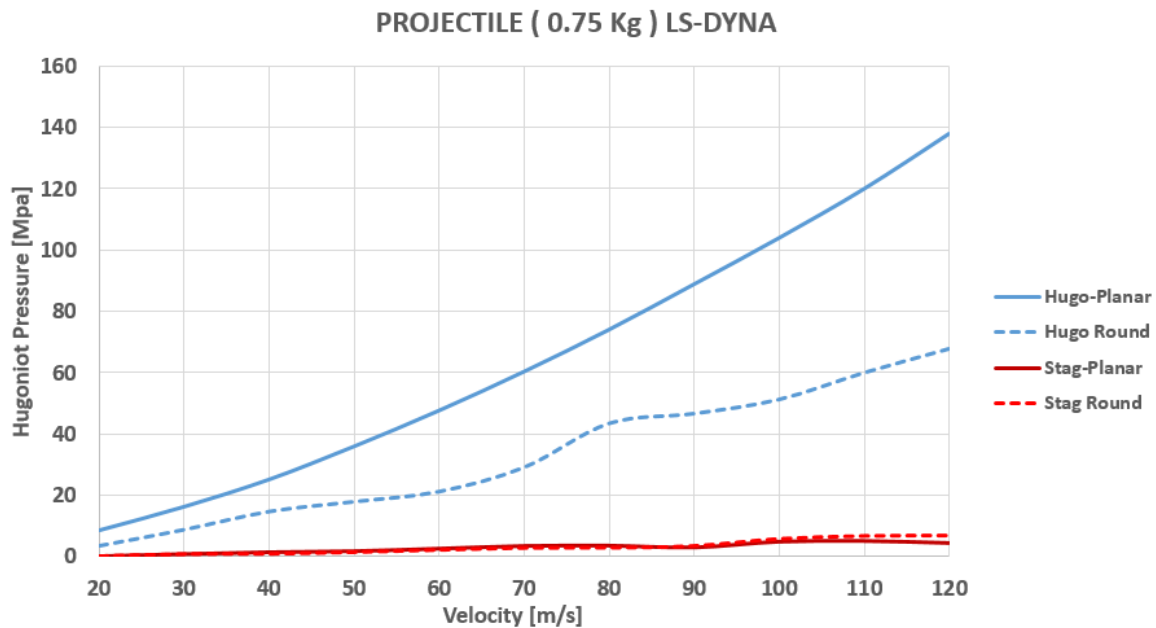
Figure 75. Hugoniot and Stagnation pressures respect to the impact velocity of a 0.75 kg planar and rounded faced projectiles.

A comparative scheme is presented for laminates #1 and #2 when they are impacted at different velocities with different projectile geometries (mass of 0.75 Kg), planar and round respectively (See Diagram 1). This analysis is performed on the back ply of the laminate (Layer #1), following the same arrangement of previous schemes.

Regarding MC in laminate #1, it is observed that the cracks develop in a very similar way (spiral shape) for the rounded impactor as compared to the planar, but its magnitude is far lower up to velocities of 50 m/s, after which, while being lower, becomes more alike in both shape and magnitude. In terms of Fiber Rupture, the differences are more noticeable: for a rounded projectile, the rupture is smaller up to velocities of 80 m/s, after which the failure becomes sudden and the back ply fails entirely (this can be observed as well in the Fig.74).

As laminate # 2 is concerned, a similar analysis can be made. The Matrix Cracking evolves in a similar manner (oval shape) but being smaller up to 60 m/s, after which becomes similar to the planar face impactor, but again in smaller magnitude. In contrast, this time Fiber Rupture did not occur in the laminate in the entire velocity range (from 0 to 120 m/s).

In the fiberglass UD equivalent laminate, almost all the layers presented big areas with MC The inconvenience of this behavior is that probably the laminate has been suffering from delamination, which the model cannot capture adequately, focalizing then the damage only in the intra-laminar mode. For this case, some additional formulation, either empirical or numerical, is advisable in order to determine correctly the delamination threshold, therefore relating it to the model for studying correctly the stiffness degradation.

DIAGRAM 1- BACK PLY DAMAGE LAMINATE #1 BOTH PROJECTILES

BACK PLY DAMAGE – IMPACT MASS			BACK PLY DAMAGE – IMPACT MASS	
MC Laminate 1 (P)	MC Laminate 1 (R)		FR Laminate 1 (P)	FR Laminate 1 (R)

30 m/s ↔
40 m/s ↔
50 m/s ↔
60 m/s ↔
70 m/s ↔
80 m/s ↔
90 m/s ↔

DIAGRAM 2- BACK PLY DAMAGE LAMINATE #2 BOTH PROJECTILES

| BACK PLY DAMAGE – IMPACT MASS | | | BACK PLY DAMAGE – IMPACT MASS | |
| MC Laminate 2 (P) | MC Laminate 2 (R) | | FR Laminate 2 (P) | FR Laminate 2 (R) |

9.2 Variation of critical strength properties

It is known that the current model overestimates the damage occurring inside the plate after the impact for different reasons mentioned in Section 8. One of these reasons is the limitation of both shear and compressive strengths to the linear behavior of its stress-strain curves. Additional simulations were performed for the CFRP laminates, using the 0.75 Kg rounded impactor and a velocity of 80 m/s, in order to study the influence of these critical strength parameters when they are increased.

These strength properties are hard to define due to its nonlinear behavior after the elastic limit, in addition to its uncertainties related to imperfections and/or damage modes such as kinking, micro-voids, among others. Understanding how stress is developed in the different directions through the impact is critical in order to determine the importance in the variations of these strengths. Therefore, three cases were studied:

- **Case #1:** Laminates with shear and compressive properties within the linear limits (Which was used for previous simulations).
- **Case #2:** The shear strength (SLT) of the laminate is increased by the double.
- **Case #3:** The shear (SLT) and compressive strength (YT) strength of the laminate are increased by the double.

In the Figs. 76 and 77 are shown the X, Y and XY stresses of the back ply (Layer #1) of each laminate (Laminate #1 and #2) at the first Matrix Cracking. It is observed that in this stress state, the damage is induced by tension in the matrix direction (YT) as it will be expected due to the bending moment, although some compression is occurring in the tensile ply at this instant due to a stress wave (See Fig .78). The center of the plate is submitted to around 38 MPa in tension in the laminate #1 for both directions, which is near to the tensile strength of the matrix (See Appendix 15.2), is even bigger in the case of laminate # 2 due to its UD nature. For the shear stresses, although appreciable, they do not exceed 13 MPa for both laminates, which is near half of the capacity of the laminate with respect to the shear strength. However, it must be remembered that the shear is coupled to both tensile and compressive matrix damage modes, limiting then the capacity of the laminate. Nevertheless, no influence was observed when increasing these strengths by half for this impact case, allowing to conclude that the damage starts purely as matrix tension failure, where both shear and compressive induced failures caused by bending or stress waves are negligible.

Figure 76. Variation of critical strengths for laminate #1, 0.75 kg rounded impactor.

BACKPLY: STRESS X (45° FIBER DIRECTION) AT FIRST MATRIX CRACKING
LAMINATE # 2 (UD) / V = 80 M/S   / MASS IMPACTOR=0.75 Kg

CASE #1
YC (UD) = 80.7 MPa
SLT (UD) = 25.6 Mpa

CASE #2
YC (UD) = 80.7 MPa
SLT (UD) = 51.2 Mpa

CASE #3
YC (UD)   = 161.4 MPa
SLT (UD) = 51.2 Mpa
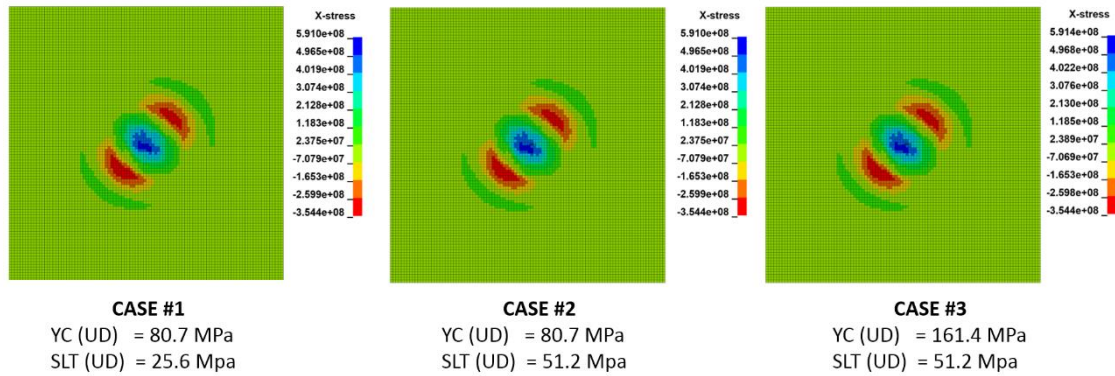
BACKPLY: STRESS Y (-45° DIRECTION) AT FIRST MATRIX CRACKING
LAMINATE # 2 (UD) / V = 80 M/S   / MASS IMPACTOR=0.75 Kg

CASE #1
YC (UD) = 80.7 MPa
SLT (UD) = 25.6 Mpa

CASE #2
YC (UD) = 80.7 MPa
SLT (UD) = 51.2 Mpa

CASE #3
YC (UD)   = 161.4 MPa
SLT (UD) = 51.2 Mpa
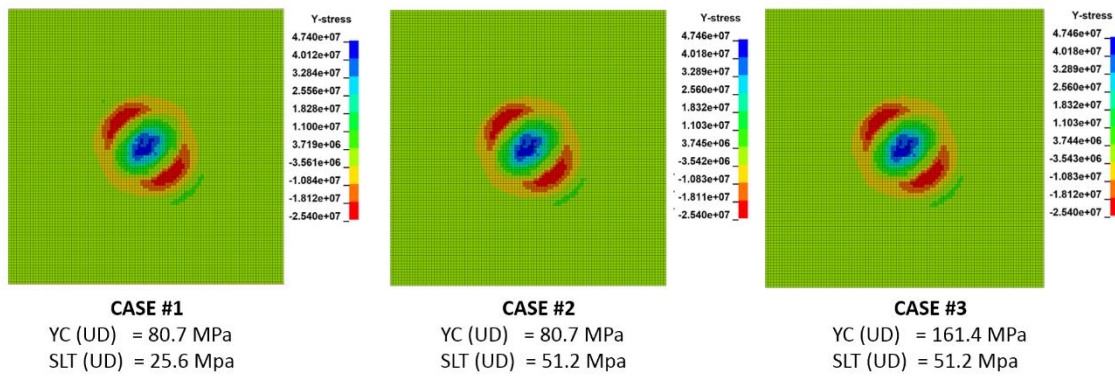
BACKPLY: STRESS XY (IN-PLANE SHEAR) AT FIRST MATRIX CRACKING
LAMINATE # 2 (UD) / V = 80 M/S   / MASS IMPACTOR=0.75 Kg

CASE #1
YC (UD) = 80.7 MPa
SLT (UD) = 25.6 Mpa

CASE #2
YC (UD) = 80.7 MPa
SLT (UD) = 51.2 Mpa

CASE #3
YC (UD)   = 161.4 MPa
SLT (UD) = 51.2 Mpa
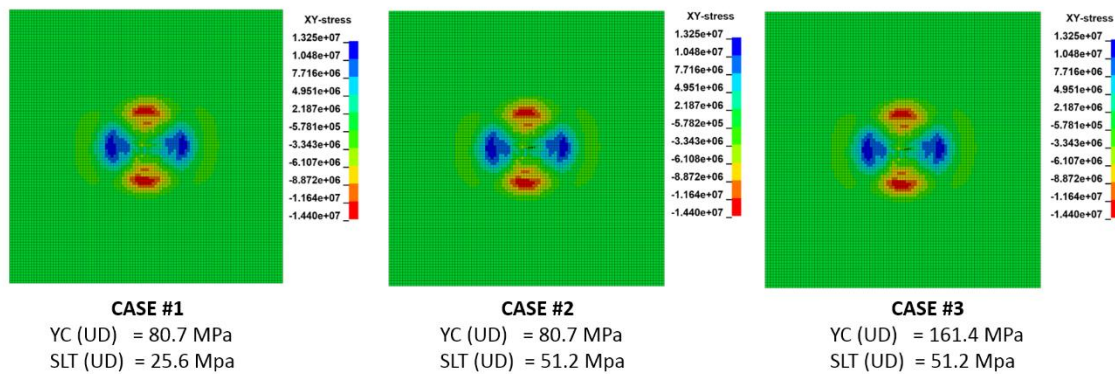
Figure 77. Variation of critical strengths for laminate #1, 0.75 kg rounded impactor.
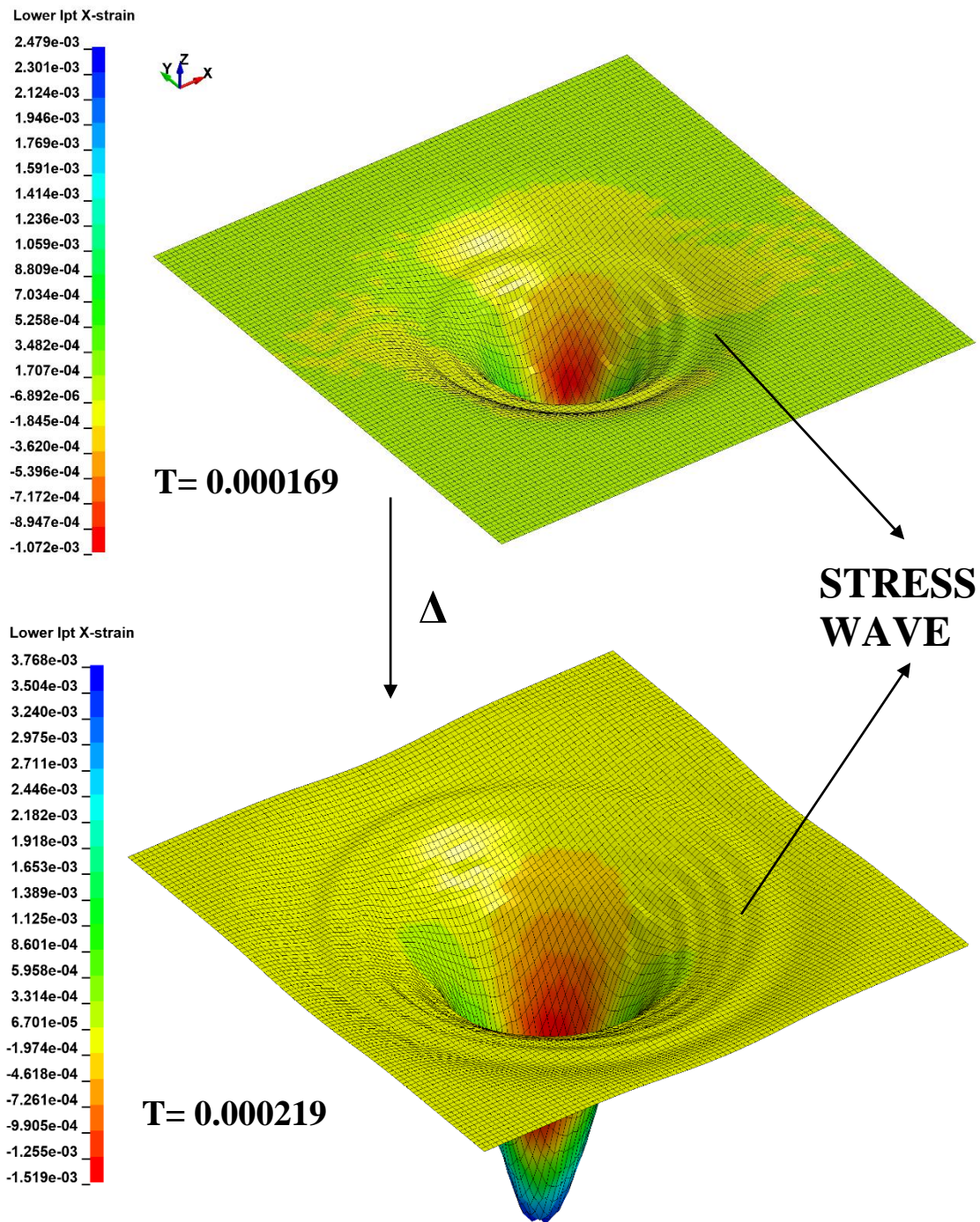
Figure 78. Initial Stress wave propagation though the plate. (100 m/s, 0.75 Kg projectile, laminate #2, back-ply)

9.3 Observations

- Biaxial fabrics reduce the matrix cracking damaged area when compared to a UD at the same velocity, which will enhance the properties against delamination. However, the disadvantage is that the reduction in longitudinal strength compared to a UD with the same fiber volume will force it to have Fiber Rupture earlier.

- The laminate #1 presented total failure (Element Deletion) much more lately than laminate # 2 for all the cases. The failure sequence of this laminate begins, after Matrix Cracking initiation, as fiber rupture of fabric layers, while delaying the rupture of UD layers compared to laminate #1. However, laminate #2 presented a much stiffer behavior in the range of velocities between 0 and 80 m/s for all impactor cases, being more evident for higher mass projectile impacts.

- GFRP laminate #3 presented the worst resistance to impacts. After 30 m/s, the laminate completely failed according to numerical simulations. Simulations between 20 and 30 m/s need to be performed in order to study in a more detailed way the laminate damage evolution. An equivalent UD GFRP laminate was tested and it was observed a complete change in its behavior: Fiber Rupture was never reached and it presented an almost linear behavior with respect to the impact velocity.

- It was observed in the simulations that reducing the projectile mass just by decreasing its length does not have a considerable decrease in the damage. The Hugoniot pressure is still high, and it will govern the failure behavior of the laminate. On the other hand, it was been seen that decreasing the projectile diameter or the impact surface shape has a drastic effect on the magnitude of this pressure.

- The results of these numerical simulations seem to be more conservative than reality. Some parameters such as strain based criteria, strength degradation, and "crash-front" weakening need to be adjusted after experiments in order to improve the numerical model accuracy.

- It was observed that the most critical parameters in strength, that is compression strength in the transverse direction and shear strength, are not being underestimated when assuming its magnitude as the linear limit of the stress-strain curve for the initiation of damage in this impact case. However, they can highly overestimate the damage in other cases for the compressed zones of the laminate above its neutral axis, as well as in cases where high magnitude stress waves are generated.

10. EXPERIMENTAL RESULTS

In this section, some of the laminate experimental results are presented and compared in terms of deflection and strain with the numerical models developed in LS-DYNA. The author would like to express its gratitude to O. Dorival and G. Barlow for contributing with all the experimental data that shown in this work (Which is Property of their own research) as well as for all the support and feedback during the development of this master thesis.

In the experimental tests, the strain evolution data of the laminates during the impact was gathered as follows:

- Using two strain gauges oriented on the fiber direction, which were located on the back-ply of the laminate at two different points as it can be appreciated in Fig.79 (Center and 75 mm offset respectively)

- Using the Digital Image Correlation (DIC) equipment of the STIMPACT laboratory for acquiring the deflection and strain fields of the laminate along the impact.

The experimental results presented in this section, are the ones obtained with the DIC equipment, after the tests of two specimens for each laminate. In the comparison analysis, only one specimen for each laminate was chosen, based on the impact that was closest to the center of the plate.
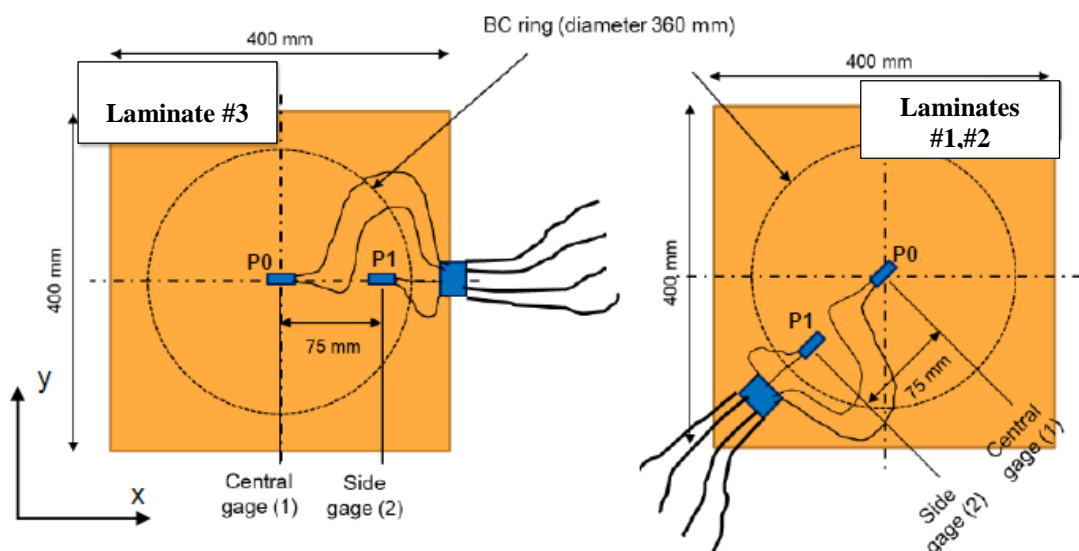
Figure 79. Strain gauges location diagram for the different laminates: Laminate #3 (Left) and Laminates #1, #2 (Right). From: G.Barlow

6.1 Laminate #1

The deflection history for the experimental and numerical tests for the two different measuring points is shown in the Fig.80. During the experiments, it was seen that the projectile was not always impacting in the plate center. For this reason, some additional simulations were performed for un-centered impacts with an offset distance of 90mm from the center.

It was observed that in terms of maximum deflection, the numerical model correlates very well with the experiments, presenting less than 8% of relative error for both measuring points for the centered impact. However, the period of the plate response in the numerical simulations is lower than the experiments for 0.5ms, which is possibly due to differences in the real and theoretical stiffness, as well as initial voids or defects in the real plates, the latter being observed at ICAM for some specimens after ultrasonic nondestructive testing.

On the other hand, it can be appreciated that the un-centered impact affects considerably the plate response in terms of maximum deflection, subsequently affecting the strain fields that will be generated during the impact. Therefore, an adequate calibration in the impact zone must be guaranteed for having a good correlation between the experiments and numerical models.

In the Fig.81 can be seen the deflection contours at different instants of the impact. Again, good correlation is obtained when comparing both experimental (DIC) and LS-DYNA results. However, this comparison is made at the moment in which the laminates reaches a determinate maximum deflection rather than comparing the same instant, which was difficult due to the problems related to the modal response.

Figure 80. Experimental and numerical deflection history at 60 m/s for Lam. #1.

Figure 81. Deflection contours at three different instants for experimental DIC (Left column) and numerical DYNA (Right column) for Lam. #1 at 60 m/s impact.
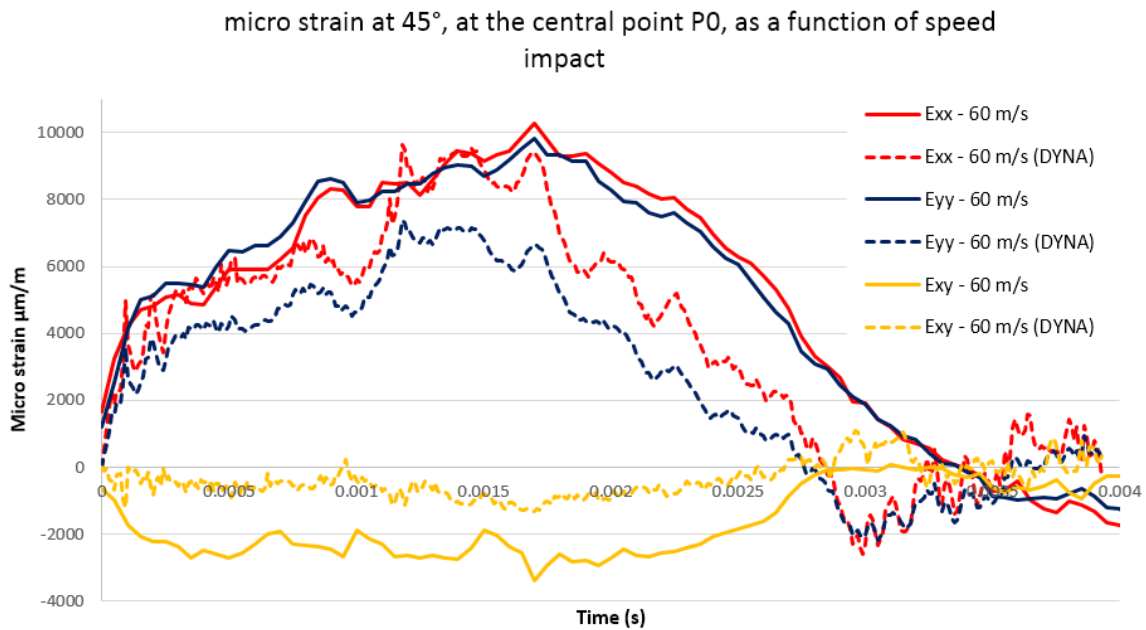
Figure 82. Experimental and numerical strains history in the fiber direction at point P0 for Lam. #1 at 60 m/s.

Figure 83. Experimental and numerical strains history in the fiber direction at point P1 for Lam. #1 at 60 m/s.

The strains at the back-ply in the different directions (Longitudinal, transversal and shear) for the points P0 and P1 are presented in the Figs.83 and 84. The numerical strain profiles are in good agreement at the central point in all strain directions. It has to be remembered that the back-ply of this laminate is a fabric, the reason for which both strains ε_{xx} and ε_{yy} are quite similar. However, this laminate possesses a bigger percentage of 0° plies, reason why the strain in the ε_{xx} global direction should be slightly higher.

For P1, the results are not that accurate for ε_{yy} and ε_{xy}. In the case of ε_{xx}, it can be observed an initial compressive strain due to the second mode response of the laminate, as well as the stress wave propagation along this point, which magnitude is almost the same for both numerical and experimental approaches. Moreover, both ε_{xx} (Numerical and experimental) increases at a similar rate up to 1ms, after which the experimental strain rate becomes smaller, ending up in a numerical strain almost 28% bigger than the experimental one.

These differences could be explained by the initiation of internal damage of the experimental plates at locations near to the back plate perimeter, having into account that this laminate (a different specimen) failed at similar velocities due to fiber rupture and internal de-bonding during the experimental campaign. Differences in the propagation of stress waves due to differences in the projectile deformation during the impact and the influence of the squared plate induced folding into the circled geometry can highly affect the overall behavior of the strain.

6.2 Laminate #2

The results obtained for laminate #2 in terms of maximum deflection were quite satisfactory. In the Figs.84 and 85 can be appreciated the deflection history of this laminate, as well its deflection contours after an impact of a 0.75Kg projectile with a velocity of 64 m/s. The modal response for both numerical and experimental laminates are very similar, this time presenting only a difference of 0.2ms between its periods. For the maximum central deflection, a difference of 6% is obtained, while for the offset point P1, there is a 12% of the difference. This can be better observed in the strains profiles shown in the Figs.87 and 88, where the central point P0 presents again a very nice fitting. The magnitudes of ε_{xx} and ε_{yy} are very similar to each other in both experimental and numerical results, this time not being due to a fabric ply, but to the orientation of the previous UD layer, which had a 90° offset respect to the back-ply.

Furthermore, the magnitudes of ε_{xx} and ε_{yy} at P0 are far lower than the ones obtained in the experiments, now due to the damage presented in the numerical simulation back-ply due to a big area with matrix cracking. In the case of P1, although the results were much more accurate than the ones in the previous laminate, it can be observed a big compressive strain at the beginning of the strain history of ε_{xx} compared to the numerical, while the maximum strain in tension and strain rates agrees very well. Further comparison along the strain gauges should be performed in order to discard errors in these values due to either possible errors in the DIC data, or the present numerical model.

Additional results with an un-centered projectile at the same conditions than the ones presented in the previous section subsection are presented in Fig.84. However, these are not further discussed as the conclusions are the same than the previous case, and they are shown only as a reference for the reader.
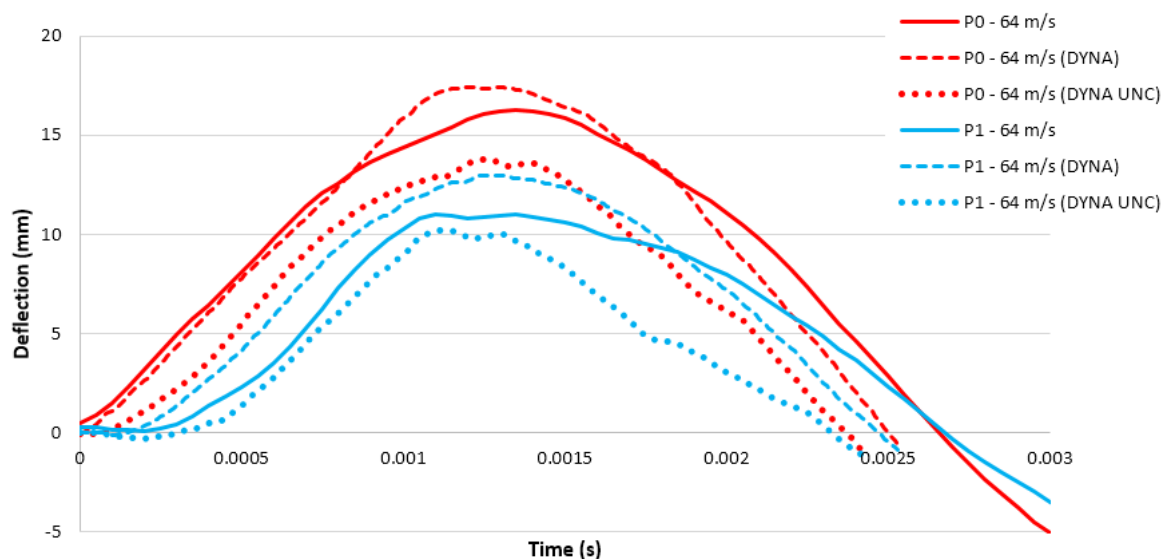
Figure 84. Experimental and numerical deflection history at 64 m/s for Lam. #2.
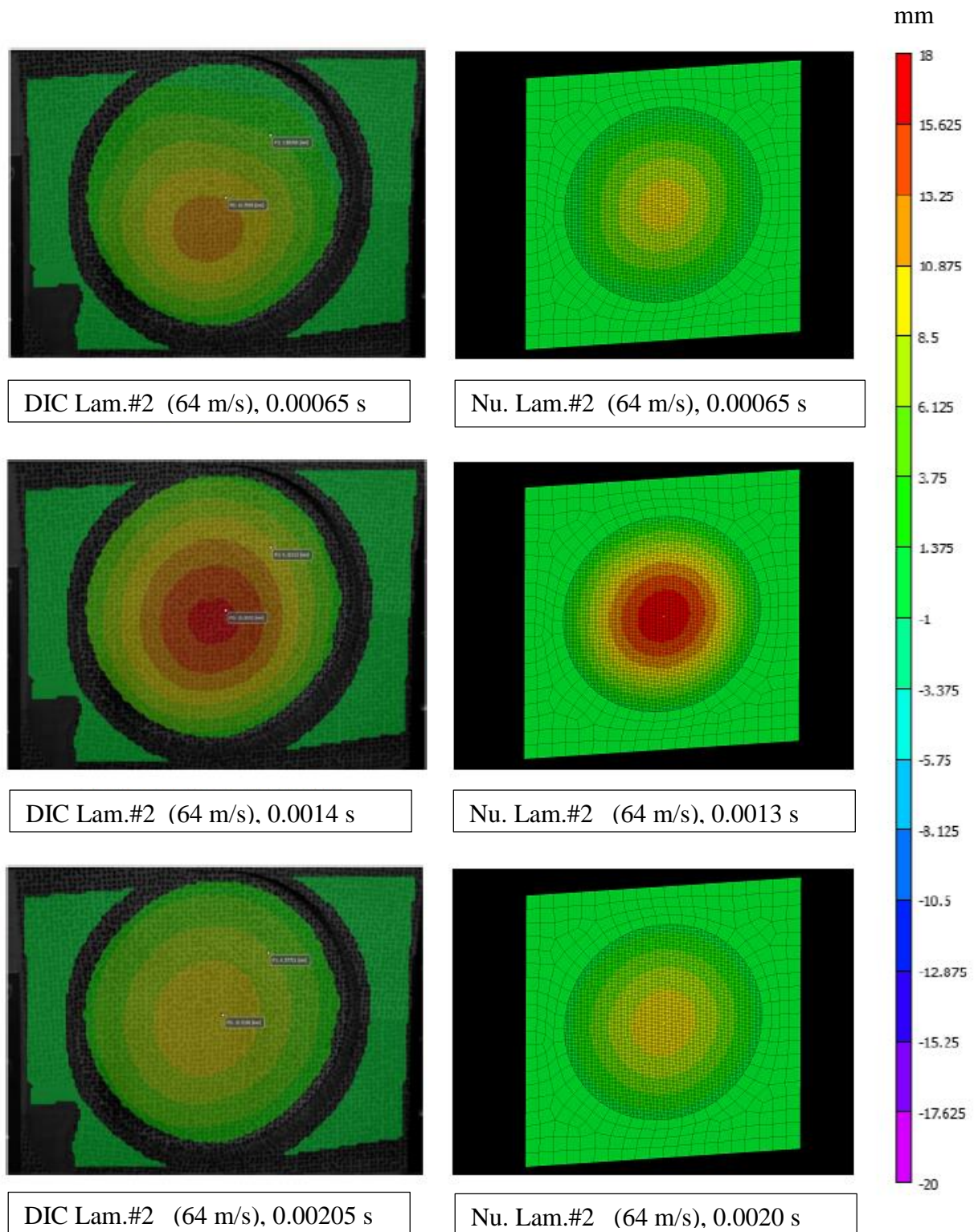
Figure 85. Deflection contours at three different instants for experimental DIC (Left column) and numerical DYNA (Right column) for Lam.#2 at 64 m/s impact.

micro strain at 45°, at the central point P0, as a function of speed impact
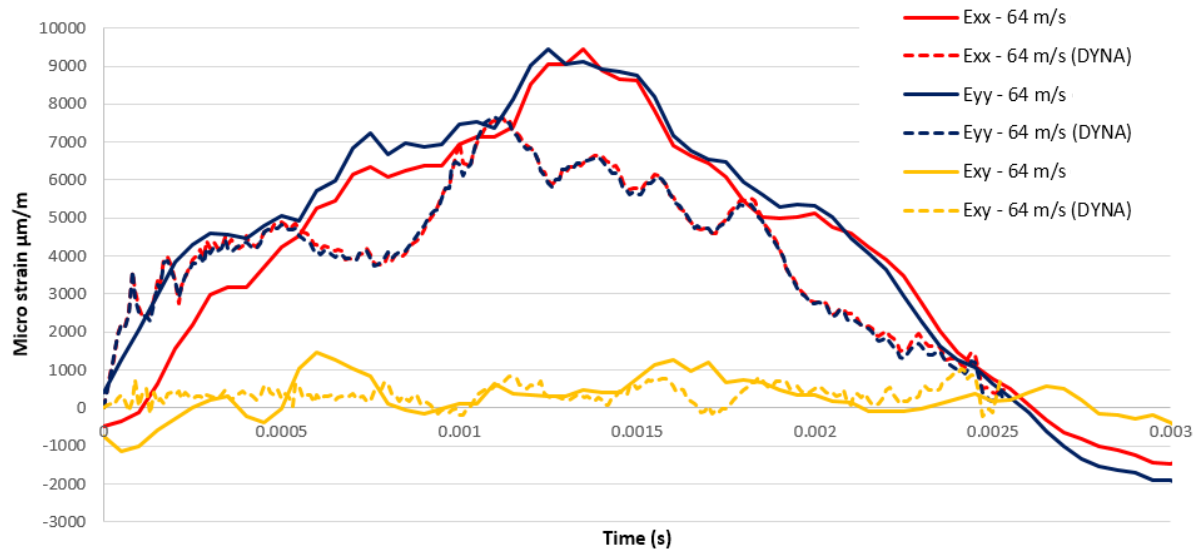
Figure 86. Experimental and numerical strains history in the fiber direction at point P0 for Lam.#2 at 64 m/s.

micro strain at 45°, at the offset point P1, as a function of speed impact
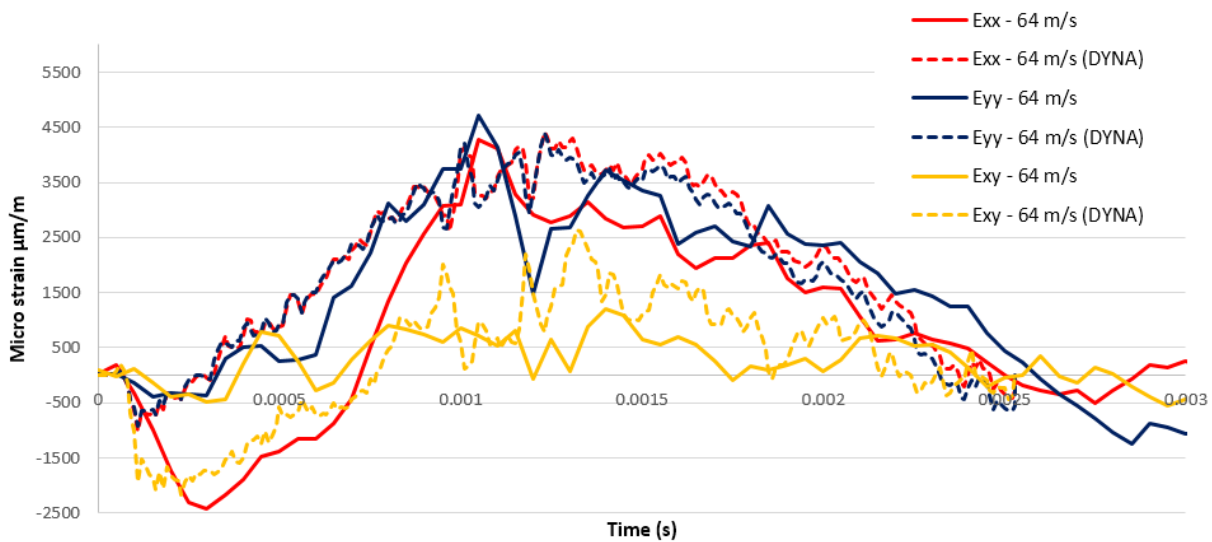
Figure 87. Experimental and numerical strains history in the fiber direction at point P1 for Lam.#2 at 64 m/s.

6.3 Laminate #3

The fiberglass laminate (Laminate #3) presented the most accurate results in terms of maximum deflection in the points P0 and P1 (5 % and 13% respectively), but was also the laminate that presented the higher difference in the modal response against the experimental tests, with a difference of almost 0.8ms in between its periods (See Figs. 88 and 89). This difference can be explained either by the overestimation of the present model in terms of intra-laminar damage, increasing this way the period of response in the numerical model, or either due to the viscoelastic behavior of the fiberglass in the experimental case, which is more susceptible to fast strain rates than the carbon fiber laminates.

In the Figs.90 and 91 are shown the history of strains at P0 and P1 locations. It can be observed that the experimental plate reaches higher strains faster than the numerical simulation. This shows that the difference in frequency should either be due to mass or initial stiffness differences, rather than stiffness increasing due to rate strain effects for similar velocities. Despite the difference in frequency between both strain graphs, the overall shape agrees very well, both presenting strain rates very similar, as well as downfalls in the strain due to the stress waves. In the Fig.90, it can be appreciated again a high initial compressive strain ε_{xx} as it happened in the previous case.
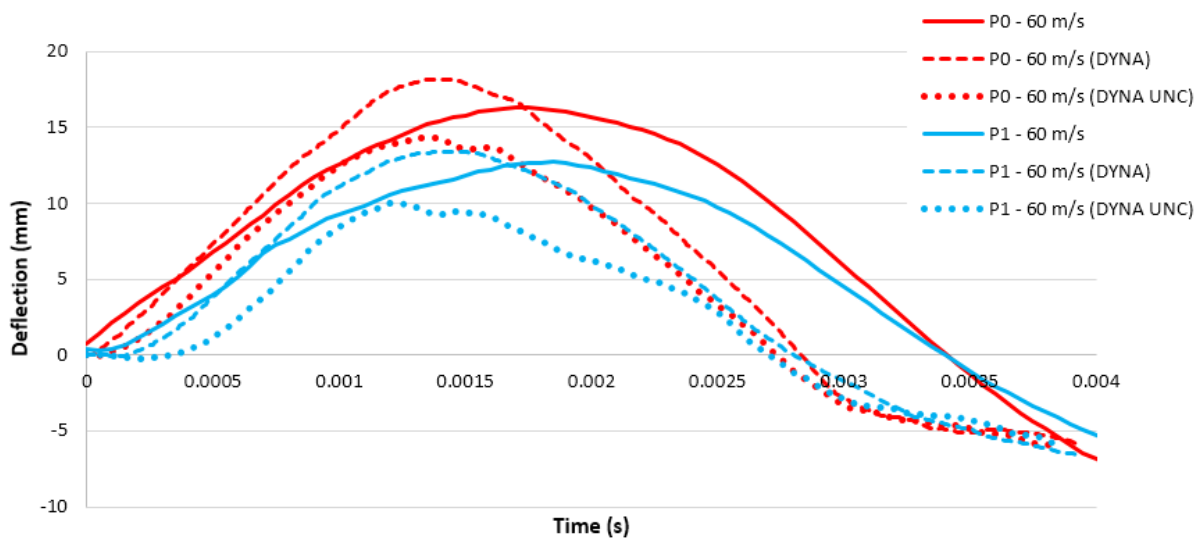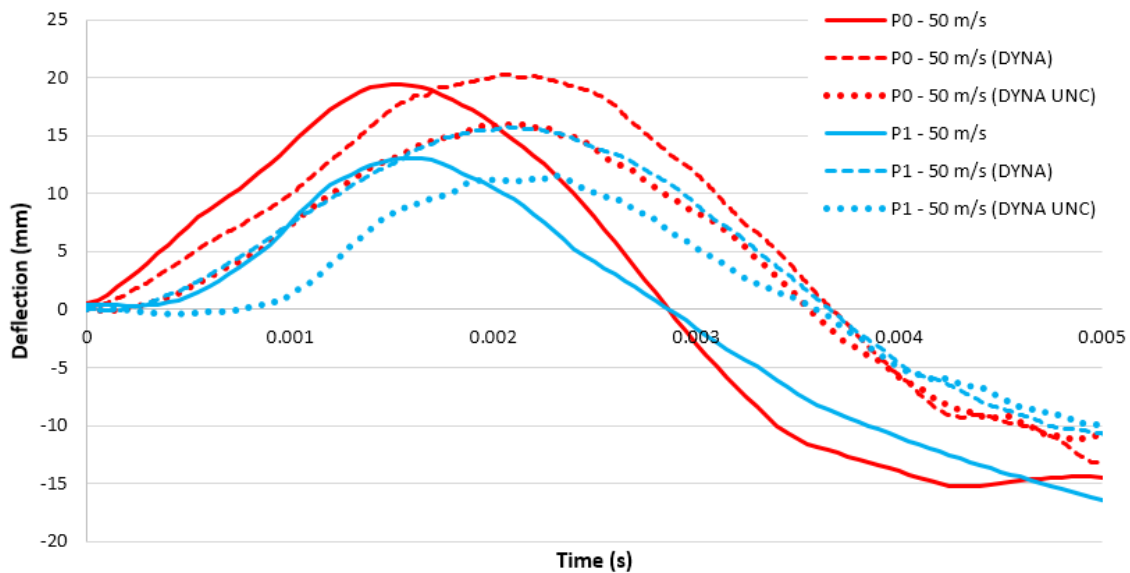

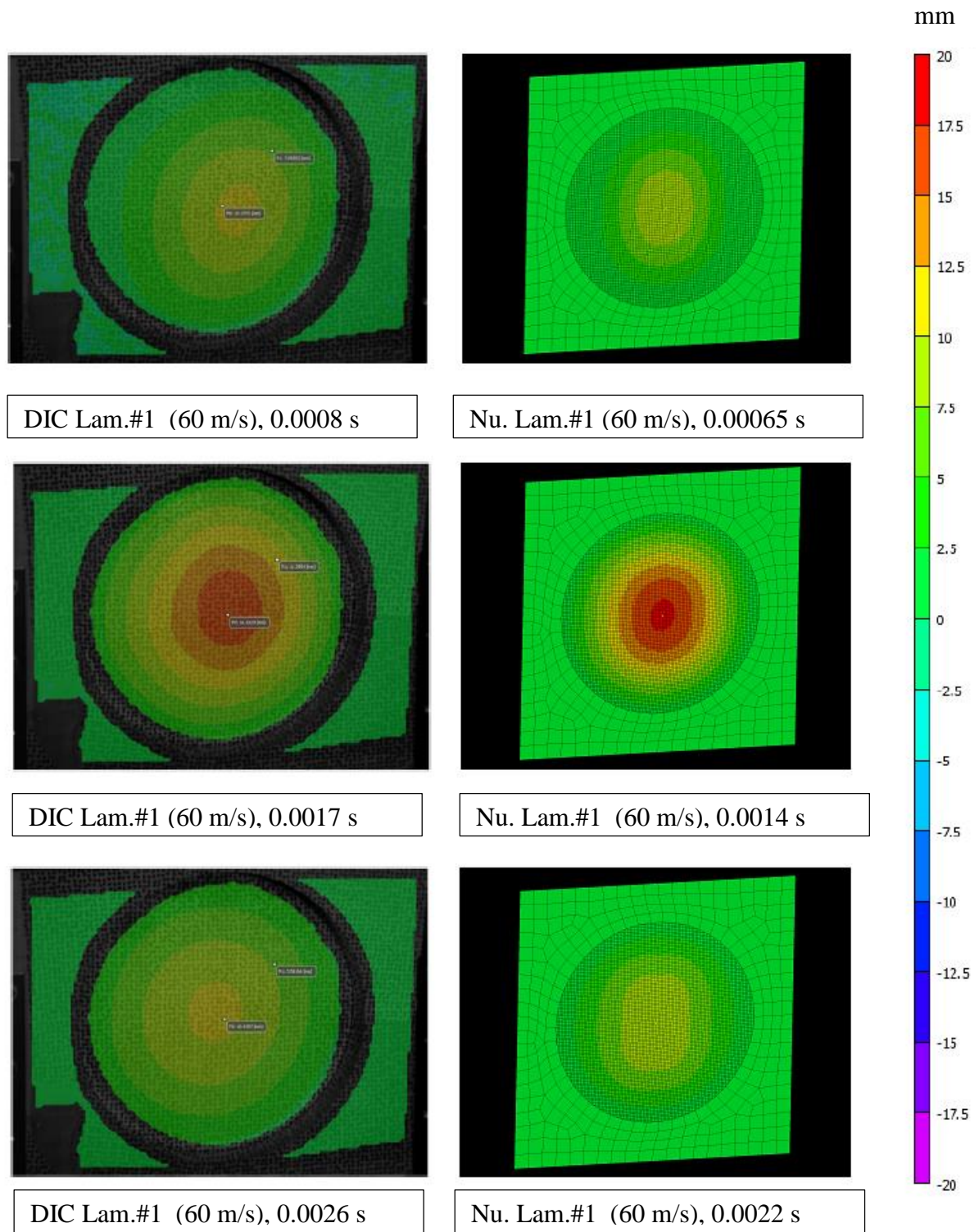**Figure 88. Experimental and numerical deflection history at 50 m/s for Lam.#3.**
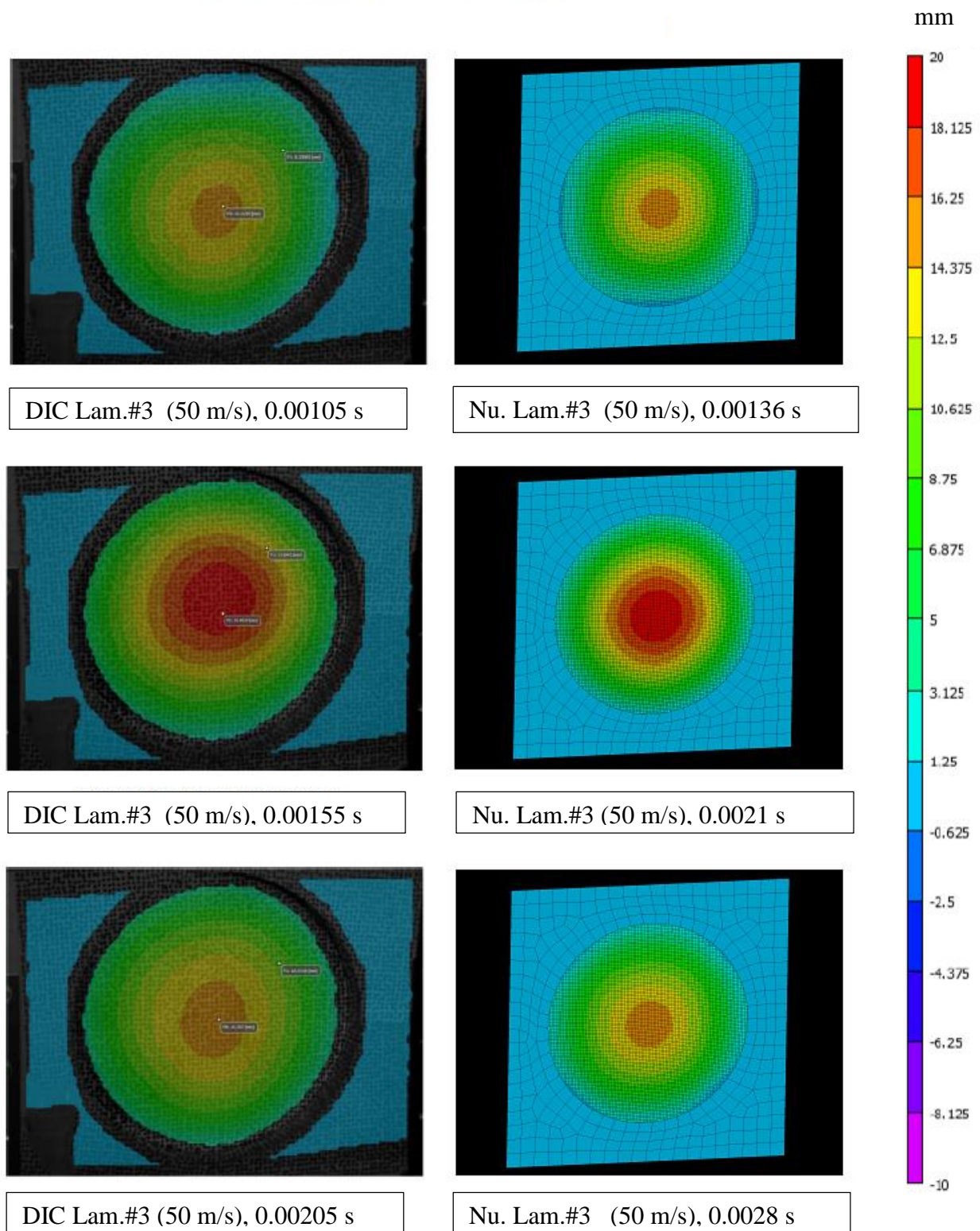
**Figure 89. Deflection contours at three different instants for experimental DIC (Left column) and
numerical DYNA (Right column) for Lam.#3 at 50 m/s impact.**

micro strain at 45°, at the central point P0, as a function of speed impact

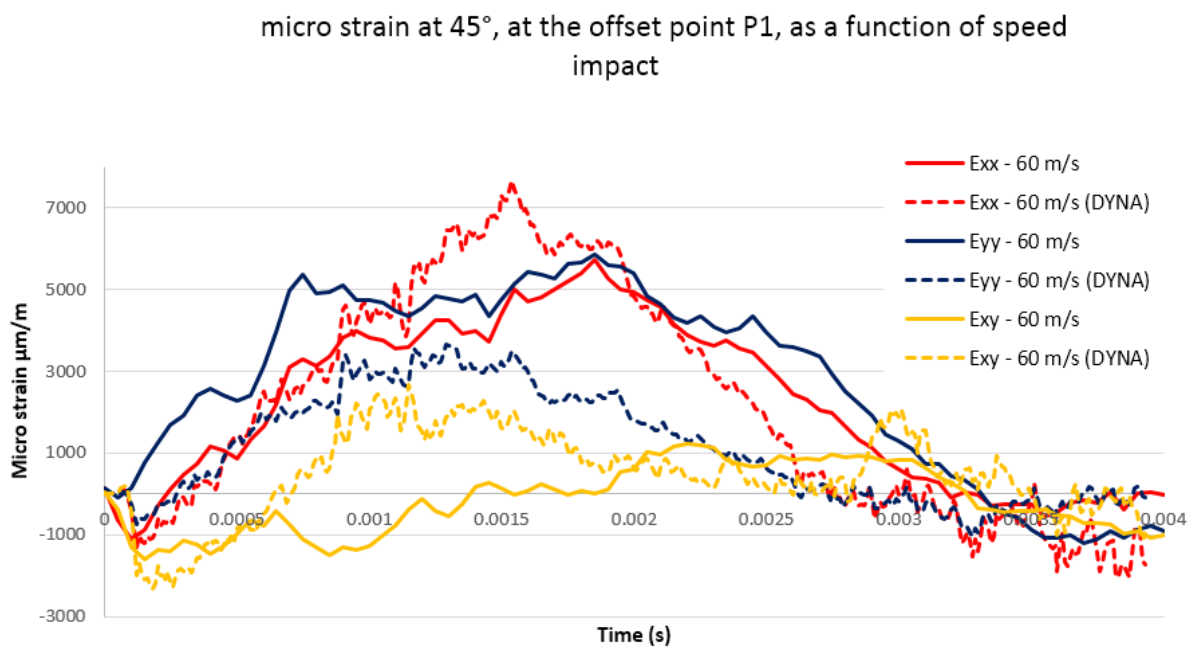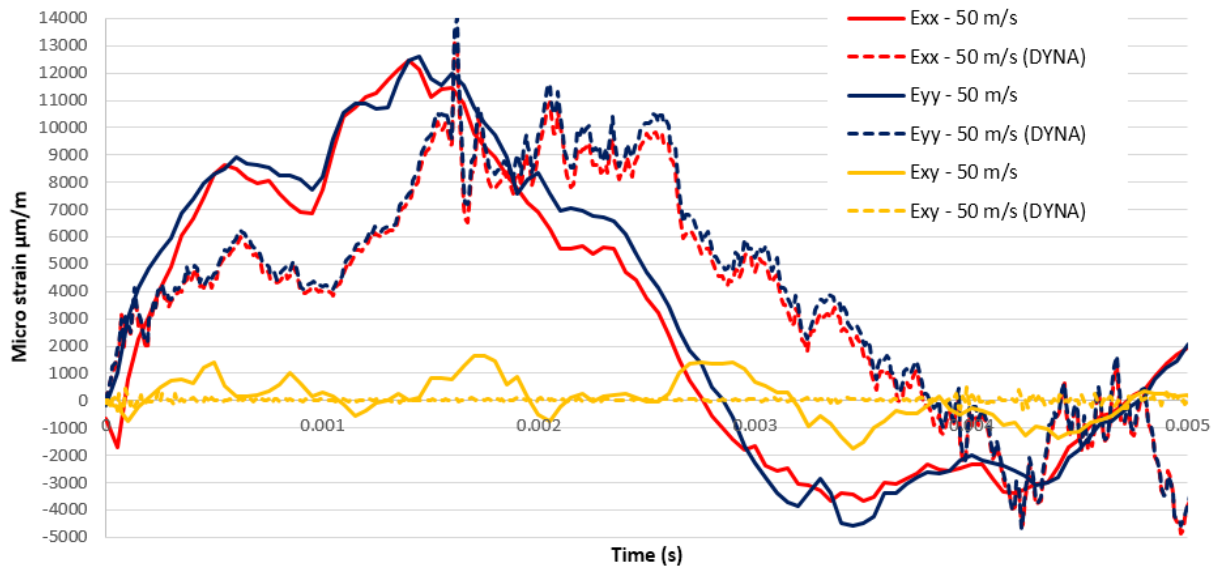**Figure 90. Experimental and numerical strains history in the fiber direction at point P0 for Lam.#3 at 50 m/s.**

micro strain at 45°, at the offset point P1, as a function of speed impact
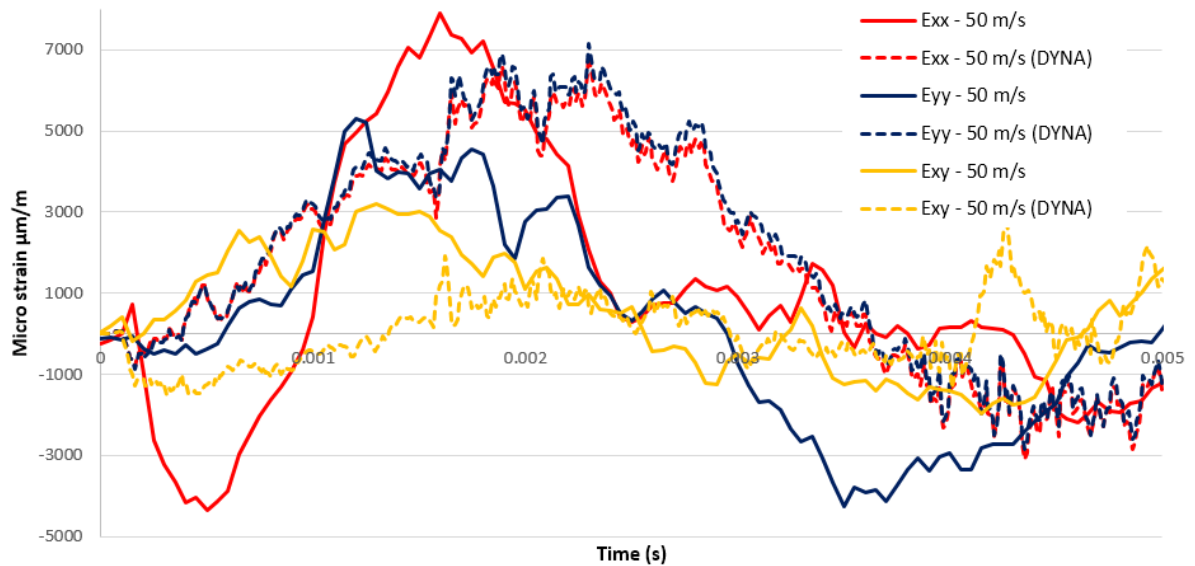
Figure 91. Experimental and numerical strains history in the fiber direction at point P1 for Lam.#3 at 50 m/s.

6.4 Further Calibration and observations

After the modifications presented in Section 9 for the fiberglass laminate (Laminate #3), and the modelling of the fabrics in the carbon fiber laminate (Laminate #1) as Unidirectional plies, the damage modes and deflection of each laminate as a function of the impact velocity was obtained (See Fig.92). This graph shows a good correlation in terms of maximum deflection with the experimental tests that have been performed at the Clement Ader Institute until the moment this Master thesis was written.

Respect to both matrix and fiber damage, a C-SCAN on the tested laminates must be carried out, therefore correlating to the results along the intra-laminar history variables obtained with LS-DYNA, subsequently performing a correct tuning of the damage parameters present in MAT 54, as discussed in Section 6. An important aspect to remark is that for all the laminates, especially the ones that present fabric plies, the modal response during the impact is not the same than the experiments, this being especially true in the case of the fiberglass laminates. No element deletion (Penetration) was observed for velocities up to 120 m/s for all the laminates, and no fiber rupture was obtained in the case of the fiberglass, which could be attributed to a dominant delamination failure in the laminate.
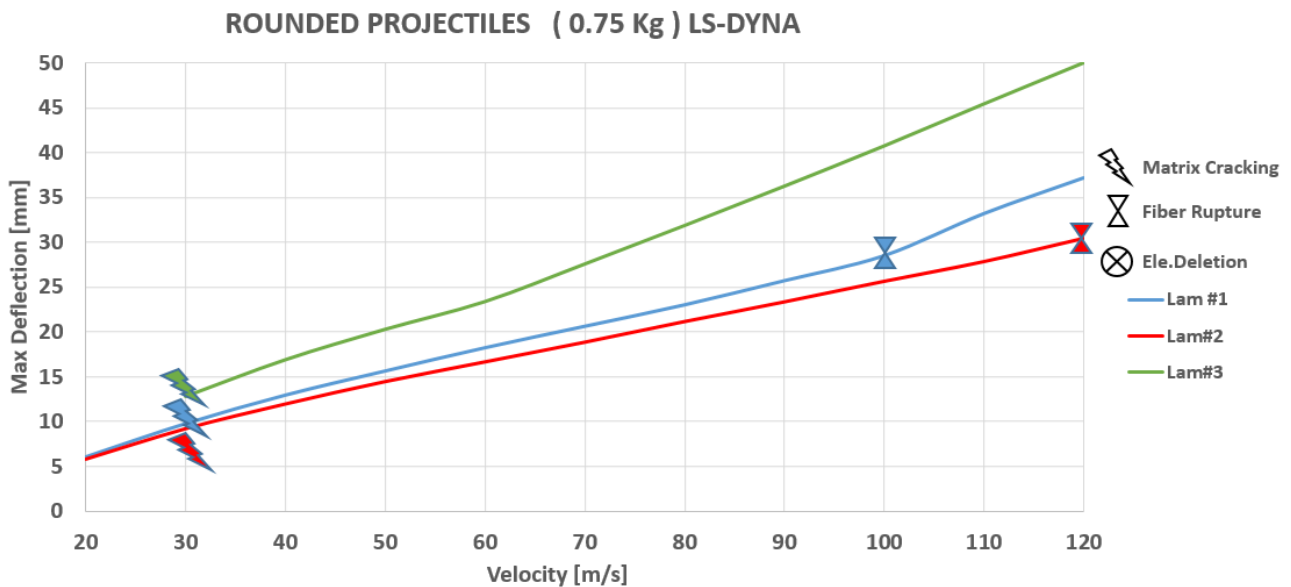
Figure 92. Maximum deflection and damage modes of laminates subjected to the impact of 0.75Kg Rounded Projectiles.
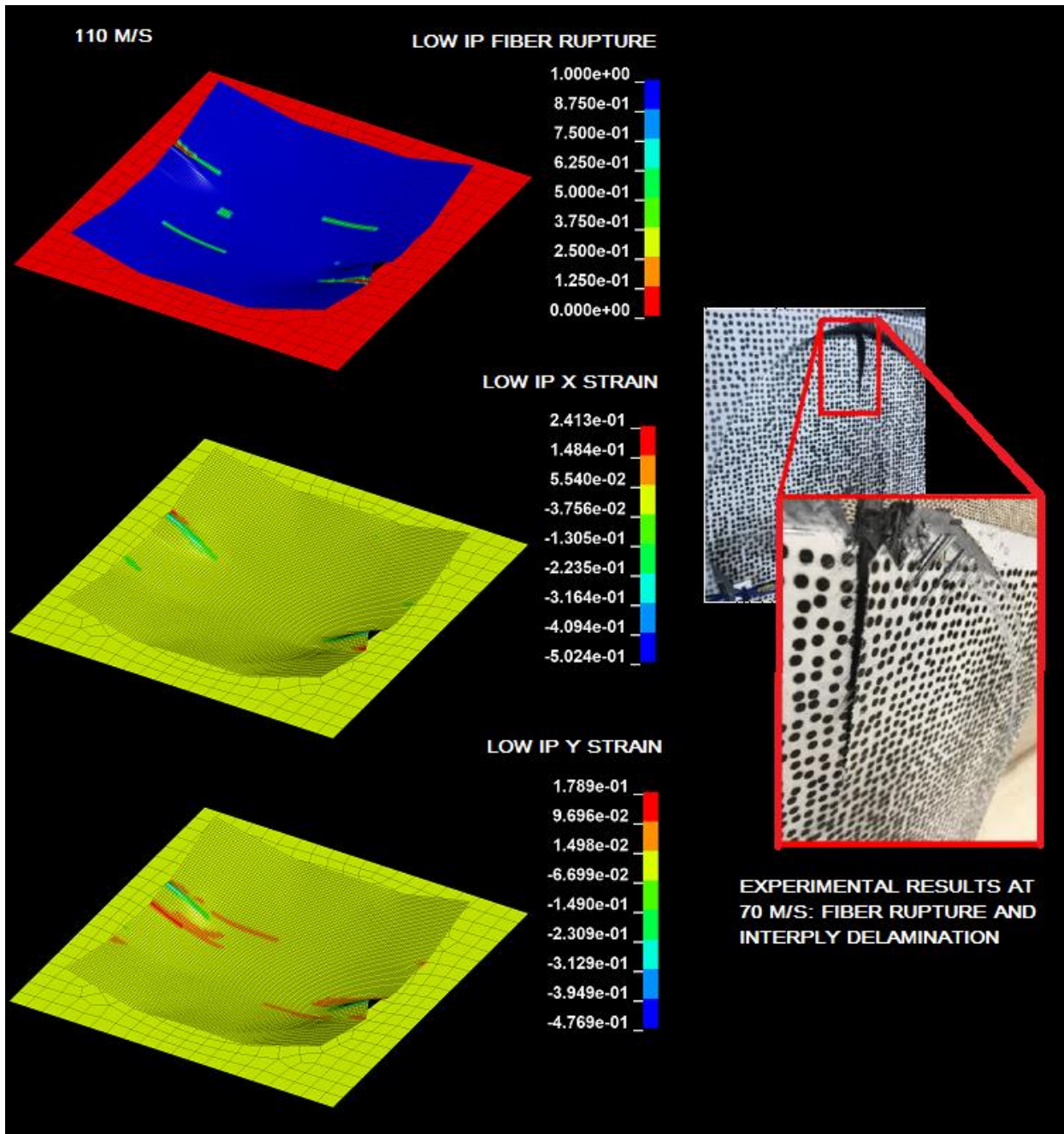
Figure 93. Fiber rupture and strain contours after the impact at 110 m/s (Left) and damage obtained during the tests after a 70 m/s impact (Right) in the back-ply of laminate #1. Photo From: G. Barlow

On the other hand, the Fig.93 shows the failure of the back-ply obtained in a laminate #1 specimen during the experimental tests campaign after an impact of 70 m/s. This case is particularly interesting because the failure begins in the outer part of the laminate instead of the center, as one would expect. With the numerical simulations, using an impact velocity of 110 m/s, a similar pattern was obtained, caused by huge tensile and compressive loads due to the folding of the laminate from the edge to the center induced the overall folding into the circle

hole. Additionally, this simulation shows that the strain rates of the laminates at velocities near to 70 m/s plays an important role, the ones that the model was only able to detect at 110 m/s, considering that the present numerical model does not include hardening by high strain rates.

A summary of the possible reasons that could have affected the strains and modal response of the laminates respect to the experimental tests are given as follows:

- Mass Variations between the real and numerical laminate and impactor, as well as differences in the initial impact location.

- Discrepancies in the stiffness of the real laminates compared to the theoretical values, which were calculated using Classic Laminate Theory along Tsai Hill Criteria. This is especially true in the case of the shear strength, which theoretical value was the elastic limit.

- Initial defects in the real plates. Although pre-impregnated materials were used during the manufacturing of these laminates, some defects were detected when an ultrasonic scanning was performed prior to the tests. These voids affect mainly the shear strength of the laminate and creates undesired stress concentration spots.

- Possible deviations in the cutting process of the real laminates, resulting in an orientation discrepancy between the real and numerical laminates.

- Inter-laminar failure of the laminates during the experiments.

- Strain rate effects of the laminates cannot be captured in the numerical model.

- Difficulties related to the DIC equipment calibration, in addition to the error associated with the capture frequency of cameras for the calculation of the strain fields from the deflection data.

11. CONCLUSIONS

Modelling a correct Hugoniot pressure is critical in soft body impacts analysis. This shockwave pressure presents a nonlinear behavior that depends on the material density, impact velocity, shock wave propagation parameters of the material, the geometry of the impactor, as well as on the thickness and material of the impacted structural member. The theory presented in the initial section of this work applies only to rigid targets, which is in good agreement against experimental results for these cases, an according to different research works. However, additional formulations need to be considered for extending the theory to flexible targets, especially in the case of multi-layered structures. As it was seen in this work, the Hugoniot pressure highly influences both Matrix cracking and Fiber Rupture thresholds.

The model developed in this work is in good agreement with Lavoie´s work respect to the material definition and ALE mesh for modelling the impactor, presenting a difference only of 8% on the Hugoniot Pressure, whereas the stagnation pressure differs only by 0.1% compared with both numerical and analytical studies. In addition, it was observed that the Hugoniot Pressure increases when the ALE mesh size is decreased. Good results were obtained with a 4mm ALE mesh, which is backed by Lavoie´s results and the theoretical impulse calculation.

A more chaotic pressure profile was observed for the elastoplastic case, which was expected due to the flexural behavior of the plate. However, accurate results were obtained when including these materials to the present model. The Hugoniot pressure decreased for the same velocity with respect to the rigid case. In addition, it was also observed that the Hugoniot pressure decreased with the increasing of the impacted plate mesh. It was found that 4 mm mesh is suitable for modelling these events in the elastoplastic case for similar projectile characteristics, and the model correlated well to the experimental tests carried out by Welsh, with less than 8% of error in terms of maximum deflection.

When modeling impact against composites plates, it is very important to take into account all damage modes for having an accurate numerical model. Although the present model only considers intra-laminar formulation using Chang-Chang criteria (due to the requirements of industrial applications for fast solution times) it seems to be a good approximation for both low and high velocity cases, in which similar deflection profiles were obtained against experimental tests found in the literature. This model allows studying the initiation and propagation of intra-laminar damage at different velocities and impacts conditions, which can help not only to

understand better the response of structures submitted to shocks but also to set up an optimal gas cannon experimental arrangement.

The model developed in the present work, for composite materials, seems to be more conservative than the numerical models that include inter-laminar damage, as well as against experimental tests. This is especially true for laminates where fabrics are used, due to uncertainties in its strength parameters, where the use of classical laminate theory is not enough. Axial coupon test of the fabric plies must be performed rather than using first ply failure criterion before implementing a damage mode approximation in order to avoid underestimations of the actual strength. Furthermore, Strain based criteria, as well as strength degradation factors, must be used in addition to Chang-Chang criteria when correlating the numerical simulations to the experiments in order to capture accurately the overall plate response.

A numerical model for studying soft body impacts against plates was developed successfully, for modelling both elastoplastic metallic plates and Intra-laminar damage in composite plates. The advantages in terms of computational cost using ALE approach compared to CEL techniques are evident: calculation times up to 1 hour are obtained when using near 200000 Eulerian elements in the ALE approach, against 3 to 4 hours that will take the CEL approach due to the increase of elements needed for modelling the entire impact domain.

12. FURTHER WORK

This work helped to understand in a general manner some of the physics occurring in both soft body impactors and composite plates tested in the experiments developed at Clement Ader institute. Because the data gathered from these experiments is still under a post-processing phase, a correlation and calibration of the current numerical model could not be performed. Therefore, is recommended for future work to use this experimental data for calibrating and correlating the numerical model against the experiments.

The current model is based on an ALE scheme due to its accuracy for capturing the impactor deformation through impact without penalizing the pressure transferred to the plate by deformation of elements, as it happens in pure Lagrangian approaches. Nevertheless, after the ALE model is calibrated against the experimental tests, an equivalent Lagrangian approach can be used and tuned accordingly in order to reduce the computational cost without compromising the accuracy of the results. SPH impactor models can be built and compared in the same manner in order to reduce the simulation times obtained so far.

This model can be improved by including Inter-laminar damage for research purposes, knowing that this approach will highly increase the computational times. However, some investigations have been focused in the simplification of these cohesive layers or tiebreak contacts through the thickness, while having the same grade of accuracy than models with complete multi layered cohesive interfaces. Nevertheless, care must be taken when using cohesive elements, as these elements reduce the bending stiffness of the laminate.

13. ACKNOWLEDGEMENTS

Firstly, I would like to thank the invaluable support and guidance of Professor Hervé Le Sourne from ICAM, who introduced me into structural dynamics problems, always explaining this subject in a very understandable way; and who was always there for helping and supporting me whenever a problem aroused during my research work. I am also really in gratitude with Yeye, Ph.D. student at ICAM/GeM Institute, for all the support and explanatory lessons about structural dynamics and LS-DYNA. I hope to have learned something from your methodical work, which will be indeed very useful in my future work.

Besides, I will be always in grateful with MECA CALCUL for allowing me to perform my internship in its facilities under the tutelage of Jean Christophe Petiteau. To him, my unconditional gratitude and admiration. Thanks for always helping and guiding me to improve the numerical models developed on this work.

None of these unique academically and personal experience would have been possible without the people of EMSHIP. I thank Professor Rigo, and all the EMSHIP staff, for giving me the opportunity to be part of this amazing program, which not only increased my professional skills but also allowed me to get know and share amazing moments with great people from across the world.

Last, but not least, my gratitude goes to my family. I will be always in debt, with whatever that controls the apparently stochastic nature of this Universe, for allowing me to be raised by such excellent parents.

This thesis was developed in the frame of the European Master Course in "Integrated Advanced Ship Design" named "EMSHIP" for "European Education in Advanced Ship Design", Ref.: 159652-1-2009-1-BE-ERA MUNDUS-EMMC.

Lucas Márquez Duque

14. REFERENCES

[1] F. A. Costanzo and W. Bethesda, "Underwater Explosion Phenomena and Shock Physics," *Proc. IMAC XXVIII*, 2010.

[2] H. U. Mair, "Hydrocodes for Structural Response," 1801.

[3] A. S, "Novel experimental and 3D multiphysics computational framework for analyzing deformation and failure of composite laminates subjected to water blasts," *Int. J. Impact Eng.*, vol. 106, pp. 223–237, 2017.

[4] R. Hedayati and M. Sadighi, *Bird Strike : An Experimental, Theoretical and Numerical Investigation*. Woodhead Publishing, 2016.

[5] J. . Wilbeck, "Impact Behavior of low strength projectiles," vol. 5, no. c, pp. 107–109, 1978.

[6] M. Lavoie, A. Gakwaya, M. Nejad Ensan, and D. G. Zimcik, "Validation of Available Approaches for Numerical Bird Strike Modeling Tools," *Int. Rev. Mech. Eng.*, vol. 1, no. 4, pp. 380–389, 2007.

[7] M.-A. Lavoie-Perrier, "Soft Body Impact Modeling and Development of a Suitable Meshless Approach," 2008.

[8] V. Goyal, C. Huertas, T. Leutwiler, J. Borrero, and T. Vasko, "Robust Bird-Strike Modeling Based on SPH Formulation Using LS-DYNA," in *47th AIAA/ASME/ASCE/AHS/ASC Structures, Structural Dynamics, and Materials Conference
 14th AIAA/ASME/AHS Adaptive Structures Conference
 7th*, 2006, no. May.

[9] R. Hedayati and S. Ziaei-Rad, "A new bird model and the effect of bird geometry in impacts from various orientations," *Aerosp. Sci. Technol.*, vol. 28, no. 1, pp. 9–20, 2013.

[10] A. Challita and J. P. Barber, "The Scaling of Bird Impact Loads," 1979.

[11] B. Wu, Z. Chen, X. Zhang, Y. Liu, and Y. Lian, "Coupled Shell-Material Point Method for Bird Strike Simulation," *Acta Mech. Solida Sin.*, vol. 31, no. 1, pp. 1–18, 2018.

[12] C. J. Welsh, "Aircraft transparency Testing - Artificial Birds technical reports arnold air force station, tennessee air force systems command," 1986.

[13] M. Hormann, U. Stelzmann, M. A. Mccarthy, and J. R. Xiao, "Horizontal Tailplane Subjected to Impact Loading," pp. 11–30, 2000.

[14] S. Heimbs and T. Bergmann, "High-velocity impact behaviour of prestressed composite plates under bird strike loading," *Int. J. Aerosp. Eng.*, no. April 2012, 2012.

[15] M. A. X. Ericsson, "Simulating Bird Strike on Aircraft Composite Wing Leading

Edge," 2012.

[16]   D. Kreculj and B. Rašuo, "Review of Impact Damages Modelling in Laminated
       Composite Aircraft Structures," vol. 3651, pp. 485–495, 1848.

[17]   J. Cheng and W. K. Binienda, "Simulation of Soft Projectiles Impacting Composite
       Targets using an Arbitrary Lagrangian-Eulerian Formulation," *J. Aircr.*, vol. 43, no. 6,
       pp. 1726–1731, 2006.

[18]   M. Staniszewski, "Simulation of Tri-axially braided composites half-cylinder behavior
       during balistic impact," 2007.

[19]   Z. Tang *et al.*, "Numerical and experimental investigation on hail impact on composite
       panels," *Int. J. Impact Eng.*, vol. 105, pp. 102–108, 2017.

[20]   S. Heimbs, S. Heller, and P. Middendorf, "Simulation of Low Velocity Impact on
       Composite Plates with Compressive Preload," *LS-DYNA Anwenderforum*, pp. 11–24,
       2008.

[21]   S. Heimbs, "Bird strike simulations on composite aircraft structures," *2011 SIMULIA
       Cust. Conf. Barcelona, Spain*, pp. 1–14, 2011.

[22]   H. Kim and K. T. Kedward, "Modeling Hail Ice Impacts and Predicting Impact
       Damage Initiation in Composite Structures," *AIAA J.*, vol. 38, no. 7, pp. 1278–1288,
       2000.

[23]   A. Blair, "Aeroengine Fan Blade Design Accounting for Bird Strike," *Ind. Eng.*, no.
       March, 2008.

[24]   M. Souli and D. J. (David J. . Benson, *Arbitrary Lagrangian-Eulerian and fluid-
       structure interaction : numerical simulation*. 2010.

[25]   C. A. Huertas-ortecho, "Robust Bird-strike Modeling Using LS-DYNA," University of
       Puerto Rico, 2006.

[26]   S. Heimbs, "Computational methods for bird strike simulations: A review," *Computers
       and Structures*, vol. 89, no. 23–24. Elsevier Ltd, pp. 2093–2112, 2011.

[27]   S. Shankar and M. M. Mayuram, "Effect of strain hardening in elastic-plastic transition
       behavior in a hemisphere in contact with a rigid flat," *Int. J. Solids Struct.*, vol. 45, no.
       10, pp. 3009–3020, 2008.

[28]   L. Olovsson, M. Souli, and I. Do, "LS-DYNA -ALE Capabilities." .

[29]   J. Day, I. Do, and J. Farstad, "Guidelines for ALE Modeling in LS-DYNA," no. July,
       2009.

[30]   D. Gay, *Composite Materials*, Third edit. CRC Press, 2015.

[31]   M. V Donadon, S. F. M. De Almeida, I. T. De Aeronáutica-ita, S. José, and S. Paulo,

Damage Modeling in Composite Structures, vol. 2. Elsevier, 2014.

[32]   Elsevier, "World wide failure exercise on failure prediction in composites," *Compos. Sci. Technol.*, 2002.

[33]   F. Paris and K. E. Jackson, "A Study of Failure Criteria of Fibrous Composite Materials," *NASA/Technical Publ.*, no. March, p. 76, 2001.

[34]   Ever J. Barbero, "Introduction to Composite Materials Design." Taylor and Francis, p. 336, 1999.

[35]   N.-Z. Chen and C. Guedes Soares, "Ultimate strength and reliability of composite material structures," *Mar. Technol. Eng.*, no. January 2011, 2011.

[36]   F. K. Chang and K. Y. Chang, "A Progressive Damage Model for Laminated Composites Containing Stress Concentrations," *J. Compos. Mater.*, vol. 21, no. 9, pp. 834–855, 1987.

[37]   L. S. Technology, *LS-DYNA Theory Manual*. 2006.

[38]   Z. Hashin *et al.*, "Failure Criteria for Unidirectional FibreComposites," *Compos. Sci. Technol.*, vol. 69, no. 5, pp. 683–706, 2015.

[39]   A. Tabiei, "Modelisation des Materiaux Composites." LSTC, 2017.

[40]   M. Andersson and P. Liedberg, "Crash behavior of composite structures - A CAE Benchmarking Study," 2014.

[41]   B. Wade, P. Feraboli, and M. Osborne, "Simulating Laminated Composites Using LS-DYNA Material Model MAT54 Part I : [0] and [90] Ply Single-Element Investigation," 2012.

[42]   A. F. Johnson and M. Holzapfel, "Modelling soft body impact on composite structures," *Compos. Struct.*, vol. 61, no. 1–2, pp. 103–113, 2003.

[43]   OASYS, "Inter-laminar material modelling in LS-DYNA." .

[44]   M. Osborne, "Single-Element Characterization of the LS-DYNA MAT54 Material Model," 2012.

[45]   L. Daudeville and P. Ladevèze, "A damage mechanics tool for laminate delamination," *Compos. Struct.*, vol. 25, no. 1–4, pp. 547–555, 1993.

[46]   A. F. Johnson, A. K. Pickett, P. Rozycki, A. F. Johnson, A. K. Pickett, and P. Rozycki, "Computational methods for predicting impact damage in composite structures To cite this version : HAL Id : hal-01005986 Computational methods for predicting impact damage in composite structures," 2017.

[47]   M. A. Lavoie, A. Gakwaya, M. N. Ensan, D. G. Zimcik, and D. Nandlall, "Bird's substitute tests results and evaluation of available numerical methods," *Int. J. Impact Eng.*, vol. 36, no. 10–11, 2009.

[48]   Autodesk, "Von Mises material Properties." [Online]. Available:
http://download.autodesk.com/us/algor/userguides/mergedprojects/setting_up_the_anal
ysis/nonlinear/materials/von_Mises_Material_Properties.htm. [Accessed: 01-Dec-
2018].

[49]   y. p. sone oo, "development of analytical formulae to analyse the submerged composite
structural response subjected to an underwater explosion," p. 20, 2018.

[50]   M. Stec, "Modeling Fatigue Failure in Elasto-plastic Materials," 2016. [Online].
Available: https://www.comsol.com/blogs/modeling-fatigue-failure-in-elastoplastic-
materials/. [Accessed: 25-Nov-2018].

[51]   M. Stec, "STIMPACT laboratoire" 2016. [Online]. Available: http://www.insa-
toulouse.fr/fr/institution/listedeslabos.html [Accessed: 25-Nov-2018].

15. APPENDICES

15.1 MECHANICAL PROPERTIES

15.1.1 Mechanical characteristics of fibers

Physical properties at 23°C	Units	E glass	T700 Carbon
Density	kg/m3	2540	1800
Axial thermal expansion	µm/m/°C	5.3	0.38
Transverse thermal expansion	µm/m/°C	5.3	5.5
Axial Young modulus	MPa	73000	235000
Axial Poisson ratio		0.22	0.22
Transverse Young modulus	MPa	73000	18700
Transverse Poisson ratio		0.22	0.25
Axial shear modulus	MPa	29900	13800
Transverse shear modulus	MPa	29900	6890
Tensile strength	MPa	1916	3780
Compressive strength	MPa	1155	2450
Shear strength	MPa	1155	1790

15.1.2 Mechanical characteristics of the matrix

Physical properties at 23°C	Units	Epoxy
Density	kg/m3	1200
Glass transition temperature	°C	120
Thermal expansion	µm/m/°C	68
Young modulus	MPa	3200
Poisson ratio		0.37
Tensile strength	MPa	74.4
Compressive strength	MPa	126.5
Shear strength	MPa	43.0

15.1.3 Mechanical characteristics of plies

Type	Units	UD	UD	Biaxial	Biaxial
Matrix		Epoxy	Epoxy	Epoxy	Epoxy
Fiber		T700 Carbon	E glass	T700 Carbon	E glass
Fiber mass fraction		67.4%	63.0%	67.4%	63.0%
Volume fiber fraction		58.0%	44.1%	58.0%	44.1%
Density	kg/m^3	1548	1779	1548	1779
Thickness for 100g/m²	mm	0.096	0.089	0.096	0.089
Stiffness					
Young Modulus X	MPa	137665	34142	73617	22268
Young Modulus Y	MPa	8983	10043	73617	22268
Young Modulus Z	MPa	8983	10043	8983	10043
Shear Modulus XY	MPa	3662	3032	3662	3032
Shear Modulus XZ	MPa	3662	3032	3440	3284
Shear Modulus YZ	MPa	3243	3582	3440	3284
Poisson Ratio XY		0.281	0.297	0.034	0.135
Poisson ratio XZ		0.281	0.297	0.287	0.321
Poisson Ratio YZ		0.385	0.402	0.287	0.321
Strength					
Tensile strength X	MPa	2214.4	896.1	388	125
Compressive strength X	MPa	1030.1	579.2	662	213
Tensile strength Y	MPa	47.5	56.1	388	125
Compressive strength Y	MPa	80.7	95.3	662	213
Tensile strength Z	MPa	47.5	56.1	47.5	56.1
Compressive strength Z	MPa	80.7	95.3	80.7	95.3
Shear strength XY	MPa	25.6	32.3	25.6	32.3
Shear strength XZ	MPa	25.6	32.3	25.6	32.3
Shear strength YZ	MPa	25.6	32.3	25.6	32.3

15.2 LAMINATES

15.2.1 Laminate # 1 (CFRP/EPOXY)

# Layer	Type of ply	Orientation	Fiber weight (g/m²)
1	biaxial T700 carbon	+/-45	300
2	UD T700 carbon	0	300
3	UD T700 carbon	0	300
4	UD T700 carbon	0	300
5	biaxial T700 carbon	+/-45	300
6	UD T700 carbon	0	300
7	UD T700 carbon	0	300
8	UD T700 carbon	0	300
9	UD T700 carbon	90	300
10	UD T700 carbon	90	300
11	UD T700 carbon	90	300
12	UD T700 carbon	90	300
13	UD T700 carbon	0	300
14	UD T700 carbon	0	300
15	UD T700 carbon	0	300
16	biaxial T700 carbon	+/-45	300
17	UD T700 carbon	0	300
18	UD T700 carbon	0	300
19	UD T700 carbon	0	300
20	biaxial T700 carbon	+/-45	300

Theoretical thickness	5.76	mm

15.2.2 Laminate # 2 (CFRP/EPOXY)

# Layer	Type of ply	Orientation	Fiber weight (g/m²)
1	UD T700 carbon	45	300
2	UD T700 carbon	-45	300
3	UD T700 carbon	0	300
4	UD T700 carbon	90	300
5	UD T700 carbon	45	300
6	UD T700 carbon	-45	300
7	UD T700 carbon	0	300
8	UD T700 carbon	90	300
9	UD T700 carbon	45	300
10	UD T700 carbon	0	300
11	UD T700 carbon	90	300
12	UD T700 carbon	-45	300
13	UD T700 carbon	90	300
14	UD T700 carbon	0	300
15	UD T700 carbon	-45	300
16	UD T700 carbon	45	300
17	UD T700 carbon	90	300
18	UD T700 carbon	0	300
19	UD T700 carbon	-45	300
20	UD T700 carbon	45	300

Theoretical thickness	5.76	mm

Lucas Márquez Duque

15.2.3 Laminate # 3 (GFRP/EPOXY)

# Layer	Type of ply	Orientation	Fiber weight (g/m²)
1	Biaxial E glass	0/90	600
2	Biaxial E glass	0/90	600
3	Biaxial E glass	0/90	600
4	Biaxial E glass	0/90	600
5	Biaxial E glass	0/90	600
6	Biaxial E glass	0/90	600
7	Biaxial E glass	0/90	600
8	Biaxial E glass	0/90	600
9	Biaxial E glass	0/90	600
10	Biaxial E glass	0/90	600
11	Biaxial E glass	0/90	600
12	Biaxial E glass	0/90	600
13	Biaxial E glass	0/90	600
14	Biaxial E glass	0/90	600
15	Biaxial E glass	0/90	600

Theoretical thickness	8.01	mm

15.2.4 Laminate # 3 (GFRP UD/EPOXY)

# Layer	Type of ply	Orientation	Fiber weight (g/m²)
1	UD E Glass	0	150
2	UD E Glass	90	150
3	UD E Glass	0	150
4	UD E Glass	90	150
5	UD E Glass	0	150
6	UD E Glass	90	150
7	UD E Glass	0	150
8	UD E Glass	90	150
9	UD E Glass	0	150
10	UD E Glass	90	150
11	UD E Glass	0	150
12	UD E Glass	90	150
13	UD E Glass	0	150
14	UD E Glass	90	150
15	UD E Glass	0	150
16	UD E Glass	90	150
17	UD E Glass	0	150
18	UD E Glass	90	150
19	UD E Glass	0	150
20	UD E Glass	90	150
21	UD E Glass	0	150
22	UD E Glass	90	150
23	UD E Glass	0	150
24	UD E Glass	90	150
25	UD E Glass	0	150
26	UD E Glass	90	150
27	UD E Glass	0	150
28	UD E Glass	90	150
29	UD E Glass	0	150
30	UD E Glass	90	150

Theoretical thickness	8.01	mm

15.3. VALIDATION: LOW VELOCITY COMPOSITE PLATE IMPACT: HEIMBS´S MODEL

Some works can be found in the literature about the analytical and numerical modelling approaches of the response of composite structures to Underwater Explosions. However, the use of ALE or SPH methods for modelling the events of Soft Body Impact has been limited to the Aeronautical industry, and few references can be found in the case of ALE impactors modelling against CFRP plates [17], [14], [13].

It was decided that the work of Heimbs would be used as reference [20] when including composite materials on the model, due to its extensive research on the field and experimental validation of its numerical models. Although in this work [20] an ALE formulation was not implemented, the use of rigid impactors at low velocity will conduce to faster simulation results. This would allow studying in a more optimal manner how accurate LS-DYNA composite material models are with respect to the initiation of damage modes, this way analyzing the most sensible parameters in the composite models and calibrating them before implementing it in long ALE simulations.

In the work of Heimbs [20], a drop tower with a hemispherical steel impactor of 1.85 Kg mass was used to impact a composite plate (CFRP) with compressive preloading and without it, keeping the impact level energy constant at 40 J. The response of the plate was measured using strain gauges as shown in Fig.94, comparing it later with a numerical model in which a rigid steel sphere was modeled and impacted at the same experimental energy level (40 J). The CFRP laminate finite element mesh was build using cohesive elements for modelling inter-laminar damage, while the Chang-Chang damage model was used for including the intra-laminar damage.
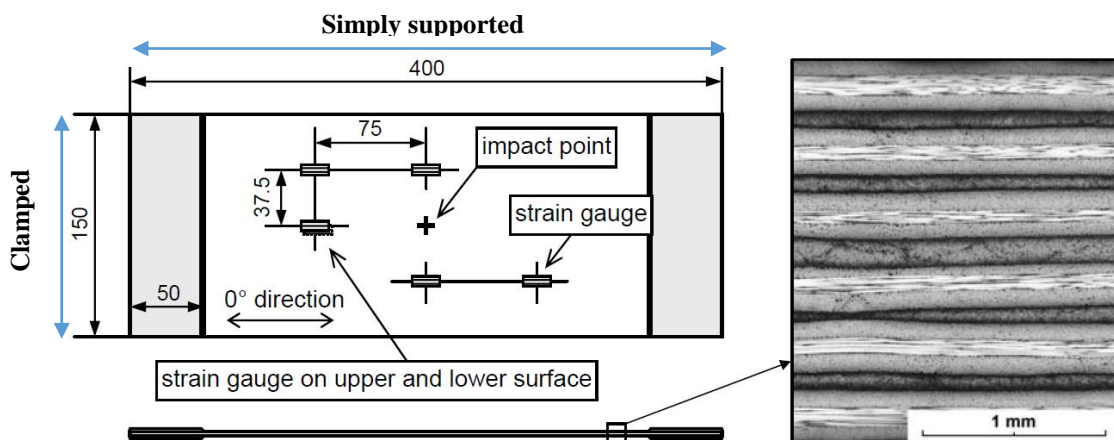
Figure 94. Dimensions and array of impact specimens and micrograph of composite laminate. Dimensions given in mm. From: [20]

CONTACT FORCE / COMPOSITE PLATE-RIGID BALL
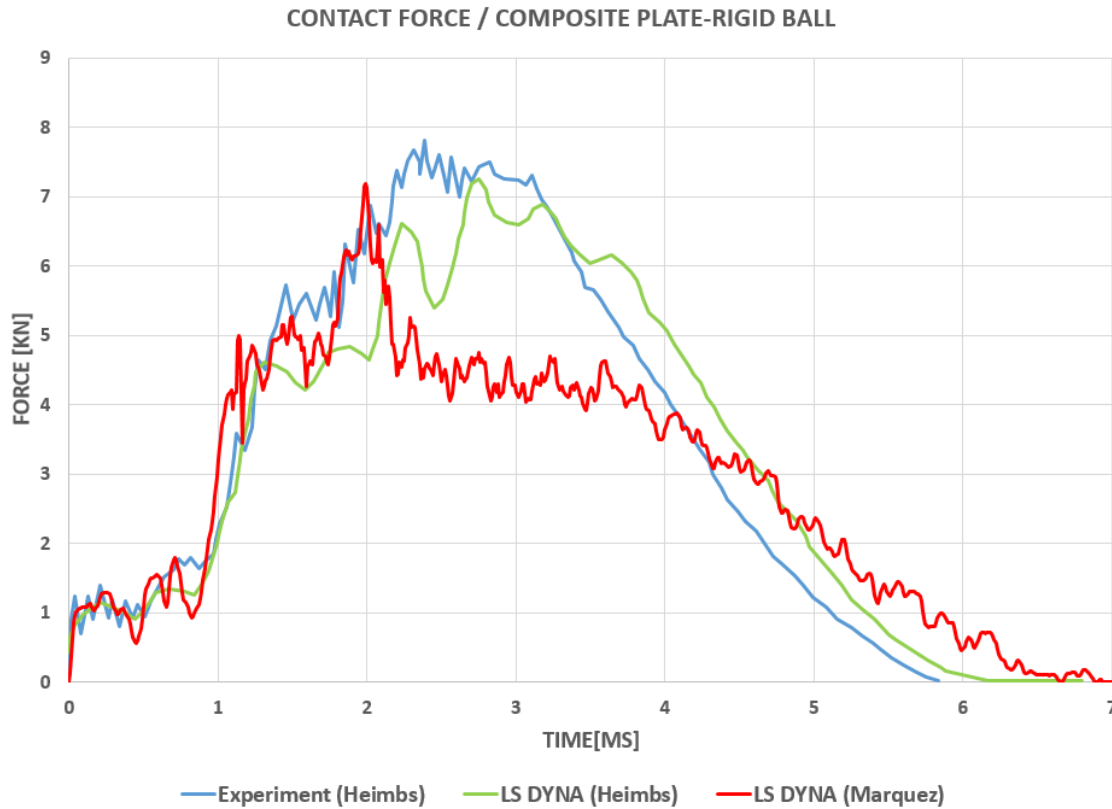
Figure 95. Contact Force between the composite plate and rigid impactor.

In the present work, the same impact energy, mesh and material characteristics of the work of Heimbs were used. However, the plate was modeled using the Single Element Shell technique, using Fully Integrated Shell Elements along with a pure intra-laminar failure material model, not being capable to include inter-laminar damage failure. The material model used for this simulation was MAT_ENHANCED_COMPOSITE_DAMAGE. As explained in Section 5.2, this material can be based in either Chang-Chang or Tsai Wu criteria for matrix failure. In the frame of this simulation, Chang-Chang criterion was used.

The properties of the CFRP prepreg were extracted from [20]. The tested laminate is symmetrical, composed of 24 plies with the following stacking sequence:

$$[-45°/0°/45°/90°]_{3s}$$

One of the main goals in the work of Heimbs was to study the response of a composite laminate when a compressive preload was defined, in addition to the impact load. However, it is presented some numerical simulations without including compressive preloading and its correspondent experimental tests, these ones being used to compare the model developed in the present work
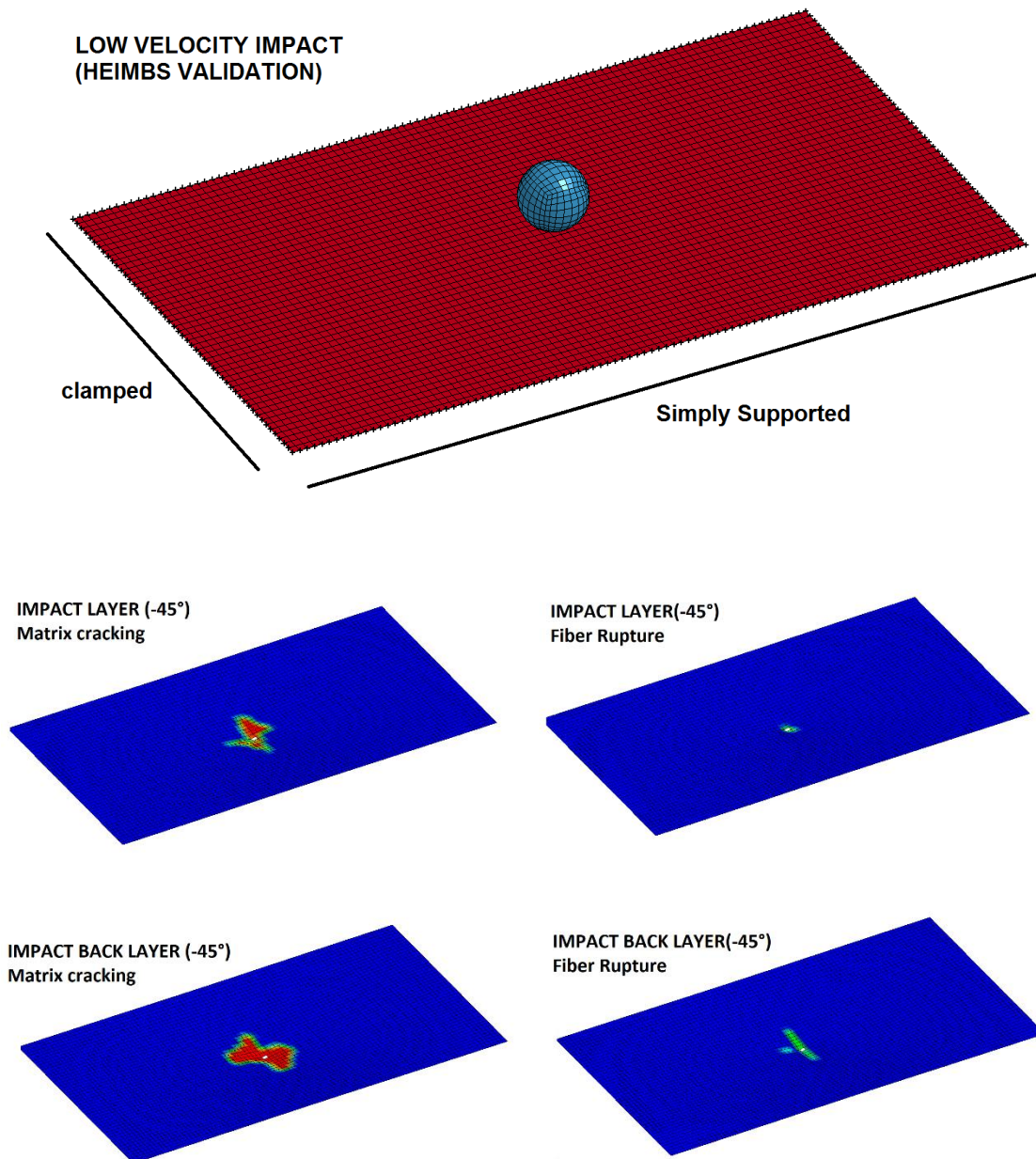
Figure 96. Numerical model developed in LS-DYNA for Heimbs Validation. Top: Boundary conditions for the composite plate. Down: Fiber and Matrix failure history variables for first and last ply at the first element deletion.

In Figs. 95, 96 and 97 are shown the results obtained for the composite plate impact. The contact forces were compared with the experimental and numerical results given by Heimbs. Although the maximum interface forces obtained were near the same than the reference results, it can be observed that the curve decreases faster after 2ms in the present work, decreasing even more abruptly after 2.3ms. This corresponds to the moment at which the laminate suffers it first element deletion, not due to fiber rupture in all layers, but for the limiting strains that were defined in the model (DFAIL). This behavior was expected, as the energy is dissipated only by

intra-laminar damage, being bigger in comparison with Heimbs model where the inter-laminar damage is also accounted for. In Fig.101, the eroded IE causing this force dropping is shown.

The history variables (damage) for the first and last plies at the first deleted element are shown in the Fig.99. It should be noted that even when the failure criteria have a logical conditional rule, that is, the element either fail or do not fail, some green contours could be observed near to the failed elements (See Fig.96). This transition is because the shell elements in this simulation are fully integrated, which means that the stresses are calculated in four gauss point per integration point per element. Therefore, the element will only fail (red contours) when all its Gaussian points have failed. As expected, there is a bigger failure in matrix tension for the back-ply (face submitted to tension), whereas the first ply is failed due to matrix crushing. On the other hand, there is a concentration of stresses near to first deleted element, which is probably causing the other elements failure in that direction by inducing a stress concentration (unbuttoning).
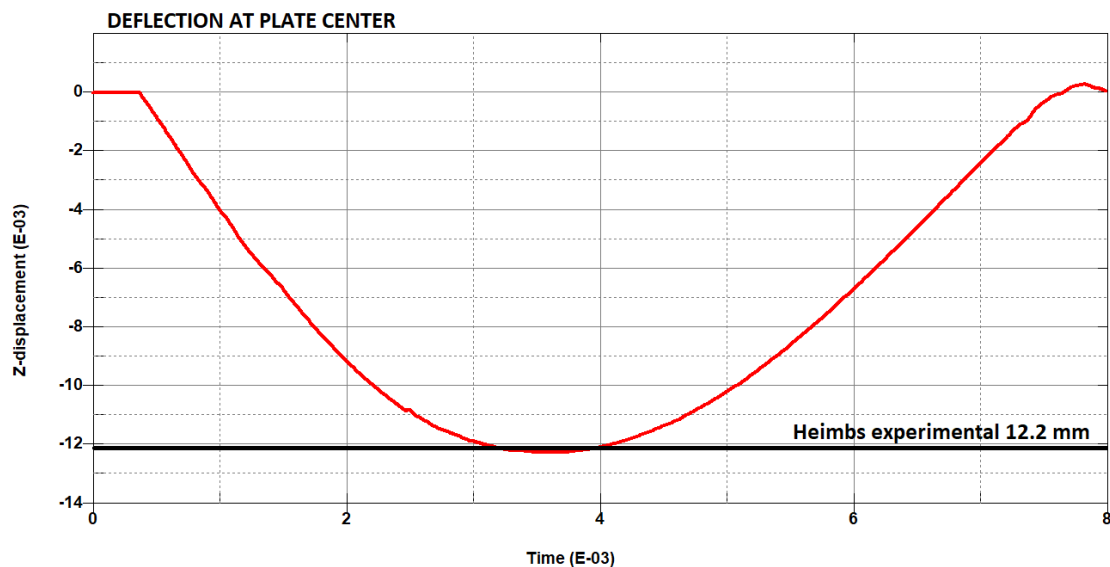
Figure 97. Deflection profile at the center of the composite plate.

Comparing the maximum deflection against Heimbs work, there is a discrepancy less than 1%. In the Fig.97 can be seen the deflection time history at the center of the plate. An elastic response can be observed, although there is remaining internal energy in the plate due to both fiber and matrix failures. It can be said from these results that the response of a plate in the present model gives accurate results in terms of maximum deflection compared to both Heimbs experimental and numerical model for low velocities, the last one including inter-laminar damage.
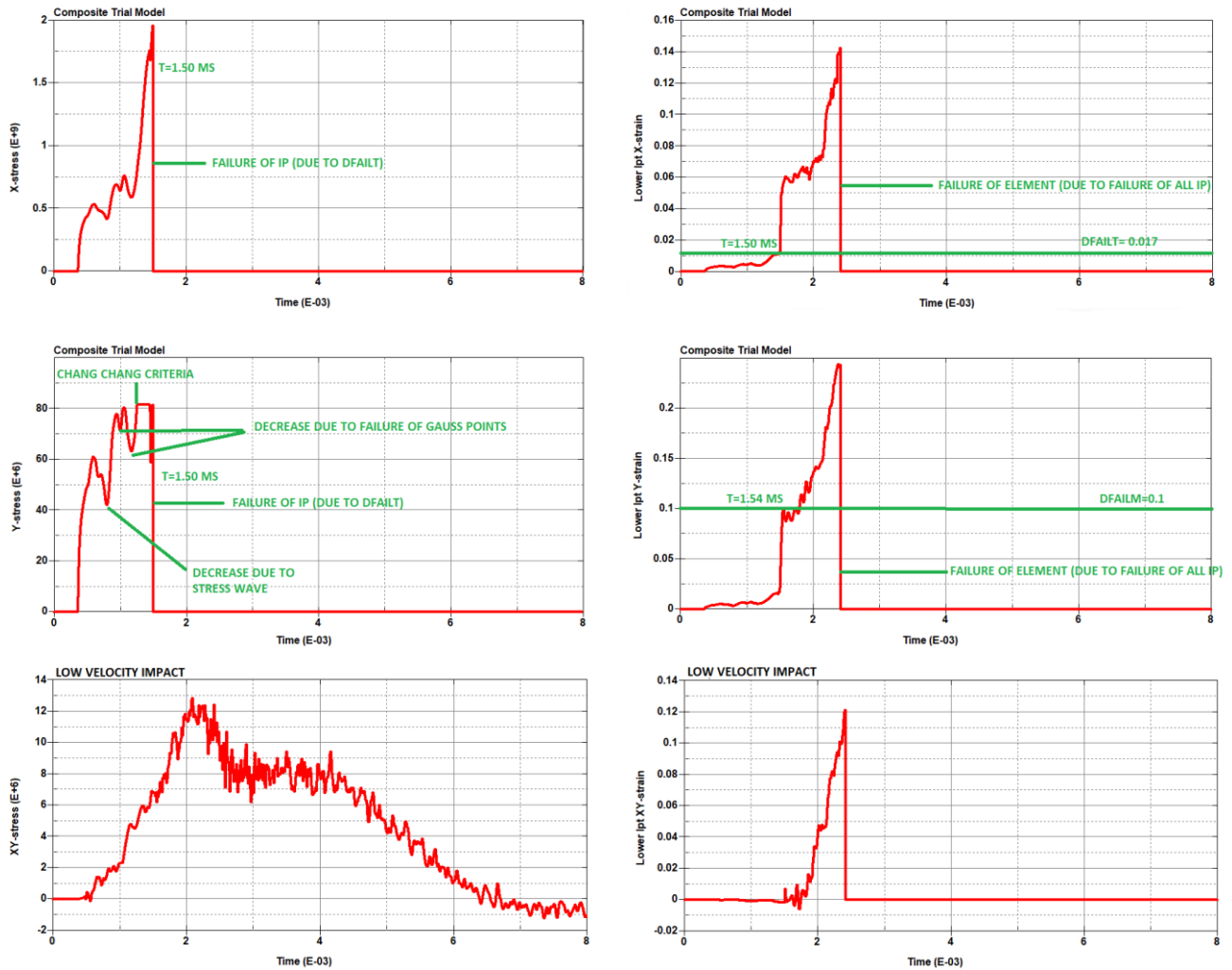
Figure 98. Stress and Strain graphs for first Integration point (Back layer) in the first element deleted.

Although, it has to be in mind that this is true as delamination does not dissipate much energy for these conditions, which is not always the case for high velocity impacts.

In Fig. 98 can be observed the behavior of the first integration point (IP) through the thickness (back-layer) at the first element deleted through the impact. The stresses in both X and Y directions (fiber and transverse direction respectively) increases in tension up to a sudden failure, which was expected because of its location on the back of the plate.

For the Y-stress (transverse direction), we can observe an initial downfall of the stress which is caused by a stress wave. Subsequently, the stress keeps rising up to a new downfall, this time caused by the failure due to Chang-Chang criteria of two of the four gauss points that compose the element in that IP (this can be observed better in the Fig.99). Around 1.3ms, all the four gauss points in the IP fails according to Chang-Chang criteria, failure caused due to matrix tension as the shear stresses are very low at this moment (See Fig.100). The IP keeps carrying the failure stress (82 MPa) in the transverse direction up to the first fiber rupture, which was triggered sooner than DFAILM. In parallel, for the X-stress (Fiber), its observed that in a time

of 1.5 ms, the fiber fails without reaching its tensile strength XT (2540 Mpa), but the strain exceeds the strain limit given by DFAILT (0.017), the reason why the IP gets deleted. After reaching DFAILT, this IP is not carrying stresses anymore, but the element is only deleted when all IP through thickness are deleted, which happens at 2.4 ms. In the Fig.100 can be seen the X, Y and XY stress for all the plies along time in the first deleted element. For each stress, it can be appreciated the plies which are subjected to tensile and compressive loads in both fiber and matrix directions, being the layer 14 the intermediate layer (Closer to the neutral axis).

As expected, the allowable magnitude of stress in fiber direction is higher in tension than in compression, and higher in compression for the matrix due to the characteristic UD composite strengths. The variation of stresses in both fiber and matrix direction is only due to the bending caused by the impact, and the orientation of each UD ply does not affect too much the stress between plies due to its quasi-isotropic-symmetrical nature. For the in-plane shear stresses, the variation between plies, positive and negative respectively, is also observed. The impacted ply (compressed ply) is the one suffering from the highest in-plane shear, diminishing from 67 MPa to 11.1 MPa through thickness up to the back ply. In overall terms, the laminate failed in a progressive manner from both top and bottom. After 1.5ms, only the seven inner plies were sustaining the load up to 2.4ms, when all these remaining plies (in the same element) failed due to the increase in longitudinal and shear stresses.
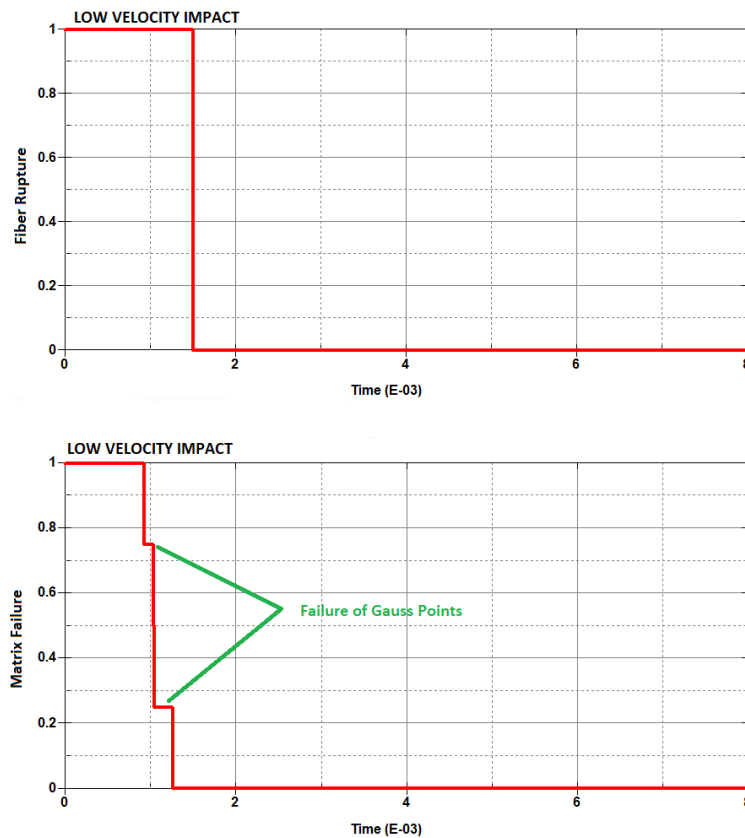

Figure 99. Failure history variables along time for the first IP in the first deleted element.
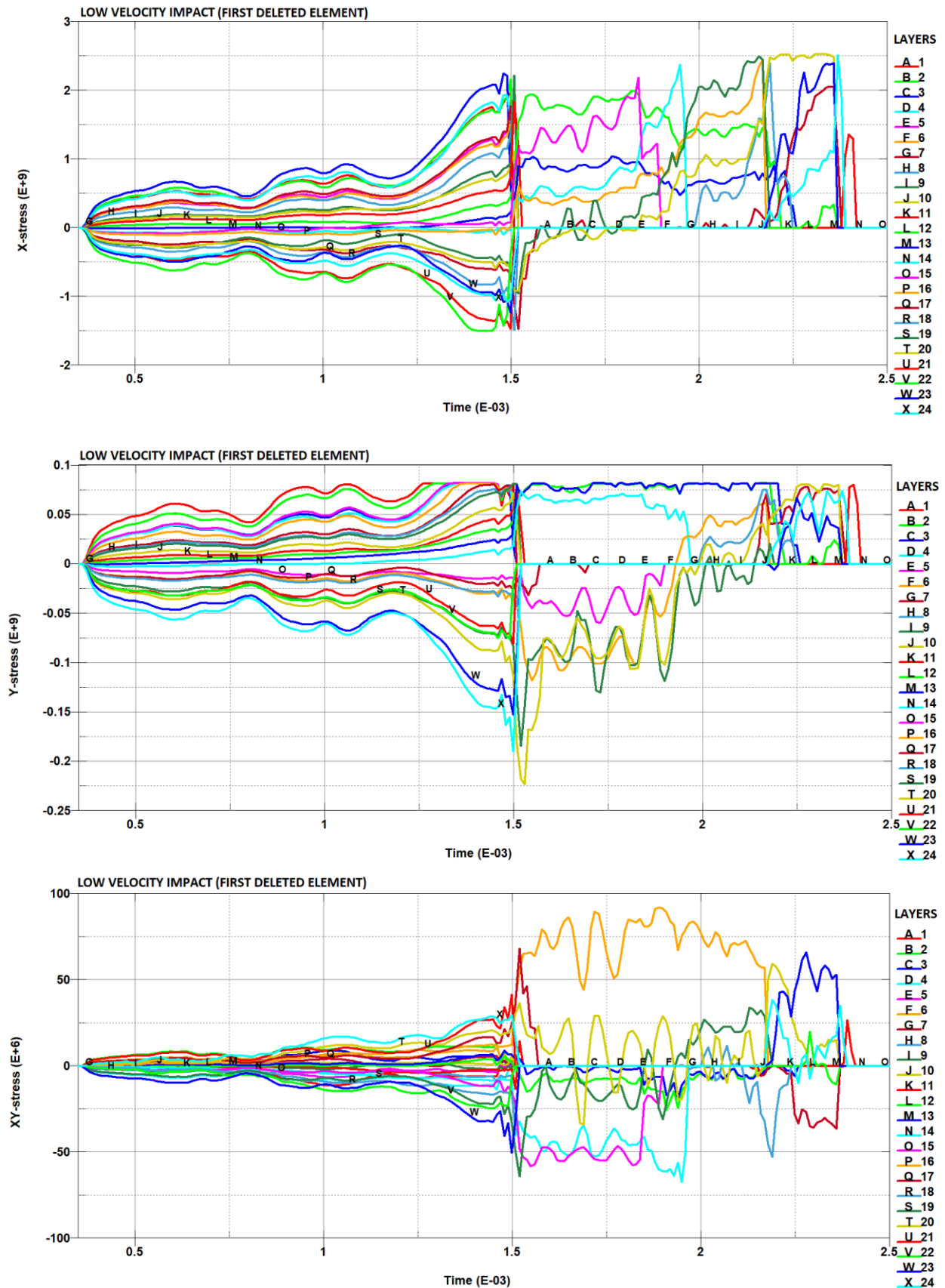
Figure 100. Stresses along time for all the layers (IP) for the first deleted element. Stresses given in Pascals.
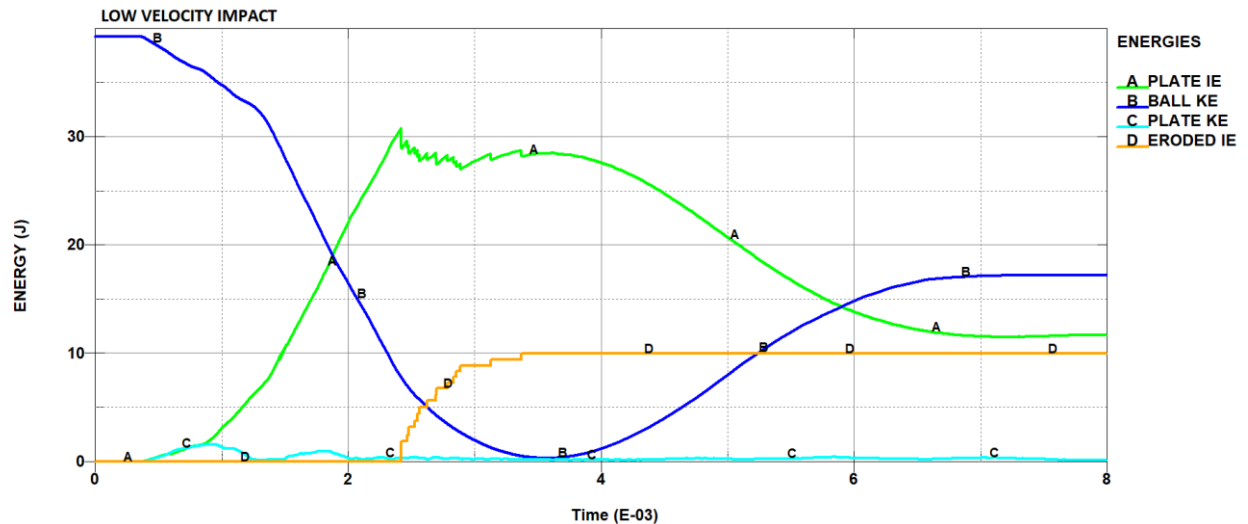
Figure 101. Energy profile for a rigid ball low-velocity impact on a CFRP plate.

In the Fig.101 can be appreciated the energy profile for the present simulation. It can be seen that all the initial KE energy from the rigid ball is transmitted to the laminate at first, causing fiber rupture and some element deletion, ending in eroded IE of the laminate. After this, part of the energy is transmitted again to the rigid ball (recoiling), and the rest stays as IE of the laminate due to the present damage and some matrix yielding.

The next step of the current work will be to implement the current model using a soft projectile instead of a rigid impactor, implementing then the ALE method and subsequently comparing it with the work of Heimbs for high velocity impact [14]. This comparison will allow increasing the robustness of the impact model developed in LS-DYNA, which objective is to pre-visualize the experiments that will take place at Clément Ader Institute. Although very satisfactory results were obtained with the current model in comparison with the Heimbs work for low velocity impacts, it is observed that the strain criteria DFAILX, as well as the restrictions in limit strengths after failure (SLIMIT), will be crucial in order to calibrate the simulations against the experimental tests.

 An inter-laminar damage model may be implemented as well in order to enhance the results in terms of damage distribution. Even though, a different model technique must be adopted using cohesive elements between layers to account for delamination. One of the main drawbacks of such techniques is that the computational cost not only increases exponentially, but the intra-laminar damage modes become less accurate due to an artificial reduction of the total bending stiffness of the laminate, making even harder to set an accurate model. However, this is out of the scope of the present work, which objective is to develop a fast and reliable numerical model from which degradation of stiffness can be predicted even when sacrificing some important aspects in the evolution of damage such as delamination.

15.4. EXPERIMENTAL SETUP: PLANAR FACE IMPACTOR

15.4.1 Case 1 - Impact with 0.75 kg planar face projectile

In this simulation, a 0.75 Kg planar projectile was impacted against three different laminates. For the first case, a total of 26 simulations were run in order to study the progression of intra-laminar damage, this being possible due to the low simulation time obtained by the single shell approach modeling, as well as the reduction in elements using an ALE mesh. The simulations took around 45 hours using the LS-DYNA Single Precision Solver along five cores.

The CFRP laminates have a thickness of 5.76 mm, and the main difference between these laminates is the orientation used for the stacking sequence, and the use of fabrics in laminate #1. On the other hand, the GFRP possesses a thickness of 8 mm, and only bidirectional fabrics (0/90°) compose it. As expected, all the simulations were presenting an initial Matrix Cracking on the back-ply due to tensile stresses, which were growing as the impact velocity was increased. It should be noted that there is a threshold limit in velocity, above which the Matrix Cracking does not grow but is rather concentrated in the impacted area. In the Fig.102 can be observed the different damage phases suffered by each laminate depending on the impact velocity, and its correspondent maximum deflection. For the GFRP laminates, first Matrix Cracking occurred at the same velocity (30 m/s).

For the CFRP laminates, at 40 m/s Fiber Rupture occurred in the fabric plies of laminate #1, after which the behavior in deflection started to become non-linear up to 120 m /s, where the first element deletion was obtained. In contrast, the laminate #2 was able to sustain the impact without any fiber breaking up to 80 m/s, after which the plies started to present a quick evolution in Fiber Rupture through the plies up to reaching element deletion at 90m/s.

In the case of the GFRP laminate, Matrix Cracking and Fiber Rupture were obtained in a more sudden manner between 20 and 30 m/s. This early failure is attributed to the fabric modeling approach, which will be discussed further along this section.
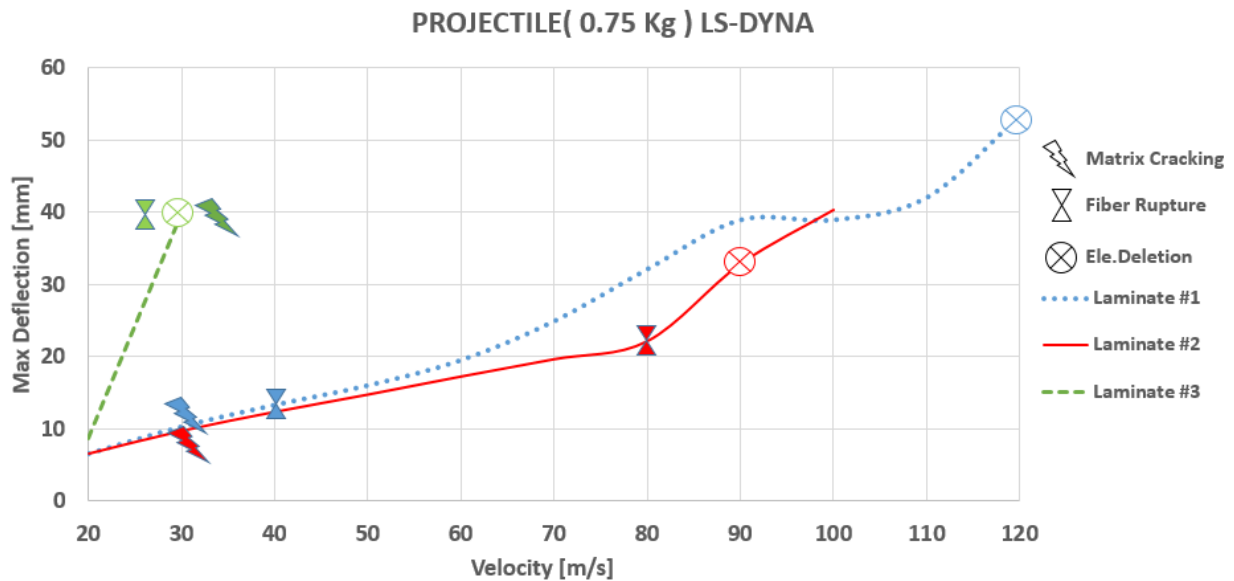
Figure 102. Maximum defletion and damage modes of laminates subjected to the impact of a 0.75 Kg planar faced projectile.

The evolution of damage along the laminate plies can be observed in a more detailed manner in Fig.103. It can be appreciated how the fabrics plies failed in FR for the laminate #1 from 40 m/s up to 80 m/s, velocity from which the UD plies could not sustain more the load in tension and started to fail. On the other hand, this progressive failure in the plies was not observed in the laminate #2, where all the plies failed in a more sudden way although they were able to resist an impact up to 80 m/s without any perceivable loss in stiffness. In both cases, all the plies presented Matrix Cracking before Fiber Rupture occurred.

The Hugoniot and Stagnation pressures for each velocity can be observed in the Fig.104. As expected, the Hugoniot pressure presented a slight non -linear behavior going from 10 to 140 MPa through the tested velocities. This pressure was not easy to post-process due to the spurious pressure profile gathered by each sensor, which was highly varying from element to element.

In the Fig.105 is presented the energy absorbed by deformation of the laminate (Internal energy) compared to the kinetic energy (KE) of the impactor. It can be said that the internal energy for both laminates never reached more than 40% (worst case) of the impact energy. A small part of the energy was transformed into KE of the plate and deformation of the impactor, whereas almost all the remaining energy was still in form of KE energy of the impactor. Some instabilities were found for the laminate #2 for impacts above 110 m/s, due to the high deformations suffered by the central elements, increasing exponentially the IE present in the plate.
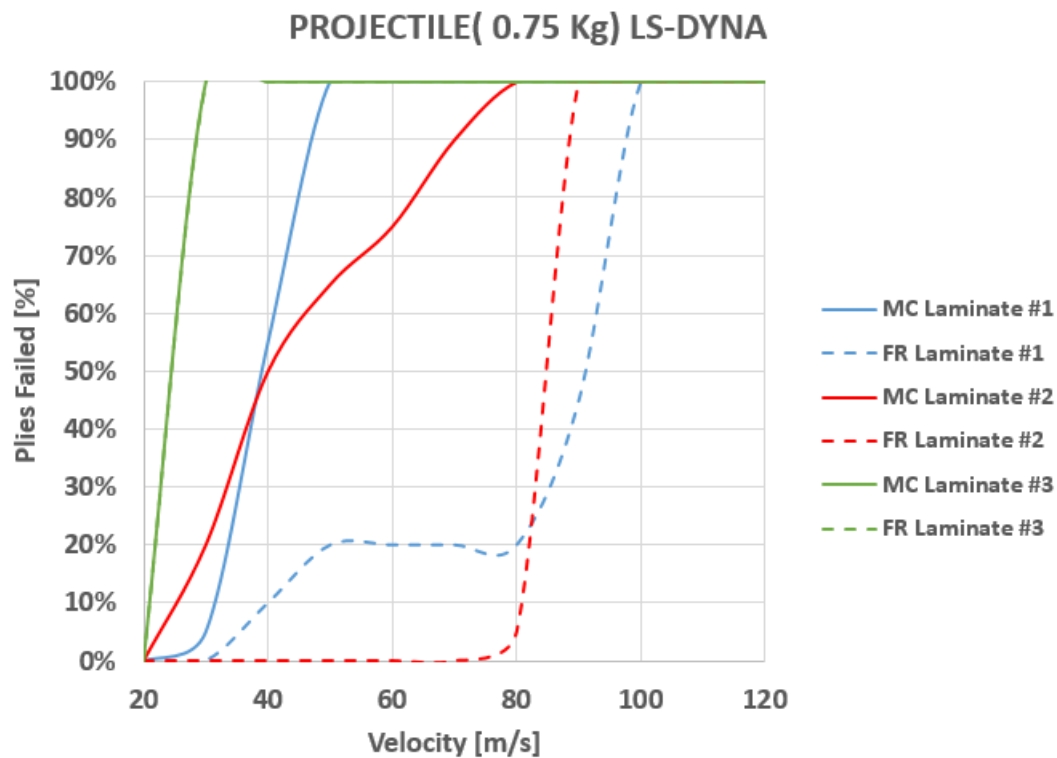
Figure 103. Percentage of plies failed for different damage modes after the impact of a 0.75 Kg planar faced projectile

On the other hand, the stagnation pressure gradually incremented in a quadratic manner with respect to the impact velocity, but within a smaller range (0 - 8 MPa), being in accordance with theoretical values obtained by using Equation 2.
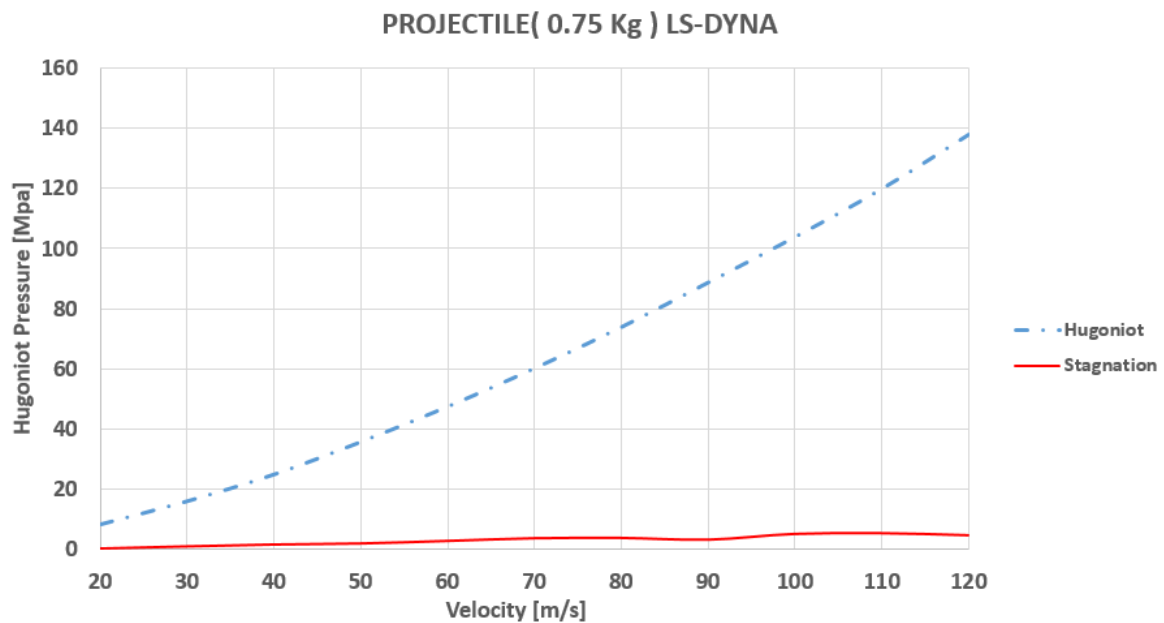
Figure 104. Hugoniot and Stagnation pressures respect to the impact velocity of a 0.75 kg planar faced projectile.
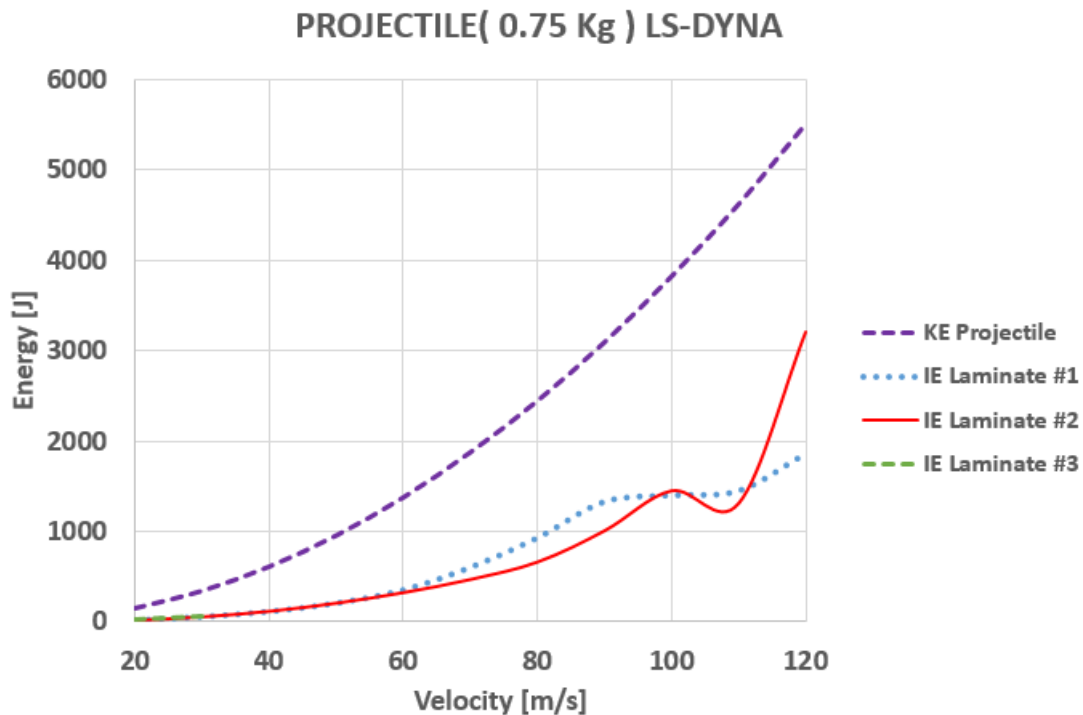
**Figure 105. Impactor Kinetical energy and maximum internal energy suffer by the plate during
the impact for a 0.75 kg planar faced projectile**

A comparative scheme is presented between laminates #1 and #2 after the impact of a 0.75 Kg
projectile at different velocities (See Diagram.3). The comparison is performed on the back ply
of the laminate at the end of the simulation: biaxial fabric (±45°) for laminate #1 and UD (45°)
for laminate #2. In the left column, is presented the comparison between Matrix Cracking
failures due to tension for both laminates, whereas the right column presents the comparison
between Fiber Rupture. It can be observed that Matrix Cracking evolution is lower on laminate
#1 (but much more plies present it compared to laminate #2), which is expected due to the better
transversal properties of the biaxial, reducing this way the tensile stress carried out by the
matrix. On the other hand, the biaxial fabrics fail in tension very early, starting the rupture from
the plate center, subsequently expanding itself in a "z" pattern.

For the Laminate #2, the Fiber Rupture starts at 90 m/s, but then all the plies start to fail in a
progressive manner. Moreover, for velocities up to 50 m/s, the Matrix Cracking appears only
in the impacted area, while for greater velocities, it gets expanded in the direction perpendicular
to the fiber (as expected) and also concentered in the circle support edge from the back plate.
Which does not happen for laminate #1, where MC contours are much more chaotic and
concentrated in the edges.

It has to be remarked that the early failure of the fabric plies is attributed to the fact that its strengths were obtained by using the first ply failure criterion of an equivalent UD laminate. However, these values are governed mainly by the weakest laminate direction (when the load is applied perpendicular to the fiber), subsequently underestimating its strength. Coupon axial tests must be performed for fabrics in order to obtain the real strength values for using adequately in this type of simulations, although in a later section another approach was used (See Section 9.4).

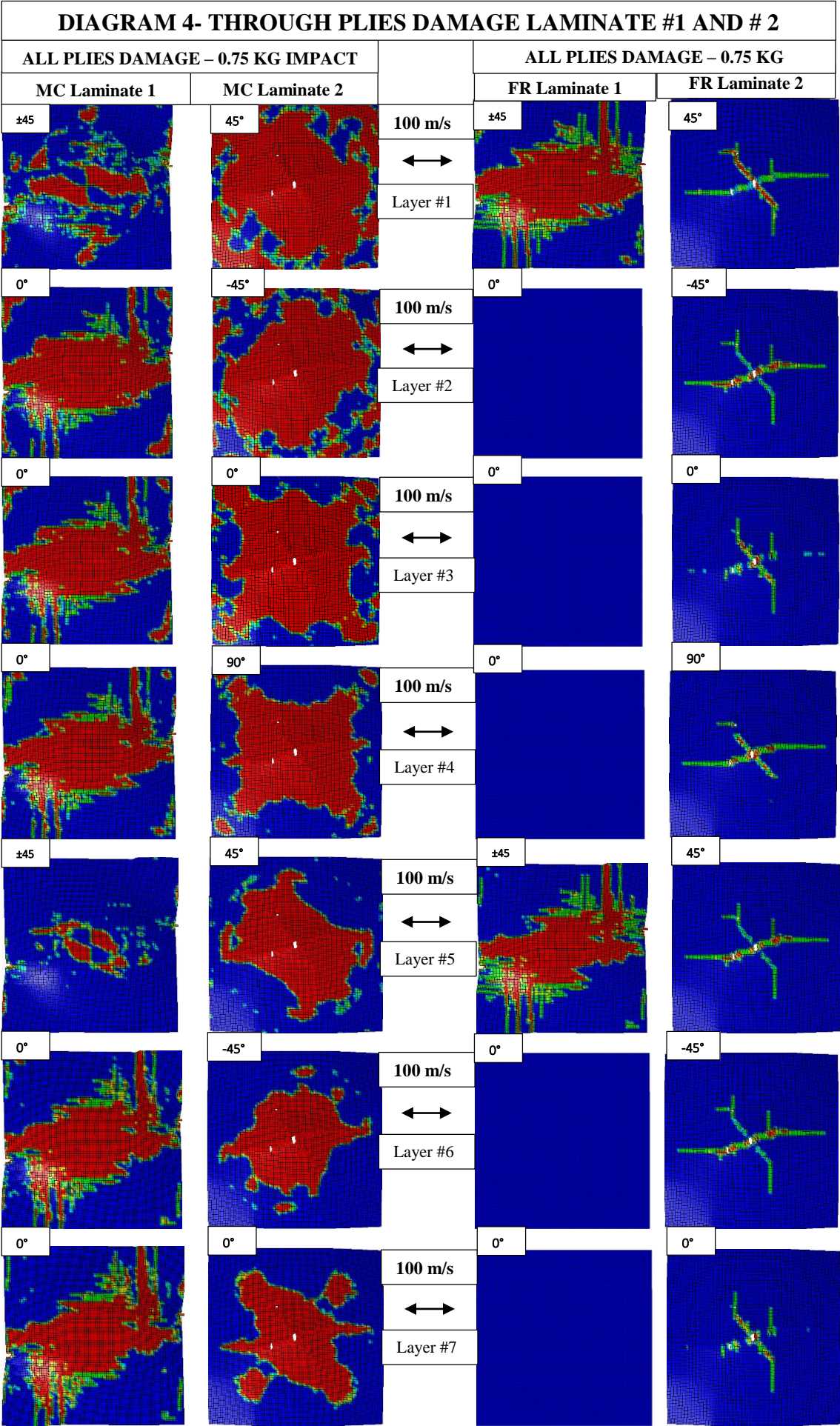A comparative scheme is also presented between laminates #1 and #2 after the impact of a 0.75 Kg projectile at 100 m/s (See Diagram.4). This time, the comparison is performed for all the plies of the laminates. Again, in the left column is presented the comparison between Matrix Cracking failure, and on the right column is presented the comparison between Fiber Rupture. Here, the failure can be observed for each ply through the thickness. As one should expect, the Matrix Cracking is lower for plies near to the half thickness, which is not subjected to either the compressive crushing load of the impact or the high tensile load due to bending. It is observed that the layers that present less MC failure are the fabrics in laminate #1. Concerning to Fiber Rupture, it is interesting to observe that the only plies which fail in the laminate #1 were the fabrics, meanwhile, the UD did not suffer any Fiber Rupture damage in contrast to the UD in laminate# 2, where element deletion was obtained. The MC contours propagation in laminate #2 is clearly different for both tension and compressive cases, the compressive failure presenting a four-petal flower shape.

DIAGRAM 3- BACK PLY DAMAGE LAMINATE #1 AND # 2

BACK PLY DAMAGE – 0.75 KG IMPACT			BACK PLY DAMAGE –0.75 KG IMPACT	
MC Laminate 1	**MC Laminate 2**		**FR Laminate 1**	**FR Laminate 2**

Lucas Márquez Duque

DIAGRAM 4- THROUGH PLIES DAMAGE LAMINATE #1 AND # 2

ALL PLIES DAMAGE – 0.75 KG IMPACT			ALL PLIES DAMAGE – 0.75 KG	
MC Laminate 1	MC Laminate 2		FR Laminate 1	FR Laminate 2

DIAGRAM 4- THROUGH PLIES DAMAGE LAMINATE #1 AND # 2

ALL PLIES DAMAGE –0.75 KG IMPACT			ALL PLIES DAMAGE –0.75KG IMPACT	
MC Laminate 1	MC Laminate 2		FR Laminate 1	FR Laminate 2

DIAGRAM 4- THROUGH PLIES DAMAGE LAMINATE #1 AND # 2

ALL PLIES DAMAGE – 0.75 KG IMPACT			ALL PLIES DAMAGE –0.75 KG IMPACT	
MC Laminate 1	MC Laminate 2		FR Laminate 1	FR Laminate 2

100 m/s — Layer #15
100 m/s — Layer #16
100 m/s — Layer #17
100 m/s — Layer #18
100 m/s — Layer #19
100 m/s — Layer #20

15.4.2 Case 2 - Impact with 0.37 kg planar face projectile

In this simulation, a 0.37 Kg planar projectile was impacted against the same three laminates in order to observe their response when the impact mass was halved. For this second case, 26 simulations were run again, taking approximately 70% of the first case simulation time due to the reduction in elements in the ALE mesh.

The results obtained for this case were very similar to the previous impactor case. Matrix cracking was observed from 30 m/s for both CFRP laminates, and the limits of Fiber Rupture were the same than the previous case. However, the most appreciable results are given in terms of maximum deflection, where the composite plates presented less deflection than the previous cases (as it would be expected). In addition, for the laminate #1, the nonlinear behavior in the Fig.106 after the first Fiber Rupture was diminished, obtaining this way a very similar response for both laminates up to 110 m/s, time for the first element deletion in laminate #2.

The GFRP laminate presented complete failure again for velocities above 30 m/s, indicating the need of performing another set of simulations where the laminate strengths are not underestimated, as it was explained previously.
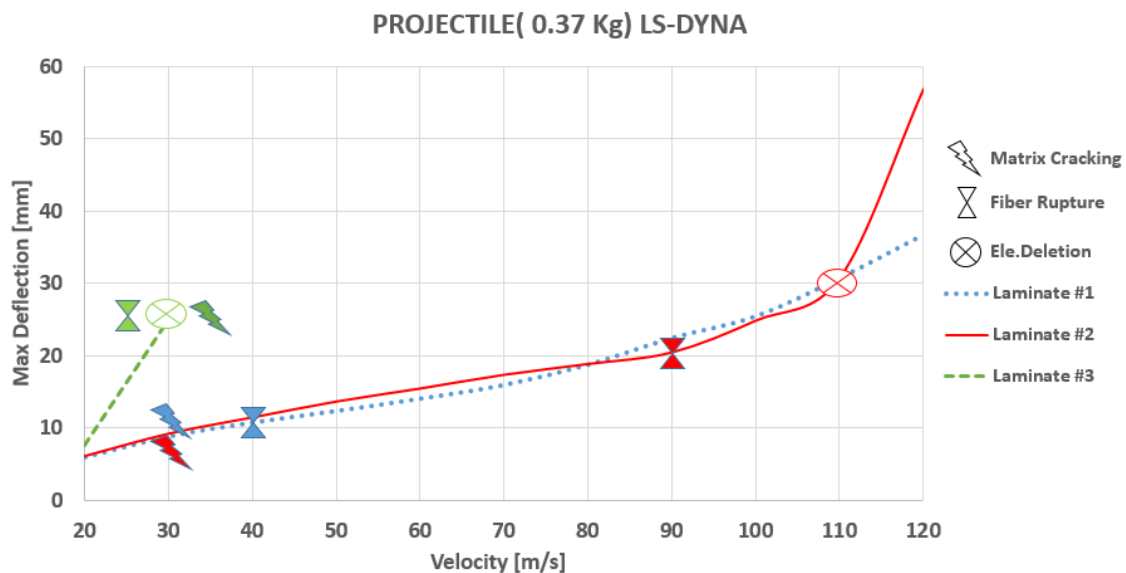
Figure 106. Maximum defletion and damage modes of laminates subjected to the impact of a 0.37 Kg planar faced projectile.
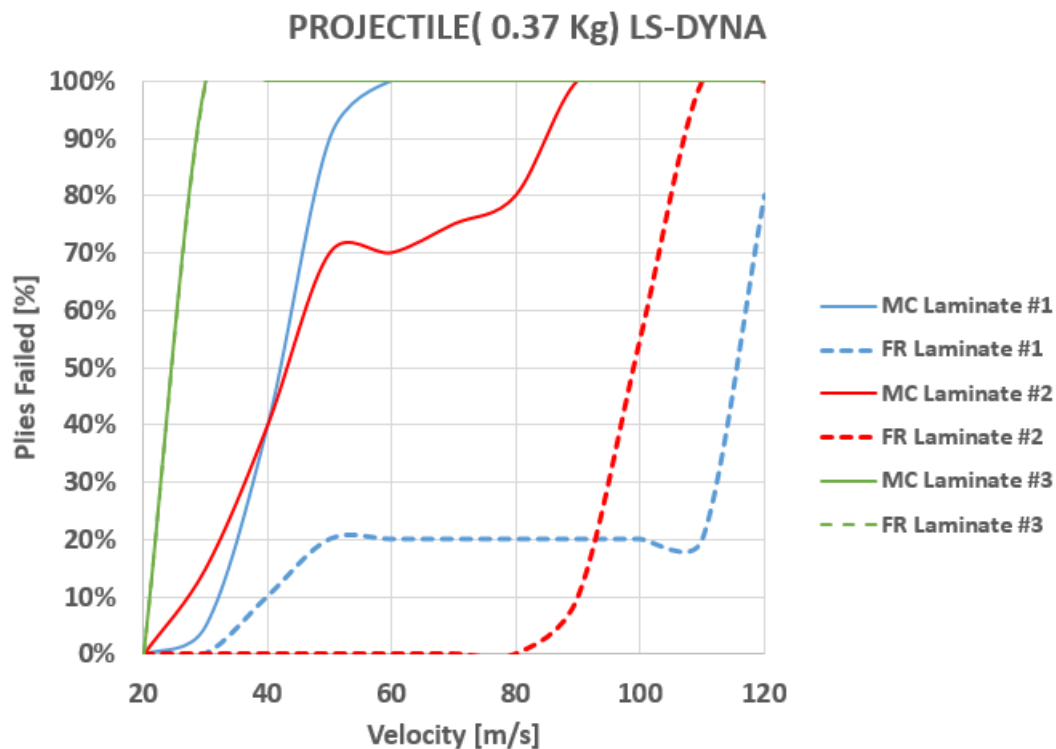
Figure 107. Percentage of plies failed for different damage modes after the impact of a 0.37 Kg planar faced projectile.
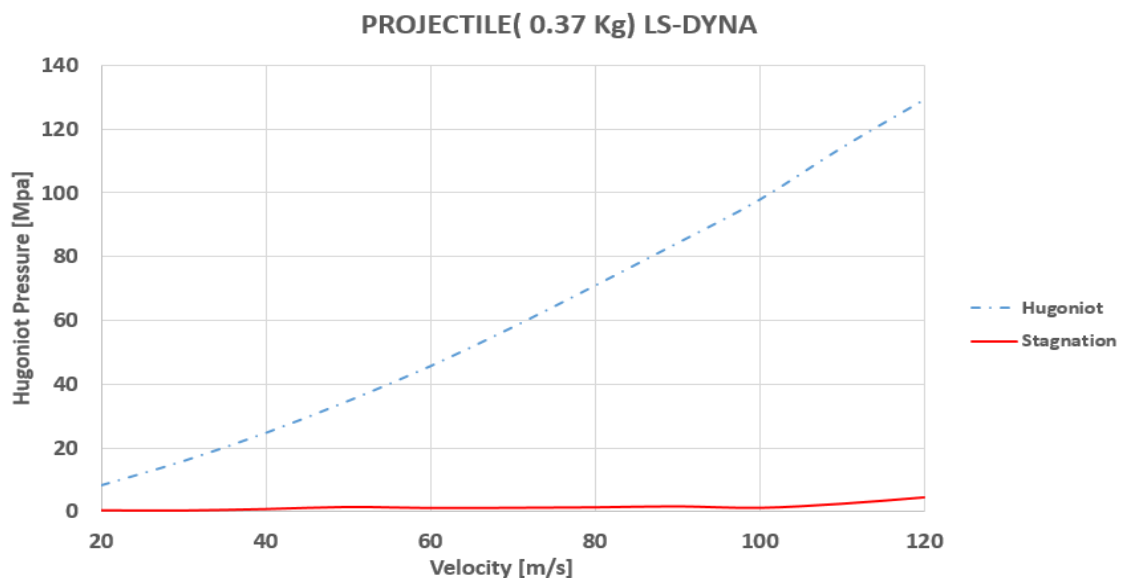
Figure 108. Hugoniot and Stagnation pressures respect to impact velocity of a 0.37 kg planar faced projectile.

In the Fig.107 can be observed that the fiber rupture in laminate #1 is presented in all the layers of fabric plies again. The UD plies in the laminate #2 are not failing that abruptly this time, now being in a range of velocities from 80 to 110 m/s for the complete plies failure (in the case 1, this range was 80 to 90m/s). There is also an appreciable reduction of plies failure in MC

between 50 and 80 m/s compared to the previous case, which is discussed in the coming subsection.

The plate IE of both CFRP laminates fits very good in this case again, which means that the overall strain fields deformation of both plates are very similar. It is interesting to observe that in this case, the maximum IE of the plate does not exceed 30%, being 10% lower than the maximum absorption for the double of impacting mass.

Moreover, the Hugoniot and stagnation pressure were not highly influenced by this change in mass, as it was expected. This is compared and discussed further on the next section, but it should be noted that if this pressure wants to be reduced, the best way will be changing either the impact face geometry or/and the initial contact area.

Figure 107. Impactor Kinetic energy and maximum plate internal energy vs impact velocity for a 0.37 kg planar faced impact.

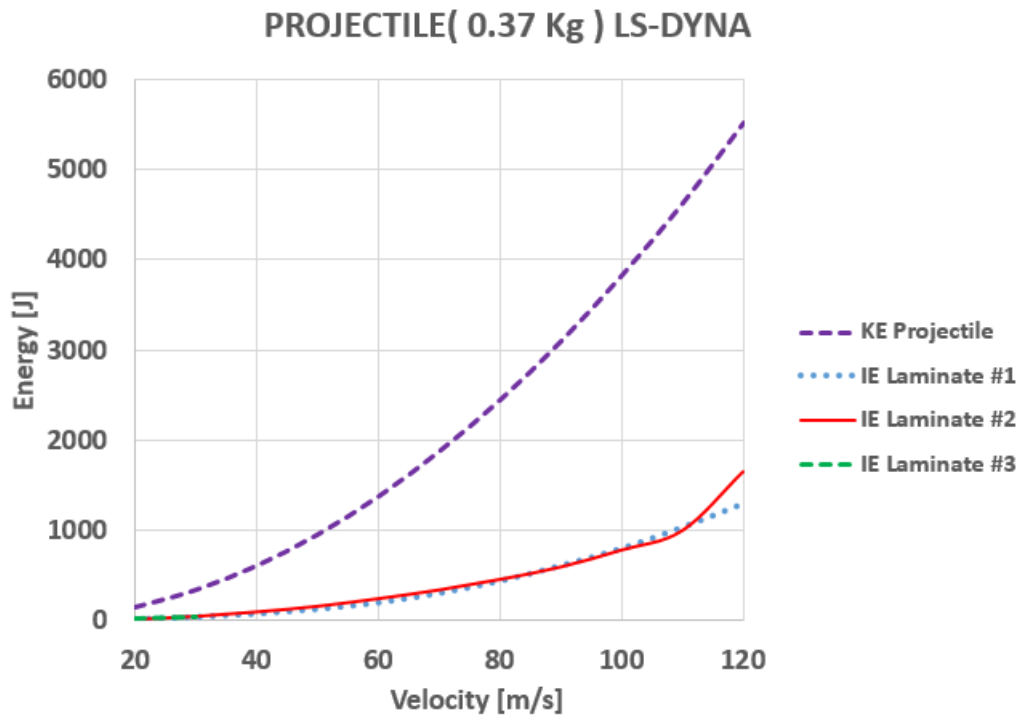## 15.4.3 Analysis and Comparison: Planar impactors

According to the simulations performed so far, the model seems to overestimate the damage, which was expected due to the assumptions are shown in Section 9, is especially true due to the neglecting the energy dissipated by inter-laminar damage. For this reason, some additional parameters such as DFAIL will need to be implemented when calibrating the numerical model against the experimental results. In addition, Matrix Cracking due to the tension was developed very early in the laminates (from velocities greater than 30 m/s), which is not adequate considering that the minimum velocity which can be obtained in the gas cannon facilities is around 50 m/s for this type of impactors.

In Fig. 110 can be observed the maximum deflection comparison for each laminate within the studied range of velocities, including the two different planar impactor masses (0.37 and 0.75 Kg). In the first instance, it can be seen that the GFRP laminate (Laminate # 3) is presenting a sudden failure when the two projectiles are shot at a velocity of 30 m/s no matter the mass of the projectile. Respect to CFRP laminates, we can divide its failure into three phases: the beginning of Matrix Cracking due to tension, Fiber Rupture, and Element Deletion according to Chang-Chang criteria. It is observed that Matrix Cracking is happening at the same velocity (30 m/s) for both CFRP laminates with the two different projectiles, failure initiated by the Hugoniot pressure and which, according to the Fig.111, it is almost the same for both projectiles.
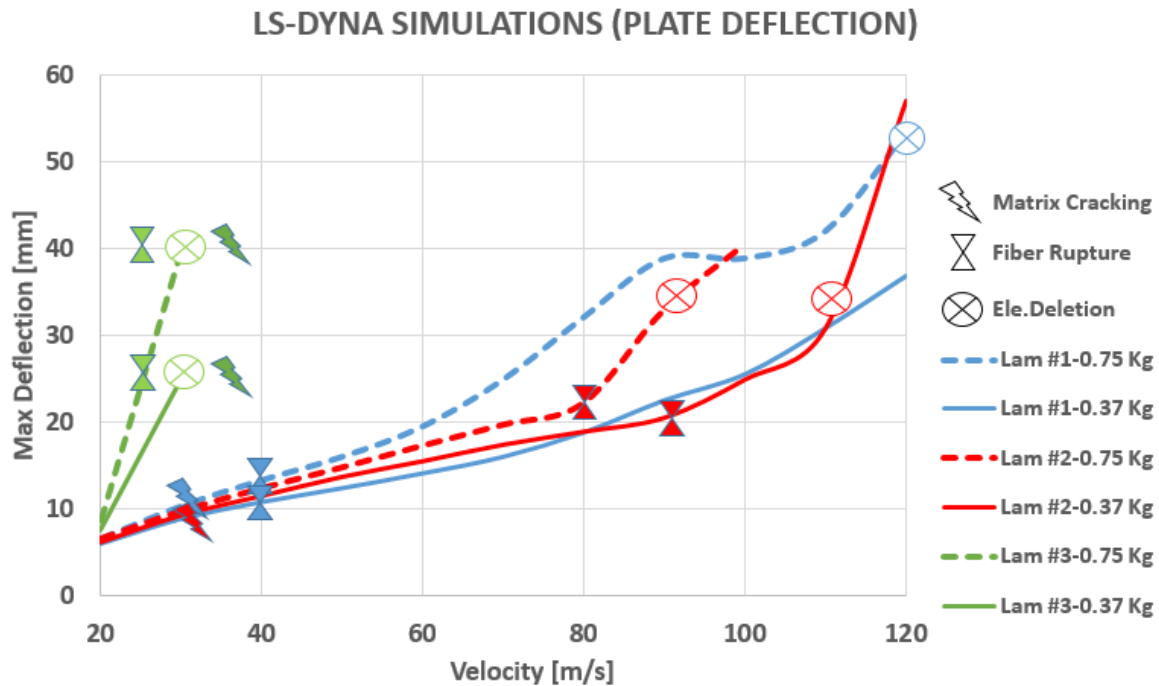
Figure 108. Maximum deflection and damage modes of laminates subjected to the impact of a 0.37 Kg and 0.75 kg planar faced projectile.

The laminate #1, which includes carbon fiber biaxial fabrics, reaches the fiber rupture at 40 m/s for both projectile masses, due to the reasons which were discussed in Section 9 and which solution will be either considering a UD equivalent laminate, or performing axial coupon tests. Moreover, the laminate #2 presents less deflection until it reaches the Fiber Rupture at 80 m/s, suddenly increasing its deflection reaching the element deletion phase even sooner than laminate #1.

When half of the mass is shot, the behavior is very much alike. Both laminates #1 and #2 present a similar stiffness behavior until laminate #2 with 0.375 kg reaches Fiber Rupture at 90 m/s (almost 10% more compared to the 0.75 Kg projectile), subsequently reducing its stiffness up to the element deletion phase at 110 m/s (almost 20% more compared to the heavier projectile). On the other hand, laminate #1 do not present element deletion, but its maximum deflection is very high. In Table 10 are shown the deflection ranges in which each type of failure occurs for each laminate.
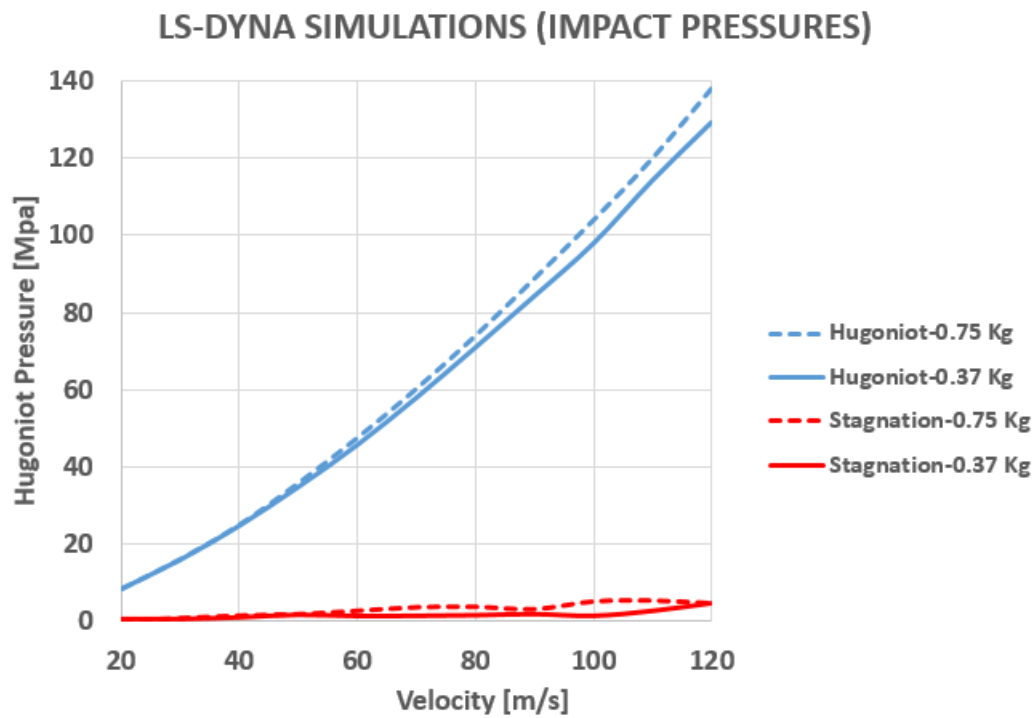
Figure 109. Hugoniot and Stagnation pressures vs impact velocity of a 0.37 kg and 0.75 kg planar faced projectiles.

The Hugoniot pressure was measured by averaging the data collected from 16 sensors located in the middle of the plate. In the Fig.111, it can be seen that the Hugoniot and Stagnation pressures are very similar for both projectiles, even when their masses are different by a magnitude of two. This behavior was expected because the Hugoniot pressure depends mainly on the initial contact area, projectile shape, material density and impact pressure, and less on the projectile mass. (See Section 3).

In order to analyze the different damage progression across the plies in each laminate, the Fig.112 was prepared. The percentage of failed plies for each damage criteria can be observed for all the laminates. As it was mentioned before, the GFRP (laminate #3) early damage took place in a suddenly way, all plies failing and being deleted for a velocity of 30 m/s. For laminate # 1, the number of plies suffering matrix cracking is increasing faster than laminate #2 when increasing the impact velocity (but in a lower ply area than laminate #2).

On the other hand, the fiber failure of the UD laminate #2 is much more sudden compared to laminate #1, where the fabrics suffer from Fiber Rupture at low velocities, followed by a

sudden UD fiber failure at higher velocities (being desirable in cases where progressive damage is required). Again, it is interesting to observe that matrix cracking is being developed in a very similar way for both CFRP laminates up to velocities of almost 40 m/s. Respect to Fiber Rupture, this damage was delayed when the impactor mass was reduced for both laminates, being more noticeable for laminate #1.
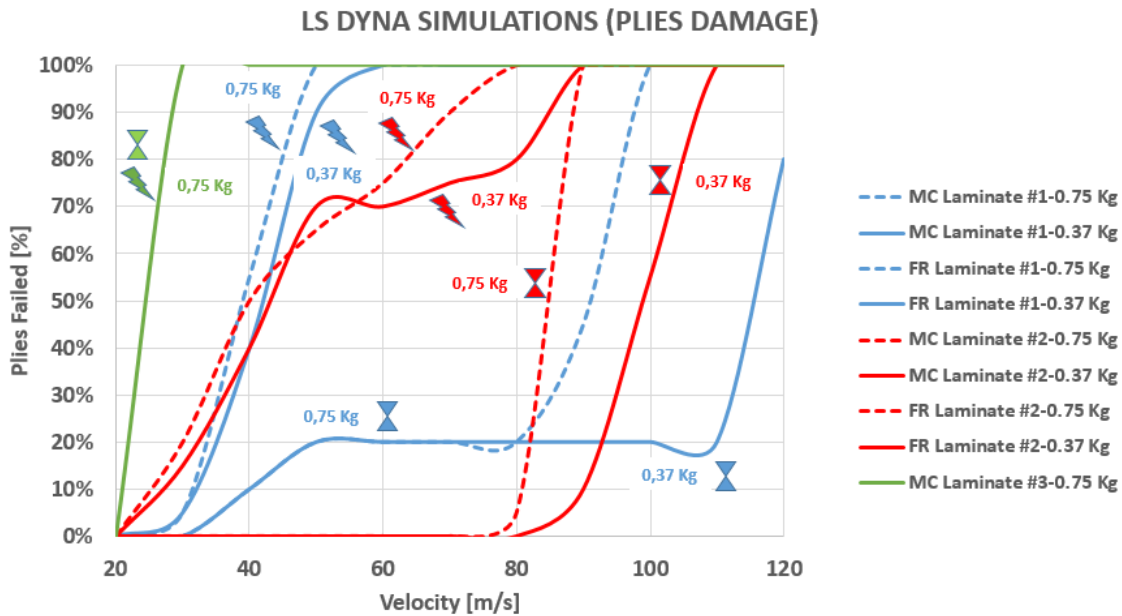
Figure 110. Percentage of plies failed for different damage modes after the impact of a 0.37 Kg and 0.75 kg planar faced projectiles.

Table 10. Deflection at which each damage modes starts to take place.

Item	Laminate # 1	Laminate # 2	Laminate # 3
Deflection at first Matrix Cracking [mm]	10-13	10-13	25-40
Deflection at first Fiber Rupture [mm]	10-15	20-25	25-40
Deflection at first of Element Deletion[mm]	=>50	35-40	25-40

A comparative scheme is presented for laminate #1 when it is impacted at different velocities with different projectile masses, 0.75 and 0.35 Kg respectively (See Diagram.5). This analysis is performed on the back ply of the laminate (layer #1), following the same arrangement of previous schemes. It is observed on this laminate, that matrix cracked area is lower for the 0.35 Kg mass up to a velocity of 60 m/s, after which becomes very similar to the contours presented for the 0.75 kg impact case where the damage gets concentrated in a spiral manner following the +-45° orientation and some damage concentrated in the edges. Regarding Fiber Rupture, patterns are very similar even when the impact energies are highly different (by a magnitude of two), being this layer destroyed after 80 m/s.

In contrast , for laminate #2 (See Diagram 6) it can be observed that the first Fiber Rupture gets delayed to almost 90m/s, but is very focalized in the center compared to the 0.75 kg projectile impact, which at 90 m/s its almost 8 times bigger in the 45° direction (Red elements). Regarding Matrix Cracking, almost the same cracked area is obtained through all the range of velocity, this time starting as a focused point in the center, subsequently expanding itself in an oval with its maximum radius in the direction perpendicular to the fiber, including some additional matrix cracks in the circle edge of the back-plate.

These results show that reducing the projectile mass by half while keeping the frontal impact area does not affect much the magnitude of damage that will be obtained at the end, even when the impact energies highly differ. This should be taken into account when deciding the impactor mass and shape for the experiments: a good agreement between mass (gas cannon capabilities) and frontal area/shape (Hugoniot pressure) must be reached in order to be able to reproduce experimentally the range of velocities in which the all the damage phases occurs.

DIAGRAM 5- BACK PLY DAMAGE LAMINATE #1 BOTH PROJECTILES

BACK PLY DAMAGE – PROJECTILE			BACK PLY DAMAGE – PROJECTILE	
MC Lam 1 (0.75 KG)	MC Lam 1 (0.37 KG)		FR Lam 1 (0.75 KG)	FR Lam 1 (0.37 KG)

Lucas Márquez Duque

DIAGRAM 6- BACK PLY DAMAGE LAMINATE #2 BOTH PROJECTILES

BACK PLY DAMAGE – PROJECTILE			BACK PLY DAMAGE – PROJECTILE	
MC Lam 2 (0.75 KG)	MC Lam 2 (0.37 KG)		FR Lam 2 (0.75 KG)	FR Lam 2 (0.37 KG)
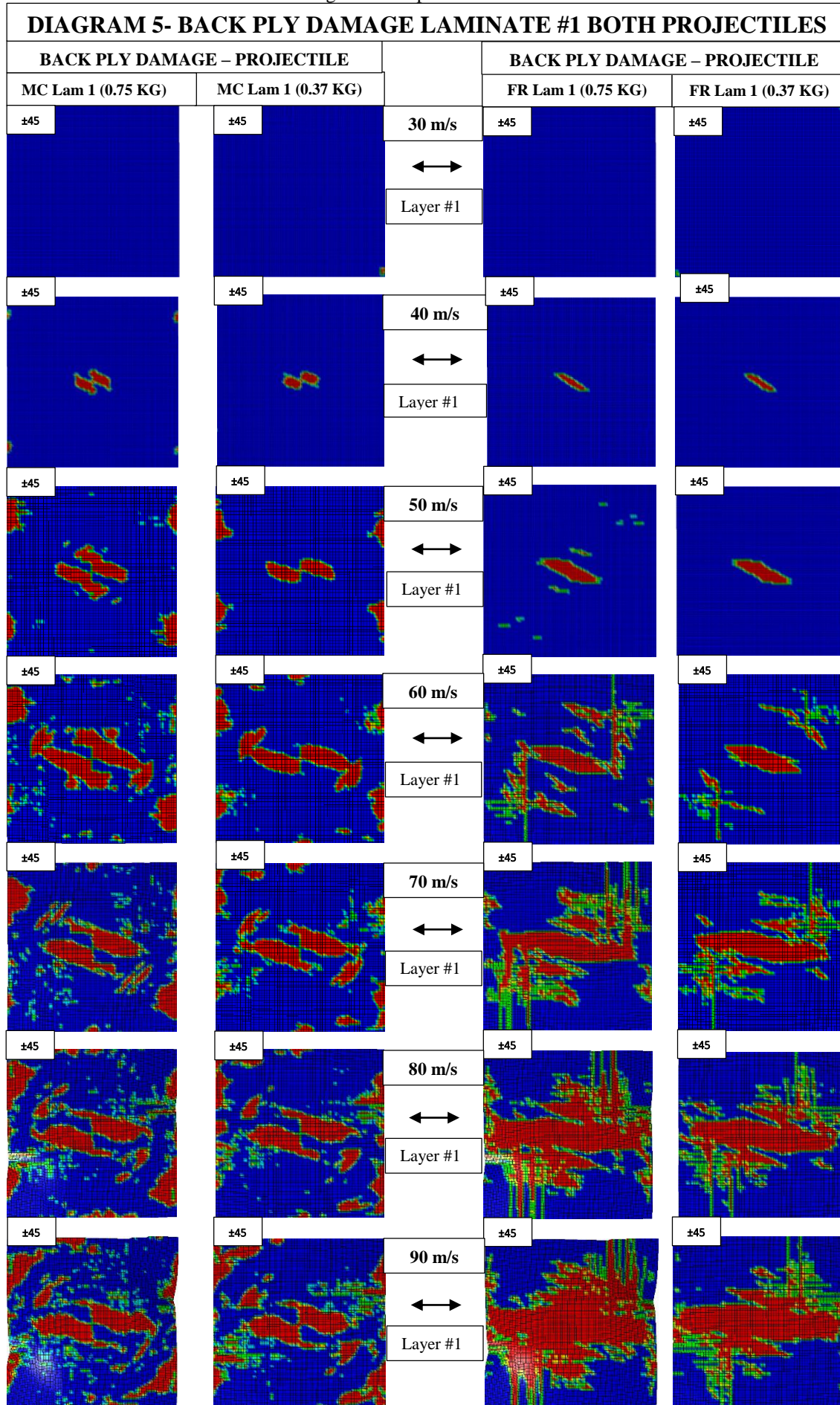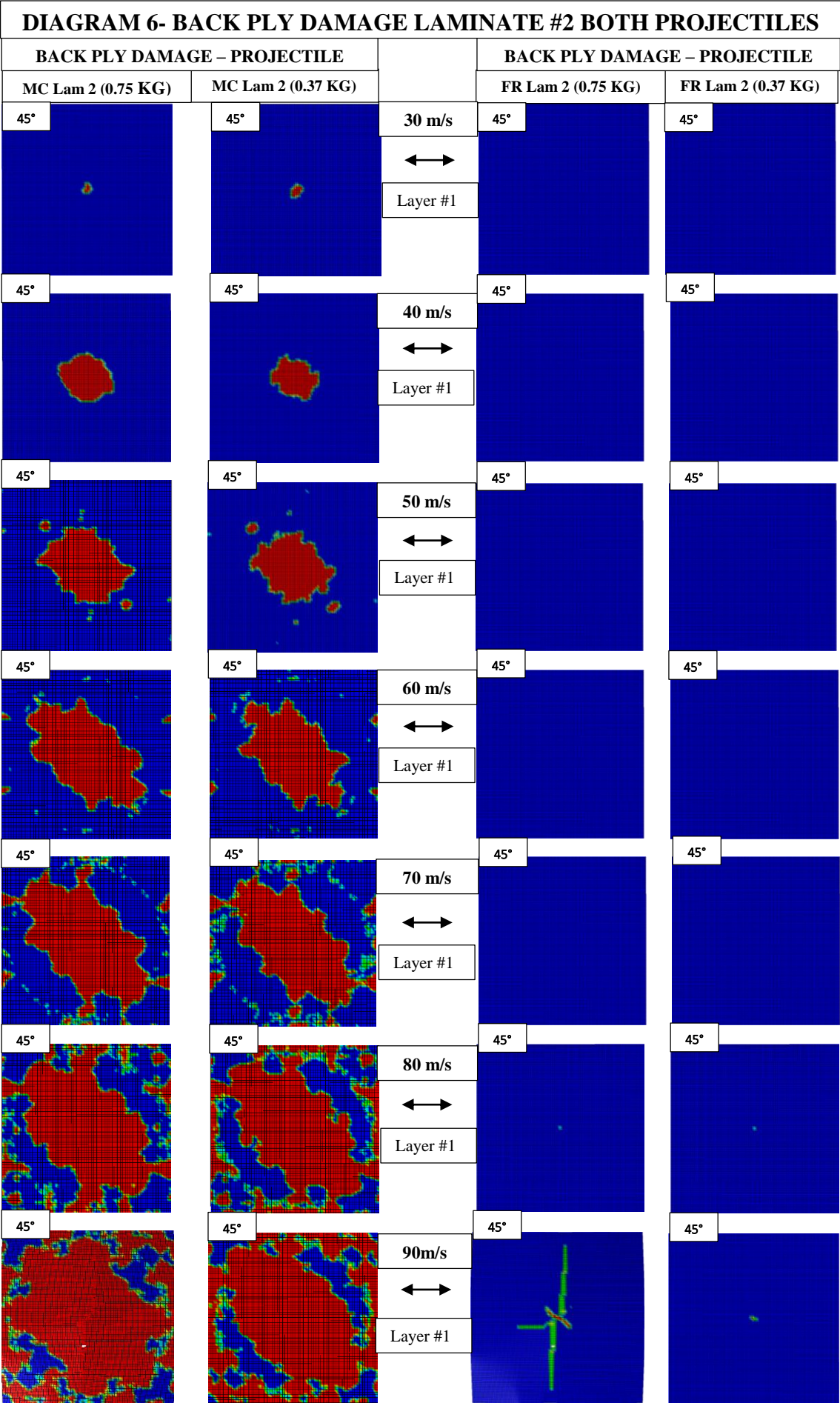
15.4.4 Time response and Strain rates

An important parameter of the plate response is the time for reaching its maximum deflection for a given velocity. This will be useful not only in the modal response analysis of each laminate for further investigations but also in the setting of the instruments and sensors that will collect data during the experiments. In the Fig.95 is shown the time that takes to each laminate to reach its maximum deflection for two different projectiles at different velocities.

It can be observed that for both laminates, it takes longer to reach its maximum deflection when they are impacted with bigger masses, which is expected taking into account that these projectiles present a longer stagnation pressure phase due to their higher length.

On the other hand, when comparing laminates #1 and #2, it is observed that for both projectiles, the laminate #2 reaches faster its maximum deflection, showing then a stiffer response in comparison with laminate #1. However, for impacts with 0.75 kg at velocities higher than 90 m/s, laminate # 2 increase its time response compared to laminate #1, which is caused by reaching the complete failure phase of this laminate, therefore decreasing its stiffness (See Fig.113). Sudden increase or decrease rates in the behavior of these curves are related to either initiation of Fiber Rupture, fast development of Matrix Cracking or Element Deletion.
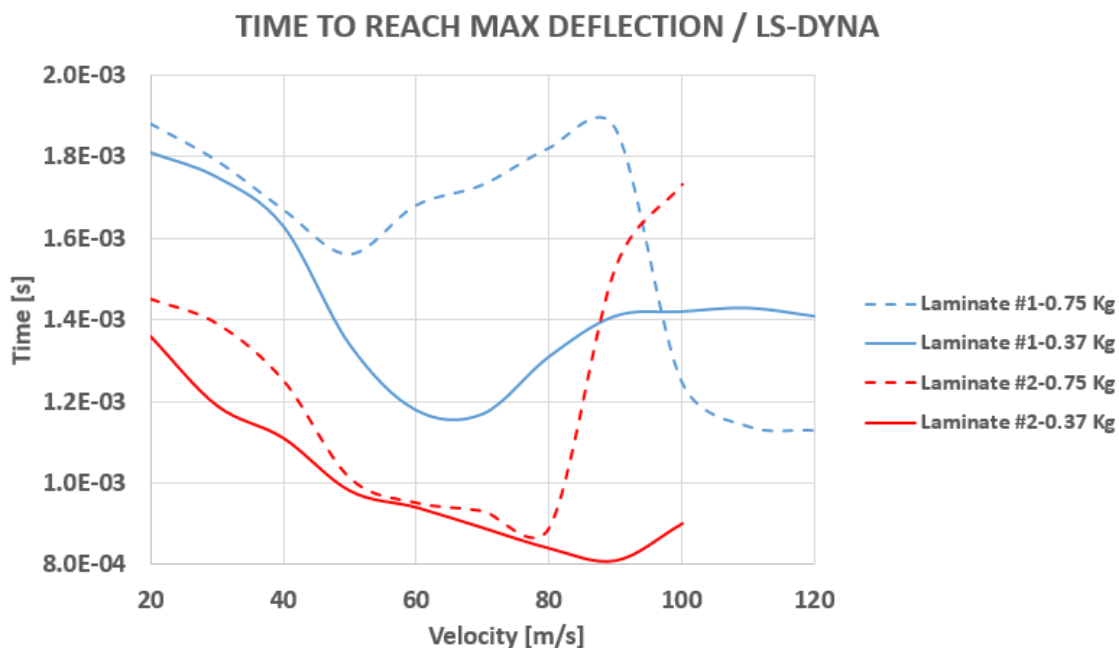

Figure 111. Time to reach the maximum deflection at different velocities for laminates #1 and #2, planar projectiles (0.37 and 0.75 Kg)

The influence of the impactor geometry at constant mass in the response time is shown in the Fig.114. The reduction in the Hugoniot pressure increases the plate response duration for all the velocities range of laminate #1 (Except at the end, where numerical instabilities occurs), and for velocities up to 80 m/s compared to the planar impactor in the case of laminate #2, moment when its reached the fiber rupture in the last case. As expected, GFRP is the laminate which presents the higher response duration, due to its lower stiffness, but only up to 60 m/s, after which it behaves in a stiffer manner compared to laminate #1, due to the Fiber Rupture on the fabrics of the laminate #1.

According to the numerical simulations, for this range of velocities, the maximum deflection of the plate is reached between 0.8 and 3.3ms after the impact, which can be used as a reference value when selecting and setting the data acquisition system during the experiments.
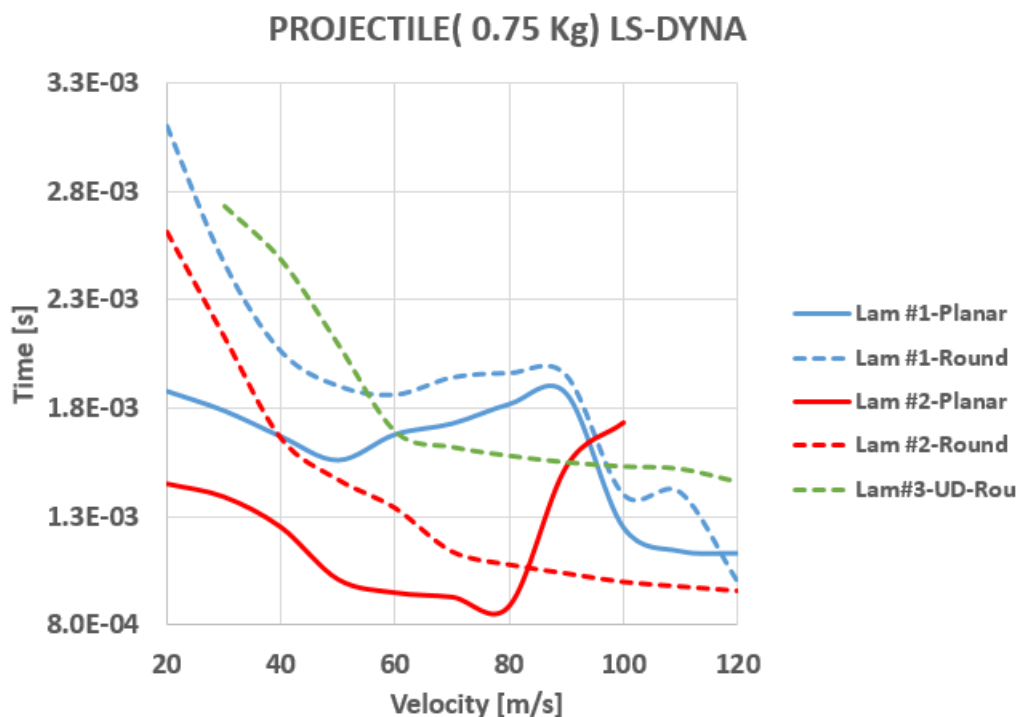

Figure 112. Time to reach the maximum deflection at different velocities for laminates #1 and #2, Round projectiles (0.75 Kg)

Table 11. Effective and first principal strain rates for a 0.75 Kg planar impact

STRAIN RATES FOR DIFFERENT LAMINATES (s⁻¹)						
0.75 Kg Projectile	**Laminate #1**		**Laminate #2**		**Laminate #3**	
Velocity [m/s]	**1st Principal**	**Effective**	**1st Principal**	**VM**	**1st Principal**	**VM**
20	0.14 -2.54	0.18 - 2.13	0.04 - 5.63	0.795-3.97	0.31 - 2.82	0.19 - 2.13
30	0.14 -4.73	0.72 - 4.29	0.32 - 14	0.921-11.3		
40	1.3 - 10.1	1.87 - 8.21	0.61 - 29.2	1.67-20.2		
50	2.7 - 13	3.34 - 13.9	1.13 - 25.3	2.4-18.1		
60	1.58 - 24.9	4.84 - 23.1	2.25 - 27.9	3.07-20.4		
70	6.33 - 28.5	7.58 - 30.5	1.38 - 43.8	4.15-30.8		
80	2.43 - 38.4	9.75 - 46.9	1.62 - 48	5.31-35.7		
90	2.3 - 44.1	17.8 - 54	23.1 - 74.9	13.9-59.8		
100	5.25 - 57.9	19.7 - 62	28.8 - 92.8	29.3-100		
110	11.5 - 74.4	26.8 - 75	46.2 - 151	43.1-140		
120	14.4 - 76	13.7 - 130	NaN	NaN		

Table 12. Effective and first principal strain rates for a 0.37 Kg planar impact.

STRAIN RATES FOR DIFFERENT LAMINATES (s⁻¹)						
0.37 Kg Projectile	**Laminate #1**		**Laminate #2**		**Laminate #3**	
Velocity [m/s]	**1st Principal**	**Effective**	**1st Principal**	**Effective**	**1st Principal**	**Effective**
20	0.14 - 3.37	0.38 - 2.63	2.38 - 5.74	0.49 - 4	0.14 - 2.55	0.16 - 2.19
30	0.98 - 4.95	0.99 - 5.27	1.13 - 11	1.48 - 8.98		
40	1.74 - 6.0	1.95 - 5.42	1.07 - 16.7	1.72 - 12.3		
50	1.93 - 14.9	2.8 - 13.8	0.31 - 28.3	2.46 - 20.7		
60	1.3 - 25.4	4.54 - 22.7	1.8 - 28	3.44 - 20.4		
70	2.95 - 41.7	7.13 - 35.5	0.72 - 41.2	3.98 - 28		
80	1.27 - 54.7	12.7 - 49.4	1.42 - 50.3	4.55 - 34.7		
90	7.1 - 51.5	14.4 - 52.2	2.23 - 64.7	9.54 - 52.2		
100	3.94 - 57.4	21.1 - 56.3	27.4 - 86.6	22.9 - 87.9		
110	10.8 - 92.6	23.3 - 70.2	59.1 - 108	47.9 - 101		
120	NaN	NaN	NaN	NaN		

The effective and first principal strain rates for all the laminates are shown in the Tables 11 and 12. The strain rates presented a considerable variation along the plate for each step of time, making of an accurate extraction a hard task. The orthotropic nature of the laminate made its post processing even harder. Even though in the case of laminates #1 and # 2 it was assumed that they can be treated as a quasi-isotropic laminate, therefore making sense to post process the effective stress rate, and after comparing it its values with the first principal averaged strain

rates. These strain rates were measured in 16 elements in the center of the plate, subsequently averaging its data and taking its range of values during the beginning and immediately after the impact, for which is presented as a range of values for each velocity. In overall terms, there is a good agreement between effective and the principal strain rates. It is known that the accuracy of these values depends strongly on the mesh size, its elements distribution and the uniformity of distribution of the applied stress. Although the mesh used in this simulation is regular, with an adequate mesh size as shown in previous sections, these values should be used only as a rough reference.